

# EARTHQUAKE SWARMS IN SOUTH AMERICA

A Thesis

Presented to the Faculty of the Graduate School  
of Cornell University

in Partial Fulfillment of the Requirements for the Degree of  
Master of Science

by

Stephen Gregg Holtkamp

February 2010

© 2010 Stephen Gregg Holtkamp

ALL RIGHTS RESERVED

## ABSTRACT

For this thesis, we performed a manual search for earthquake swarms in South America using the PDE catalog. We chose to perform a manual search because global catalogs are deficient in lower magnitude events and have a potentially low number of events per swarm. With our technique we aim to be insensitive to spatial scales, temporal scales and particularly the number of earthquakes in the potential swarms since seismicity rates vary greatly over the South American continent. However, with a manual search we sacrifice a rigorous approach for one that requires individual interpretation. We identify 35 possible swarms of varying spatial scales and tectonic locations with this search. For most of the events, discussion is limited to several implications about broader tectonic processes due to the lack of additional or higher resolution data (e.g. GPS, InSAR, local seismic catalogs). Several of the events have geodetic data available and for those cases we process and model surface deformation for various slip models and stress changes for earthquake interaction. Two swarms are examined in detail and do not show or are inconclusive for aseismic slip. Seismicity that appears to have been triggered by the Mw=8.5 2001 Peru earthquake is examined and shows that static changes in the Coulomb stress field did not trigger the events, indicating that some dynamic triggering process may have been responsible. We provide evidence that earthquake swarms show a strong degree of interaction with megathrust events by preceding and even marking the limits of large earthquake rupture propagation, showing evidence of stress interaction with megathrust events, and occurring in areas of long standing seismic gaps. We show that swarms commonly occur at the subduction of aseismic ridges and

that there may be a potential interaction between swarm locations and trench parallel gravity anomalies. The catalog produced in this thesis appears to agree with previously determined magnitude-frequency scaling laws as well as potentially agreeing with moment-duration scaling laws. Although few volcanic swarms were found, we explore a possible relationship between swarm magnitudes, the frequency of eruption, and temperature of the volcano.

## BIOGRAPHICAL SKETCH

Stephen was born July 5, 1985 in Cincinnati, Ohio. Stephen was always interested in science, particularly physics, growing up. After attending Moeller High School in Cincinnati, he attended Miami University in Oxford, Ohio. Stephen started as a physics major at Miami, where conducting an undergraduate research project is a curriculum requirement. After seeing a talk by Dr. Mike Brudzinski on slow earthquakes at the physics seminar series, Stephen decided to join Mike's seismology lab to conduct his undergraduate research project. During two years working in Mike's seismology lab, Stephen worked analyzing GPS time series associated with slow slip events in Cascadia, an experience which finalized his interest in geophysics. While working in the seismology lab got him interested in lab work, a trip to the west coast of Mexico to install and service seismometers with Mike got him interested in geology and the field work aspect of geophysics.

Work on his undergraduate project was continued at Cornell University under advisors Matt Pritchard and Rowena Lohman. Work for this thesis started the second year of Stephens two year tenure at Cornell, with Matt Pritchard, Rowena Lohman, and Larry Brown advising.

## ACKNOWLEDGEMENTS

Work for this thesis was supported by a NASA graduate research fellowship. I thank my principal advisors Matt and Rowena for always being available to provide guidance and feedback. I benefited greatly from discussions with graduate students Greg Kirkpatrck, Bill Barnhardt, Phoebe Judge, and Amanda Baker and professors Larry Brown, Larry Cathles, Muawia Barazangi, Jason Phipps Morgan, and Chris Andronicos. The friendships I made in the department with Adrienne Long, Greg Kirkpatrick, Greg McElwee, Sander Hunter, Bill Barnhardt, Phoebe Judge, Willie Guerra, and many others sustained my motivation throughout the years in Ithaca. Geology students really are the best.

## TABLE OF CONTENTS

Biographical Sketch . . . . .	iii
Acknowledgements . . . . .	iv
Table of Contents . . . . .	v
List of Tables . . . . .	vi
List of Figures . . . . .	vii
<b>Introduction</b>	<b>1</b>
<b>1 Earthquake Swarms</b>	<b>7</b>
1.1 Abstract . . . . .	7
1.2 Introduction . . . . .	8
1.3 Data and Methods . . . . .	11
1.3.1 Swarm Search . . . . .	11
1.3.2 InSAR Methodology . . . . .	17
1.4 Results . . . . .	21
1.4.1 Previously Discovered Swarms . . . . .	21
1.4.2 Newly Discovered Swarms . . . . .	61
1.5 Discussion . . . . .	90
<b>Conclusion</b>	<b>114</b>

## LIST OF TABLES

1.1	South American Earthquake Swarms . . . . .	18
1.2	South American Earthquake Swarms . . . . .	19
1.3	Interferograms Made . . . . .	20
1.4	Comparison of along strike epicentral propagation velocities . .	100

## LIST OF FIGURES

1	Magnitude distribution for the PDE and EHB earthquake catalogs.	5
1.1	Regional Map of South America and Swarm Locations . . . . .	15
1.2	1973 Copiapo Earthquake Swarm . . . . .	23
1.3	Epicenter propagation for 1973 Copiapo Swarm . . . . .	26
1.4	1979 Copiapo Earthquake Swarm . . . . .	27
1.5	2006 Copiapo Earthquake Swarm . . . . .	28
1.6	Epicenter propagation for 2006 Copiapo Swarm . . . . .	29
1.7	2006 Copiapo Swarm Neighborhood Algorithm Result. . . . .	33
1.8	2006 Copiapo Swarm Model . . . . .	34
1.9	2006 Copiapo Swarm Neighborhood Algorithm Result. . . . .	37
1.10	2006 Copiapo Swarm Model . . . . .	38
1.11	1997-1998 Punitaqui Sequence . . . . .	40
1.12	1997 Punitaqui Earthquake Swarm . . . . .	41
1.13	Epicenter propagation for the 1997 Punitaqui earthquake Swarm	42
1.14	2005 Ticsani Earthquake Swarm . . . . .	44
1.15	Interferograms of the 2005 Ticsani Earthquake Swarm . . . . .	45
1.16	Neighborhood algorithm results for Ticsani Swarm . . . . .	47
1.17	Inverse model of the 2005 Ticsani Earthquake Swarm. . . . .	48
1.18	1985 Valparaiso Earthquake and pre-shock Swarm . . . . .	50
1.19	2001 Topocalma Knoll earthquake swarm. . . . .	51
1.20	2003 Papudo Seamount Earthquake Swarm . . . . .	53
1.21	2005 Earthquake Swarm at $\sim 34^{\circ}\text{S}$ . . . . .	54
1.22	2007 Swarm near Aysen, Southern Chile . . . . .	56
1.23	1991 Swarm near Hudson Volcano, Southern Chile . . . . .	57
1.24	2008 Earthquake Swarm concurrent with eruption at Chaiten Volcano . . . . .	59
1.25	1977 Earthquake Swarm in Southern Ecuador . . . . .	63
1.26	2005 Earthquake Swarm in Southern Ecuador . . . . .	64
1.27	Possible 1985 Earthquake Swarm in Southern Ecuador . . . . .	65
1.28	Epicenter propagation for the 2005 Ecuador earthquake swarm .	66
1.29	Radar Coherence in Southern Ecuador . . . . .	68
1.30	1977 Central Peru Earthquake Swarm . . . . .	69
1.31	1980 Central Peru Earthquake Swarm . . . . .	70
1.32	1986 Bolivian Earthquake Swarm . . . . .	71
1.33	1991 Colombia Earthquake Swarms . . . . .	73
1.34	1999 Arauco Peninsula Earthquake Swarm . . . . .	74
1.35	2001 Northern Peru Earthquake Swarm . . . . .	76
1.36	2001 Peru Earthquake and Triggered Seismicity . . . . .	77
1.37	2001 Triggered Swarm at Coropuna Volcano . . . . .	78
1.38	2001 Triggered Swarm near Lake Titicaca . . . . .	79
1.39	2001 Triggered Swarm at Tutupaca Volcano . . . . .	80

1.40	2005 Pisco, Peru Earthquake Swarm . . . . .	82
1.41	Pre-Earthquake Interferogram of the Pisco Region . . . . .	83
1.42	1991 Costa Rica Earthquake Swarm . . . . .	85
1.43	1993 North Panama Earthquake Swarm . . . . .	86
1.44	1998 Swarm Activity in Central America . . . . .	87
1.45	1998 Northern Panama Earthquake Swarm . . . . .	88
1.46	1998 Southern Panama Earthquake Swarm . . . . .	89
1.47	1997 Kronotskii Earthquake and pre-shock Earthquake Swarm . . . . .	94
1.48	1973 Kamchatka Earthquake Swarm . . . . .	95
1.49	1983 Kamchatka Earthquake Swarm . . . . .	96
1.50	Magnitude-frequency analysis of Swarms . . . . .	98
1.51	Comparison of Swarm Properties for All Swarms . . . . .	101
1.52	Comparison of Swarm Properties for Megathrust Swarms . . . . .	102
1.53	Distributed slip solution for the 2006 Copiapo Swarm . . . . .	104
1.54	1973 Copiapo Tidal Comparison . . . . .	106
1.55	2006 Copiapo Tidal Comparison . . . . .	107
1.56	Conceptual model for Ticsani swarm interaction . . . . .	109
1.57	Coulomb stress changes at Coropuna Volcano . . . . .	112
1.58	Coulomb stress changes at Tutupaca Volcano . . . . .	113

## INTRODUCTION

Clustering of earthquakes in space and time indicates that interaction between earthquakes is an important phenomenon. The nature of this interaction could potentially provide insight into the physics of earthquake rupture or could be a proxy for studying other processes of interest, such as aseismic slip or fluid diffusion in fault zones. Generally, clustering is attributed to either (1) a decaying cascade of ruptures along a fault plane associated with a large main-shock event [e.g., Sykes, 1971], (2) increase in shear and confining stresses due to and in the proximity of large main-shock events [King et al., 1994], or (3) areas of magmatic or geothermal activity [Benoit and McNutt, 1996]. Earthquakes that occur in magmatic environments are often characterized as swarms because the number and magnitude of shocks in the cluster often increases with time and has no clear associated main-shock that can explain the distribution of seismicity [e.g., Mogi, 1963; Sykes, 1970; Hill, 1977]. We take this definition and in this thesis will define a swarm as an increase in seismicity rate that lacks a clear triggering main-shock earthquake.

Earthquake swarms in volcanic regions have been extensively studied because they are often associated with eruptions or intrusions. Volcanic swarms can occur before, during, after, or not at all correlated with volcanic activity [Benoit and McNutt, 1996]. Swarm-like behavior near volcanic centers may replace mainshock-aftershock behavior due to substantial heterogeneity in material properties or local stress fields that often accompany intrusive volcanic systems, or by high pore fluid pressure which acts to reduce the failure shear stress by reducing the normal stress.

Earthquake swarms not clearly associated with volcanism have been doc-

umented at strike slip and convergent boundaries around the world. Swarms along transform faults often occur at releasing bends [e.g., Shibutani et al., 2002] and in these cases explanations given for volcanic swarms can easily be applied because releasing bends are often accompanied by thinning of the lithosphere and pull-apart basins, a process that often is associated with volcanic activity. These explanations do not easily extrapolate to swarms near the deformation front (e.g. forearc) at convergent boundaries because magmatic activity, if present in the form of arc volcanism, does not occur until the downgoing slab is at  $\sim 100$  km depth, or  $\sim 200$  km from the trench in most cases.

Earthquake swarms at subduction margins have been documented in New Zealand [Evison and Rhoades, 1993], Japan [Matsuzawa et al., 2004; Fujinawa et al., 1983], Kamchatka [Zobin, 1996], Mexico [Zobin, 1996], and South America [Lemoine et al., 2001]. In most of these cases, they were studied for their relationships to larger main-shock events or for stress interactions with other groups of events. In Kamchatka, New Zealand, and Japan, earthquake swarms were studied for their precursory behavior in relation to larger main-shock events, but the mechanism of interaction remains debated. We hope that compiling a thorough catalog of swarms in South America will shed insight into the nature of interaction between large megathrust events and earthquake swarms.

Conceptual models for producing earthquake swarms require two parts: (1) a means of stressing the fault zone that will slip, and (2) a means of preventing large earthquakes relative to the fault dimensions. The means of stressing in volcanic areas is often interpreted as injection of a dyke or magma chamber and in tectonically active areas is far-field stresses (e.g. plate motions) or local stress changes associated with large earthquakes. The means of preventing

large ruptures in volcanic zones is often attributed to fluids and stress or material heterogeneity. Convergent margins where aseismic ridges or seamounts are subducting could very well have enough fluids and heterogeneity to prevent large ruptures, but observations also indicate that aseismic slip may be an important factor in earthquake swarms [Lohman and McGuire, 2007; Ozawa et al., 2007]. Seismology alone cannot provide direct evidence of aseismic slip because no seismic energy is radiated. Geodesy, the field of measuring the earth (e.g. relative motions of points on the earth's crust), most commonly provides the direct evidence seismology cannot. Aseismic slip has been suggested as coinciding with earthquake swarms based on direct geodetic evidence [Lohman and McGuire, 2007; Ozawa et al., 2007; Wolfe et al., 2007], but where no geodetic data exists this suggestion has been based on an expansion or propagation of hypocenters at rates faster than fluid diffusion can occur [e.g., Vidale and Shearer, 2006]. Geodetic data (e.g. Global Positioning System (GPS) and interferometric synthetic aperture radar (InSAR)) have provided essential tools for the discovery of several aseismic processes, such as postseismic or slow slip.

This thesis will focus on the role of earthquake swarm activity in South America. We focus on South America because several swarms have been documented in detail and the highly active margin may make it likely that more swarms exist. South America hasn't been the focus of any broad earthquake swarm studies like in Southern California or Japan, and large areas of the continent are very dry and therefore conducive to application of the InSAR geodetic technique. The tectonic importance of the region, high earthquake activity rate, and availability of geodetic data make South America a good natural laboratory for the study of earthquake swarms.

Active tectonics in South America is dominated by subduction of the Nazca oceanic plate beneath the western coast of South America. Compression dominates the region, and subduction has resulted in arc volcanism in many locations throughout the Andes mountains, although the arc is discontinuous, presumably due to flat slab subduction in northern Peru and central Chile. The core of this work is based on a search for swarm like activity all throughout the South American continent using the National Earthquake Information Center's (NEIC) Preliminary Determination of Epicenters (PDE) catalog, (available online at <http://neic.usgs.gov/neis/epic/epic.html>). Because global catalogs are deficient in smaller magnitude earthquakes, this study intends to be thorough, but only above the completeness threshold, and include swarms from all tectonic environments. The completeness threshold for the PDE catalog is spatially heterogeneous as it depends on station distribution. The PDE completeness threshold is also temporally heterogeneous, but the threshold has generally decreased over time as more stations are installed in the global network. Figure 1 shows the current magnitude distribution for the PDE catalog and Engdahl-Hilst-Buland (EHB) earthquake catalogs for the year 2006. The EHB catalogs are International Seismological Centre (ISC) reported events relocated with the algorithm described in Engdahl et al. [1998] and generally have lower hypocentral mislocation error, with significantly better depth locations. The ISC catalog is considered to be the final bulletin of hypocenters and the PDE program contributes roughly one third of the data used in the ISC compilation. At the beginning of the PDE catalog (1973), earthquakes below  $\sim M_w=5$  in South America were rare in the catalog but now magnitudes of 3 to 4 are commonly reported in many areas.

We then integrate other forms of data, such as Interferometric Synthetic

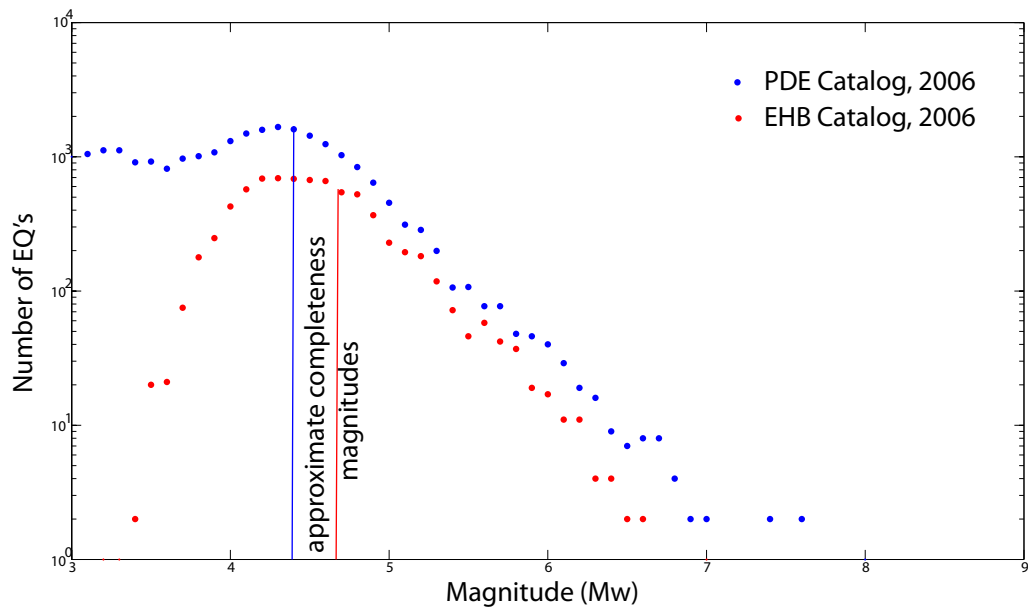


Figure 1: Magnitude distribution for the PDE and EHB earthquake catalogs. Magnitude of completeness is the magnitude at which the distribution deviates from linear at smaller magnitudes in a logarithmic scale ( $\sim 4.7$  for the EHB catalog and  $\sim 4.4$  for the PDE catalog for the year 2006)

Aperture Radar (InSAR), and apply different modeling techniques aimed at analyzing potential models for earthquake swarm generation and interaction with other earthquakes. We will report on 35 possible earthquake swarms and describe the environments in which they occurred. We perform deformation modeling for three swarms which have ample InSAR data available. We also examine triggering mechanisms for two swarms apparently triggered by a  $M_w=8.5$  earthquake in southern Peru.

# CHAPTER 1

## EARTHQUAKE SWARMS

### 1.1 Abstract

For this thesis, we performed a manual search for earthquake swarms in South America using the PDE catalog. We chose to perform a manual search because global catalogs are deficient in lower magnitude events and have a potentially low number of events per swarm. With our technique we aim to be insensitive to spatial scales, temporal scales and particularly the number of earthquakes in the potential swarms since seismicity rates vary greatly over the South American continent. However, with a manual search we sacrifice a rigorous approach for one that requires individual interpretation. We identify 35 possible swarms of varying spatial scales and tectonic settings with this search. Due to the lack of additional or higher resolution data (e.g. GPS, InSAR, local seismic catalogs) for most of the events, discussion is limited to several implications about broader tectonic processes. Several of the events have geodetic data available and for those cases we process surface deformation data and create models for the fault slip and stress changes for earthquake interaction. Two swarms are examined in detail and do not show or are inconclusive for aseismic slip. Seismicity that appears to have been triggered by the Mw=8.5 2001 Peru earthquake is examined and shows that static Coulomb stress changes due to the 2001 Peru earthquake are not consistent with increasing the likelihood of failure along fault planes active during the swarm, indicating that some dynamic triggering process may have been responsible. We provide evidence that earthquake swarms show a strong degree of interaction with megathrust events by preceding and

even marking the limits of large earthquake rupture propagation, showing evidence of stress interaction with megathrust events, and occurring in areas of long standing seismic gaps. We show that swarms commonly occur at the subduction of aseismic ridges and that there may be a potential interaction between swarm locations and trench parallel gravity anomalies. The catalog produced in this thesis appears to agree with previously determined magnitude-frequency scaling laws as well as potentially agreeing with moment-duration scaling laws.

## 1.2 Introduction

With this work we aim to address the fundamental observation that earthquake swarms occur by conducting a thorough examination of the swarm process in South America. Earthquake swarms are of scientific interest because they represent a potentially different mode of fault rupture than mainshock-aftershock sequences that may not be understood and they are of societal interest because earthquake interaction is a key aspect of earthquake hazard mitigation. Earthquake swarms, unlike Mainshock-aftershock sequences (MS-AS), do not have a single accepted definition and the definitions that exist are mostly observational in nature. Hill [1977], for example, defines swarms as clusters of “earthquakes in which the number and magnitude of shocks in a cluster gradually increase and decay in time without a distinct main shock.” MS-AS sequences have several scaling relations: 1) Gutenberg-Richter scaling, which relates the magnitude of events to the frequency with which they occur, 2) Omori’s Law, which describes the temporal decay of aftershock sequences, and 3) Bath’s Law, which relates the magnitude of the mainshock to the magnitude of its largest aftershock [Lay and Wallace, 1995]. In this study, we define a swarm of earthquakes as a seismicity

rate increase which starts and ends abruptly in time and is not accompanied by a distinct main-shock.

Several automated or semi-automated techniques have been developed to identify earthquake swarms or anomalous seismicity rate changes, and they work well within regional catalogs [Vidale and Shearer, 2006; Ogata, 2007]. Vidale and Shearer [2006] investigated earthquake bursts in Japan and Southern California with a semi-automated technique that identified seismicity rate increases which were then examined visually and labeled as swarm-like, aftershock-like, and mixed. They found 18 swarm-like bursts of seismicity in Southern California and 19 swarm-like bursts in Japan. Ogata [2007] and previous studies compared observed seismicity rates with rates predicted by the Epidemic-Type Aftershock Sequence (ETAS) model to detect anomalous seismicity rate changes, both increases and decreases, which can be explained by static stress changes caused by aseismic slip with Coulomb failure stresses on the order of millibars triggering rate changes. The ETAS model is a stochastic model based on expansion of Omori's Law for aftershock decay, an empirical law that relates the aftershock rate to the mainshock magnitude and time after the mainshock event [Shcherbakov et al., 2004], and takes into account that every earthquake in each sequence will have its own set of aftershocks. In this way the ETAS model removes the effect of aftershocks from the seismicity catalog, which is important because aftershocks are caused by the mainshock and not another underlying process, such as aseismic slip or stressing rate.

Rate and state friction dependent models have also been proposed to explain seismicity rate changes on faults [Dieterich, 1994]. Llenos et al. [2009] combine the ETAS and rate- and state- dependent models to show that after-

shock productivity within a swarm is not related to stressing rate and use the ETAS model to reduce the impact of aftershocks on their inferred aseismically triggered stressing rates.

Earthquake swarms that have occurred in regions with dense geodetic and seismic observations (e.g. Boso peninsula, Japan and Salton Trough, California) have been shown to occur coincident with large amounts of aseismic moment release in the form of a slow earthquake [Ozawa et al., 2007; Lohman and McGuire, 2007]. For the recent Boso peninsula swarm in 2007, total seismic moment release of  $3 \times 10^{24}$  (Mw=5.59) was observed, compared to the geodetically constrained moment release of  $1.09 \times 10^{26}$  (Mw=6.62) which is 36 times larger than the total seismic moment release [Ozawa et al., 2007]. Geodetic moment for two other Boso swarms in 2002 and 1996 were  $\sim 2000$  times larger than total seismic moment release. Seismicity during the Salton Trough swarm of 2005 totaled  $1.1 \times 10^{24}$  dyne-cm (Mw=5.3), 5 times smaller than the geodetically constrained moment release of  $5.25 \times 10^{24}$  dyne-cm (Mw=5.75) [Lohman and McGuire, 2007]. We will examine potential scaling relations between swarm moment release and duration.

In the Boso and Salton Trough cases, as well as the 2000 Izu Islands swarm that occurred during a dike intrusion [Toda et al., 2002], seismicity rate is shown to be directly correlated with stressing rate, either by aseismic slip or some other stress inducing event. In these three geodetically constrained cases, earthquake swarm locations are adjacent to the aseismically slipping regions. We document seismicity rate increases only as they are easy to determine visually when the background seismicity rate is low.

The purpose of this swarm search is to identify earthquake swarms in South

America and determine their basic characteristics. We then determine if geodetic data exist for each swarm. A few of the swarms for which additional data exists are examined. This provides examples for the types of applications this swarm database can provide, such as Coulomb stress change modeling or InSAR investigations. The motivation behind these investigations is the possibility of aseismic slip as a controlling factor in the generation of earthquake swarms and on stress interactions between swarms and other clusters of earthquakes. This explanation for earthquake swarms has been invoked in tectonic (which here we define as not magmatic) environments, such as the Salton trough and Boso peninsula swarms. Geodesy provides observations of deformation due to subsurface magmatic or fluid movements and can be a useful tool for studying volcanic processes. Since we document several swarms in volcanic regions, we also combine geodetic and seismic evidence to examine the role of earthquake swarms in volcanic processes. Individual studies will compare seismic observations with detailed geodetic inversions to test for the existence of aseismic slip as a potential controlling mechanism and will calculate the Coulomb stress changes associated with earthquakes to test swarm triggering mechanisms.

## **1.3 Data and Methods**

### **1.3.1 Swarm Search**

We download the complete PDE catalog for the western half of the South American continent, which spans from latitude 13N to 57S and longitude 63W to 83W.

The data are freely available online from [http://neic.usgs.gov/neis/epic/epic\\_global.html](http://neic.usgs.gov/neis/epic/epic_global.html) and contains information on time, location, magnitude, and depth for earthquakes from 1973 through February 1, 2009. Global catalogs such as the PDE are generally not as accurate as local catalogs because local Earth structure is not accounted for [Engdahl et al., 1998]. Local seismic velocity variations (e.g. due to a subducting plate) tend to impart systematic errors in global catalogs, so while global catalogs suffer in accuracy they do not suffer as much in precision in the locations since systematic errors affect accuracy but not precision [Syracuse and Abers, 2009]. Global catalogs also do not have accurate or precise measurements of depths for shallow ( $< \sim 50$  km) earthquakes because picking good depth phases in earthquake waveforms varies by earthquake and station location, making it difficult for global catalogs to constrain this information. Engdahl et al. [1998] attempted to correct for these discrepancies by using better earth velocity models and an algorithm for picking depth phases in generating the EHB catalog. Benchmarking of the EHB catalog with locally relocated seismicity has shown that the EHB catalog can still have errors on the order of 10 km [Maggi et al., 2000], but catalogs such as the PDE and ISC catalog can have errors on the order of several tens of kilometers [Engdahl et al., 2006]. With all catalogs, much of the error is in depth estimation [Maggi et al., 2000; Engdahl et al., 2006; Syracuse and Abers, 2009].

A grid search was used to extract all earthquakes in a moving window over a grid in latitude and longitude. Depth was not restricted in the search. A box size of 1.5 degrees ( $\sim 167$  km) was used and all earthquakes in that area were plotted as a magnitude vs time plot. For each iteration we shifted the grid by 0.5 degrees so there was overlap in successive plots. This was done to ensure that no swarms were missed due to improper sampling of the source area. 1.5

degrees was chosen after testing several box sizes because with larger box sizes there are too many earthquakes in the moving window to identify individual earthquake sequences.

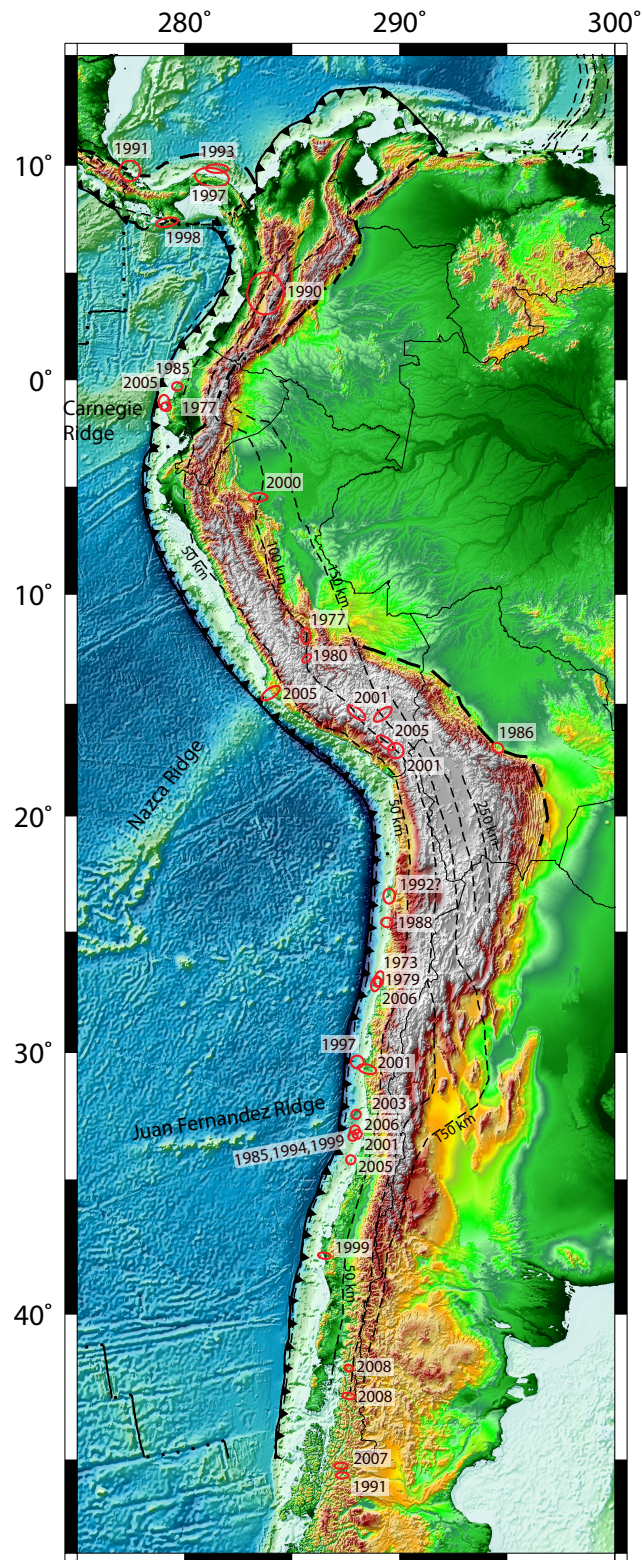
We examined the plots of earthquake magnitude as a function of time for seismicity rate changes or bursts of seismicity. For each case where an apparent increase in seismicity was not accompanied by a large earthquake, we made additional plots, like the one shown in Figure 1.5, focusing on the cluster in question to determine the nature of the seismicity. The plots show time-magnitude distribution on a 15 year time scale to get a sense of the background seismicity, time-magnitude in a short time period bracketing the potential swarm, and a map view image of seismicity in a window encompassing the potential swarm. In most cases, bursts that appear to be swarm-like were coincident with large events just outside of the grid search area and are labeled aftershock sequences as they appear to follow the scaling laws for MS-AS sequences.

The initial set of aftershocks is often interpreted to outline the rupture area of large events [Lay and Wallace, 1995]. Large earthquakes in South America, particularly on the subduction interface, consistently rupture hundreds of kilometers of the fault. Since the PDE reports the epicentral location, care must be taken that aftershocks of large earthquakes are not misinterpreted as swarms due to their distance from the mainshock epicenter. To ensure this is the case, it is important that the map view image completely encompasses the cluster of seismicity, which we ensure by expanding the area well beyond the edge of seismicity (most figures in this thesis have a box size of  $\sim 3$  degrees).

We identified 35 swarm-like clusters of earthquakes. A summary of all swarms is presented in Table 1.1, 1.2 and Figure 1.3.1. The "environment" vari-

able is determined from the tectonic environment of the swarm (between the trench and the 50km depth contour is "megathrust", anywhere near the arc is "volcanic"). The "volcanic" label only implies the swarm is in the vicinity of the arc, not that it is necessarily a volcanic earthquake swarm. The area calculation is made with an algorithm solving for the minimum volume enclosing ellipsoid (a convex optimization problem) of the earthquake hypocenters. The algorithm is freely available at the MATLAB central file repository (<http://www.mathworks.com/matlabcentral/fileexchange/9542>) under the BSD License. The two largest dimensions of the 3-D ellipsoid are taken to represent the rupture plane and the area of this ellipse is the area reported in Table 1.1. This algorithm was tested for several large mainshock-aftershock sequences in South America and was able to accurately determine strikes and dips and slightly overestimate rupture areas. The overestimation is probably due to earthquake hypocentral errors. Only areas for swarms with more than 40 earthquakes are reported because for small numbers of events hypocentral errors dominate in the area calculation. Characteristics of swarms were diverse in geologic setting, relation to other earthquakes, duration, spatial extent, number of earthquakes, and magnitudes of earthquakes. In all, close to one thousand earthquakes were identified as associated with swarms out of a total of 50,000 earthquakes in the PDE catalog, with moment magnitudes up to  $M_w=6.7$ . It is worth noting that this methodology may have some systematic problems with it. For example, swarms are difficult to determine visually in areas with high background seismicity rate (e.g. central Chile, between  $30^\circ\text{S}$  and  $35^\circ\text{S}$  contains half of the earthquakes in South America). Also, it is difficult to distinguish between swarms that follow large earthquakes or are triggered by large earthquakes and aftershock sequences.

Figure 1.1: Combined Topography/Bathymetry of South American region studied in this Thesis. Red circles and associated dates provide times and locations of all swarm events discussed in the Results section. Size of red circles is true to the zone of shocks associated with the swarms. Thick black lines provide plate boundary information from Bird [2003] and thin dashed lines show depth to slab contours every 50 km (from Syracuse and Abers [2006]).



### 1.3.2 InSAR Methodology

SAR acquisitions made from the European Space Agency's (ESA) ERS-1, ERS-2, and Envisat radar satellites were searched for acquisitions that span each swarm. In most cases, the time interval search window before and after each swarm was limited to a couple of years, but in several cases was expanded beyond that to acquire potential pairs. Tracks that have acquisitions bracketing swarms are listed in Table 1.3. These are acquired from the European Space Agency (ESA's) Earthnet On-Line Interactive (EOLI) data repository for several of the events discussed in the results section. For this study, we focused on swarms that had larger maximum magnitudes ( $\sim 6$ ) because these have the highest probability of being detected geodetically.

Interferograms were processed using the Repeat Orbit Interferometry Package (ROIPAC) software package maintained by JPL/Caltech [Rosen et al., 2004]. Interferograms were initially processed using orbits provided by the European Space Agency and available online, but for every case long wavelength ramps were present in the initial interferograms. These ramps are mostly due to orbit uncertainties and are fit using a quadratic ramp and removed. Interferograms were then down-sampled (looked down), unwrapped, and geocoded using ROIPAC.

Inversion of the geodetic data was performed using the Neighborhood Algorithm, a nonlinear inversion scheme useful in exploring several different model parameters efficiently [Sambridge, 1998]. A key advantage of the Neighborhood Algorithm is that it gives a measure of the broadness of the misfit minimum for each of the parameter spaces explored which allows the reader to visually qualify the goodness of the result. Interferograms are resampled using

Table 1.1: South American Earthquake Swarms. \* denotes previously discovered swarms. Duration is in years, area is in square meters. Lat and lon are the approximate center of the swarm.

Date	Lat.	Long.	Duration	Num. EQs	Total Mw	Fig.	Area
1973.5*	-26.83	-70.92	0.12	72	6.7	1.4.1	6.1e+09
1976.9	-11.93	-73.5	0.25	14	5.9	1.30	
1977.3	-1.36	-80.79	0.05	9	5.6	1.25	
1979.3	-27.15	-71.05	0.03	12	6.2	1.4	
1980	-12.93	-74.5	0.8	12	5.8	1.31	
1985.1	-33.08	-71.85	0.01	15	5.8	1.18	
1985.3	0	-80.5	0.2	5	4.9	1.27	
1986.15	-17.43	-65.5	0.25	7	5.8	1.32	
1990.5	3.5	-76.5	0.25	100	5.4	1.33	1.1e+11
1991.3	10.07	-82.5	0.2	15	6.3	1.42	
1991.6	-44.93	-72.5	0.07	13	6.1	1.23	
1993.6	9.5	-79	0.65	10	5.2	1.43	
1994	-33.2	-72.2	0.1	10	4.4		
1997.5*	-30.52	-71.86	0.04	32	6.9	1.12	1.8e+10
1997.6	9.5	-79	1	141	4.6	1.44	2.2e+11
1998.05	6.21	-73.87	0.35	30	5.2	1.46	
1998.1	7.3	-81	1	57	5.0	1.45	2.8e+10
1999.3	-33.33	-72.29	0.02	25	4.9		
1999.45	-33.33	-72.29	0.1	50	4.8		
1999.84	-38	-72.5	0.15	11	5.7	1.34	
2000.6	-5.36	-76.62	1.7	15	5.6	1.35	
2001.45	-15.4	-72.2	.15	31	6.1	1.37	
2001.45	-15.41	-70.36	0.5	16	5.6	1.38	
2001.45	-17	-70.25	0.15	20	5.8	1.39	
2001.8*	-33.2	-72.2	0.01	10	4.9	1.19	
2003.4	-32.34	-72.19	0.02	25	5.2	1.20	3.1e+09
2005.05	-1.36	-80.79	0.09	39	6.6	1.26	5.1e+09
2005.2	-14.77	-76.54	0.8	15	5.5	1.40	
2005.61	-34.3	-72.5	0.01	9	4.7	1.21	
2005.55*	-16.64	-70.79	0.25	38	5.8	1.14	
2006.3*	-27.02	-71.02	0.1	100	6.9	1.5	6.4e+09
2006.7	-33.2	-72.2	0.1	14	4.7		
2007*	-45.24	-72.65	0.25	15	6.4	1.22	
2008.34*	-42.7	-72.5	0.01	10	6.0	1.24	
2008.40*	-42	-72.3	0.02	7	6.1	1.24	

Table 1.2: South American Earthquake Swarms. \* denotes swarms examined with InSAR in this thesis

Date	Lat	Environment	Location	Area
1973.5	-26.83	Megathrust	Copiapo	6.08e+09
1976.9	-11.93	?	C. Peru	
1977.3	-1.36	Megathrust	Ecuador	
1979.3	-27.15	Megathrust	Copiapo	
1980	-12.93	?	C. Peru	
1985.1	-33.08	Megathrust	Valparaiso	1.57e+10
1985.3	0	Megathrust	Ecuador	
1986.15	-17.43	Sub-Andean	Bolivia	
1990.5	3.5	?	Colombia	1.13e+11
1991.3	10.07	?	Costa Rica	
1991.6	-44.93	Volcano	Hudson	
1993.6	9.5	?	Panama	
1994	-33.2	Megathrust	Topocalma	
1997.5	-30.52	Megathrust	Punitaqui	1.8e+10
1997.6	9.5	?	C. Amer.	2.19e+11
1998.05	6.21	?	S. Panama	
1998.1	7.3	?	N. Panama	2.8e+10
1999.3	-33.33	Megathrust	Topocalma	
1999.45	-33.33	Megathrust	Topocalma	
1999.84	-38	Megathrust	Arauco	
2000.6	-5.36	?	N. Peru	
2001.45*	-15.4	Volcano	Coropuna	
2001.45	-15.41	Volcano?	Titicaca	2.23e+10
2001.45	-17	Volcano	Tutupaca	
2001.8	-33.2	Megathrust	Topocalma	
2003.4	-32.34	Megathrust	Papudo	3.14e+09
2005.05*	-1.36	Megathrust	Ecuador	5.07e+09
2005.2*	-14.77	Megathrust	Pisco	3.11e+10
2005.61	-34.3	Megathrust	34S	
2005.55*	-16.64	Volcano	Ticsani	1.33e+10
2006.3*	-27.02	Megathrust	Copiapo	6.38e+09
2006.7	-33.2	Megathrust	Topocalma	
2007	-45.24	Volcano	Aysen	
2008.34	-42.7	Volcano	Chaiten	
2008.40	-42	Volcano	Hornopirén	

Table 1.3: Interferograms Made. BPerp is the perpendicular baseline between the two satellite passes. The Track column has the format 'Satellite'-T'Track Number', where satellite is either ERS or IM'number' (ENVISAT Image mode number). For example, IM2-T447 is Envisat image mode 2, track 447.

Location	Master Date	Slave Date	Track	Bperp
Copiapo	06/18/2007	08/22/2005	ERS-T96	300
	01/14/2008	08/22/2005	ERS-T96	260
	03/05/2007	09/06/2004	ERS-T96	230
Ticsani	01/22/2005	01/07/2003	IM2-T411	
	06/17/2006	12/04/2004	IM4-T361	
	06/14/2006	01/05/2005	IM2-T318	
Ecuador	02/11/2006	07/12/2003	IM2-T068	30
	02/11/2006	06/07/2003	IM2-T068	100
	07/12/2003	06/07/2003	IM2-T068	80
S. Peru (Coropuna)	01/09/2002	04/09/1996	ERS-T225	40
	01/13/2003	10/06/1997	ERS-T497	40
Peru (Pisco)	07/28/2006	02/18/2005	IM2-T447	100
	10/19/2007	10/10/2003	IM2-T354	60
	08/17/2007	2/18/2005	ERS-T447	190

the resampling tool of Lohman [2004], which uses an initial fault plane guess to identify important regions in the interferogram. Greens functions are built using Okada's rectangular dislocation solution in an elastic half space [Okada, 1985]. The inversion scheme allows for exploration of several model parameters: location of the fault patch described by an azimuth and a distance from an initial search point, depth, length, width, and aspect ratio the fault patch, strike, dip, and rake. Variations in incidence angle along the radar scene, which manifests as a ramp in the range direction, are accounted for in the inversions.

## **1.4 Results**

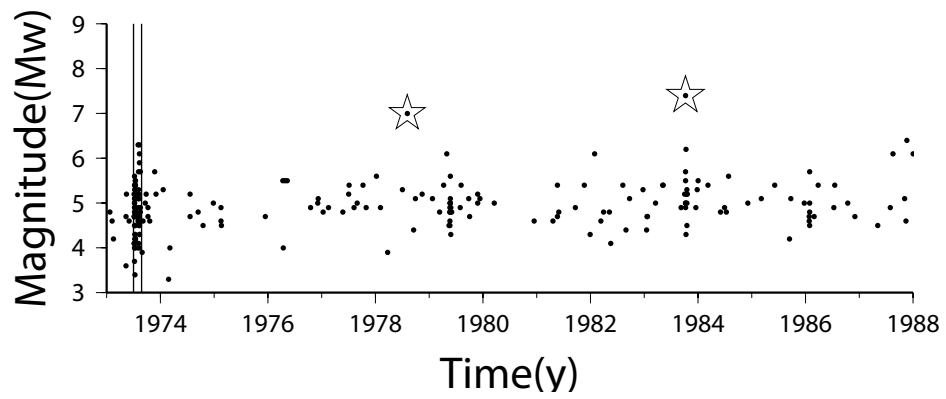
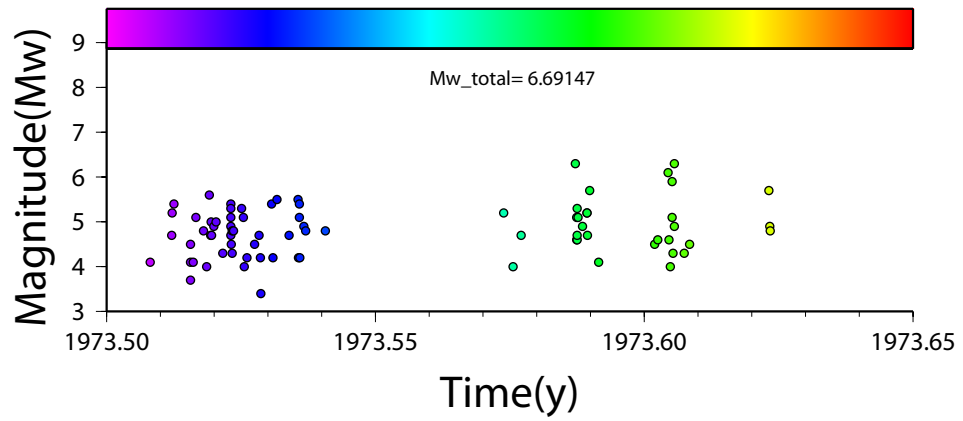
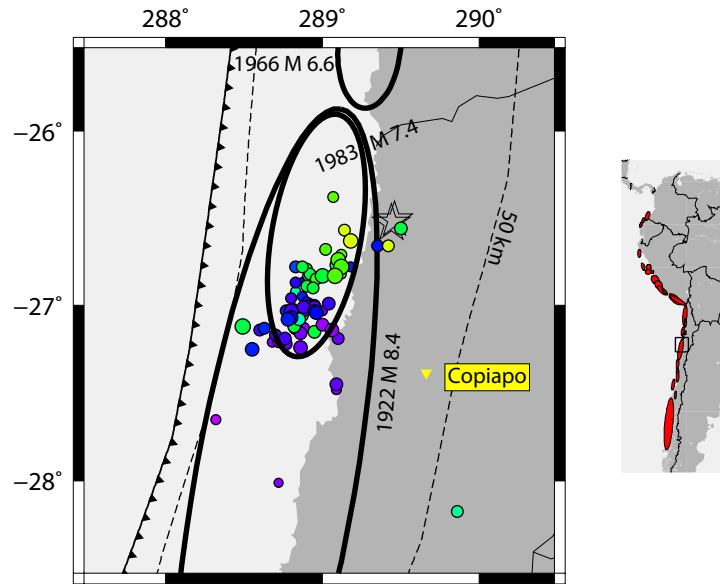
### **1.4.1 Previously Discovered Swarms**

A key test for the effectiveness of our effort to compile a thorough list of swarms is comparing swarms found with this method to previously discovered swarms documented in literature or meeting abstracts. Individual swarms documented by previous researchers will be discussed in the following sections. Most of these swarms were studied individually and discovered with local seismic networks. Our search was blind in the sense that the swarm search described above was done before a literature search for swarms. All of the swarms known in the literature and above or near the catalog completeness threshold ( $\sim 4-5$ ) were found by our swarm search method.

### Central Chile, 1973, 1979, and 2006 Copiapo Swarms (27°S)

Comte et al. [2002] report a swarm during July and August of 1973 using ISC reported earthquakes. The swarm search presented in this thesis also documents this swarm, and shows it contains at least 72 earthquakes with a maximum magnitude of  $M_w=6.3$ . The first earthquakes occurred near 27°S and propagated to the north. They report this swarm to be in the middle of the 1922  $M_w=8.2$  rupture zone and show that this swarm marks the southern terminus of the 1983  $M_w=7.4$  earthquake. They suggest that if this swarm were on the interface and not in the continental crust above it, this indicates that the region north of the swarm was not ready to rupture in 1973. The 1973 Copiapo swarm and its relation to the 1983 earthquake is shown in Figure 1.4.1. Figure 1.4.1 shows that the events appear to have started at the southern edge of the rupture zone and ended at the northern edge, so we plotted the along strike position of epicenters to determine if any propagation had actually occurred. Figure 1.3 shows the along strike epicentral propagation. While a linear fit to the along-strike distances favors this south to north propagation at  $\sim 3$  km per day for the initial swarm and  $\sim 0.6$  km per day when averaged over the whole sequence, we feel there is not enough resolution to differentiate between smooth propagation of epicenters, discrete jumps in epicenters, or random scatter.

Figure 1.2: 1973 Copiapo Earthquake Swarm. Top panel shows mapview of seismicity with circle size representing  $M_w$  and color representing time as shown in the middle panel. The dashed lines on the map show depth to slab contours from Syracuse and Abers [2006] and represent the 6, 50, 100, 150, and 200 km depth contours. Middle panel shows PDE reported seismicity in a small time window just bracketing the seismicity and within the area shown in the top panel. The bottom panel contains 15 years of seismicity to show the background seismicity rate. Thin vertical lines in the bottom panel show the begin and end times of the middle panel. When present, stars in the top and bottom panels show epicenters of earthquakes with  $M_w > 6.5$  within the 15 year timespan shown in the bottom panel. The same scheme will hold for all subsequent plots of swarm seismicity.



Comte et al. [2002] also report that this is the only swarm in the Copiapo region, but this swarm search identified an additional swarm in 1979, though much smaller in number and magnitudes of earthquakes. This swarm is shown in Figure 1.4 and contains only 12 earthquakes with a maximum magnitude of  $M_w=5.6$ .

More recently, in April to May of 2006, a swarm consisting of approximately 180 earthquakes observed within the PDE catalog occurred overlapping with and to the south of the 1973 Copiapo swarm. This swarm was also identified and examined by Comte et al. [2006]. They present evidence that seismicity within this swarm is correlated with a subducting seamount. In addition, they find that events occur in areas of low  $V_p$  and high  $V_p/V_s$  ratio. Seismic anomalies of low  $V_p$  and high  $V_p/V_s$  ratio are consistent with the presence of excess fluids in the area because fluids are seismically slow but affect shear velocities more than compressional velocities.

The 2006 Copiapo swarm is shown in Figure 1.5. Figure 1.6 shows that this swarm may exhibit north to south propagation of hypocenters, but again there is not enough resolution in the PDE to rule out discrete jumps in seismicity or just random scatter. A best fit line to the main part of the seismicity, from  $\sim 2006.335$  to  $\sim 2006.345$ , prefers a rate of  $-7.4$  km/day of along-strike epicentral propagation. North to south propagation is opposite to the 1973 swarm but is similar to the overall trend of north to south propagation during recent large megathrust events in Chile [Pritchard et al., 2007]. Seismicity within the swarm was clustered at the beginning and after 1/3 of the sequence, with the largest event occurring in this second burst of earthquakes.

The onshore region next to the site of the 2006 Copiapo swarm lies at the

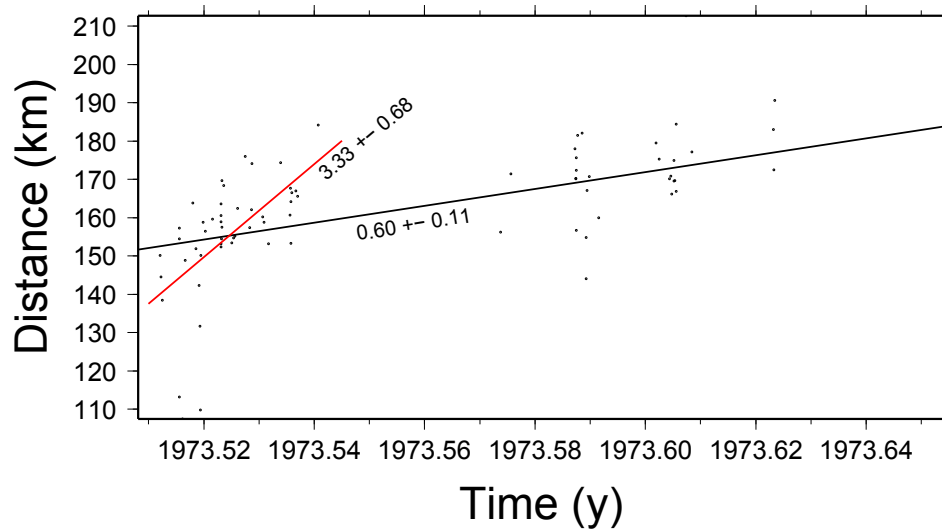


Figure 1.3: Earthquake epicenter propagation for the 1973 Copiapo earthquake swarm. Distances on the y-axis are taken from the southernmost event in the cluster so the y axis has north at the top and south at the bottom and represents along-strike propagation. Depths are not included because of poor depth resolution in the global catalog. Values shown are in km per day and the error is one standard deviation.

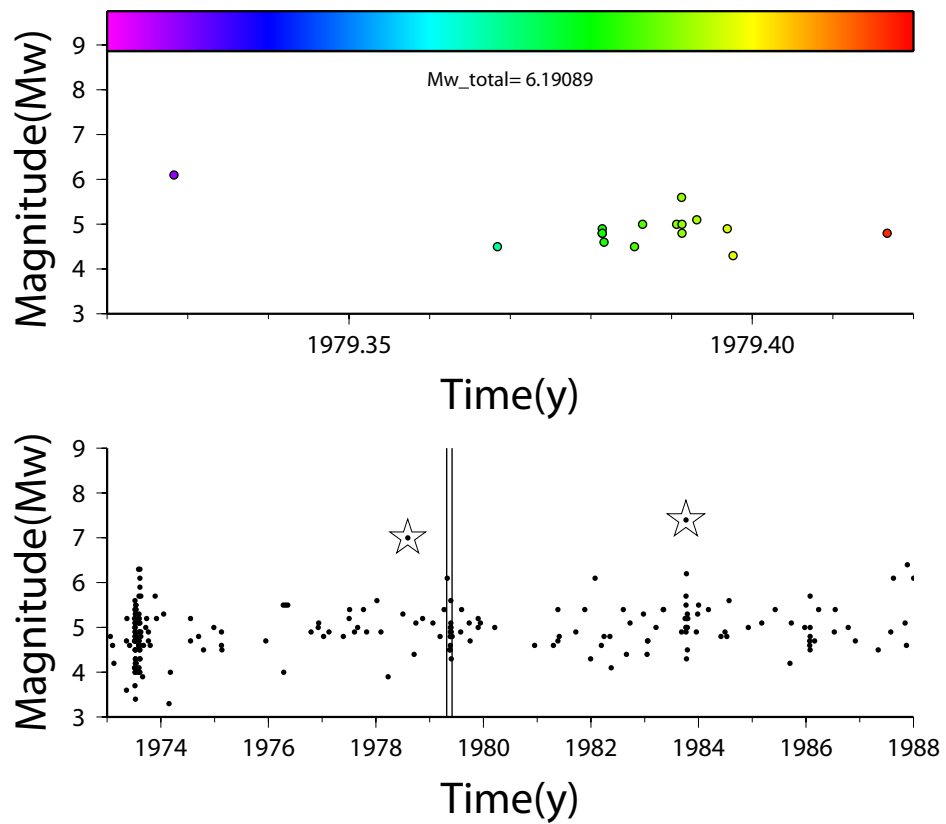
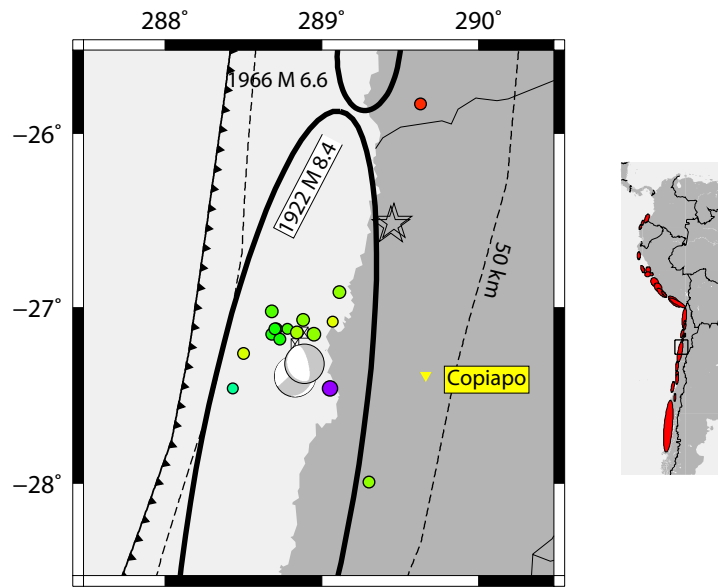


Figure 1.4: 1979 Copiapo Earthquake Swarm.

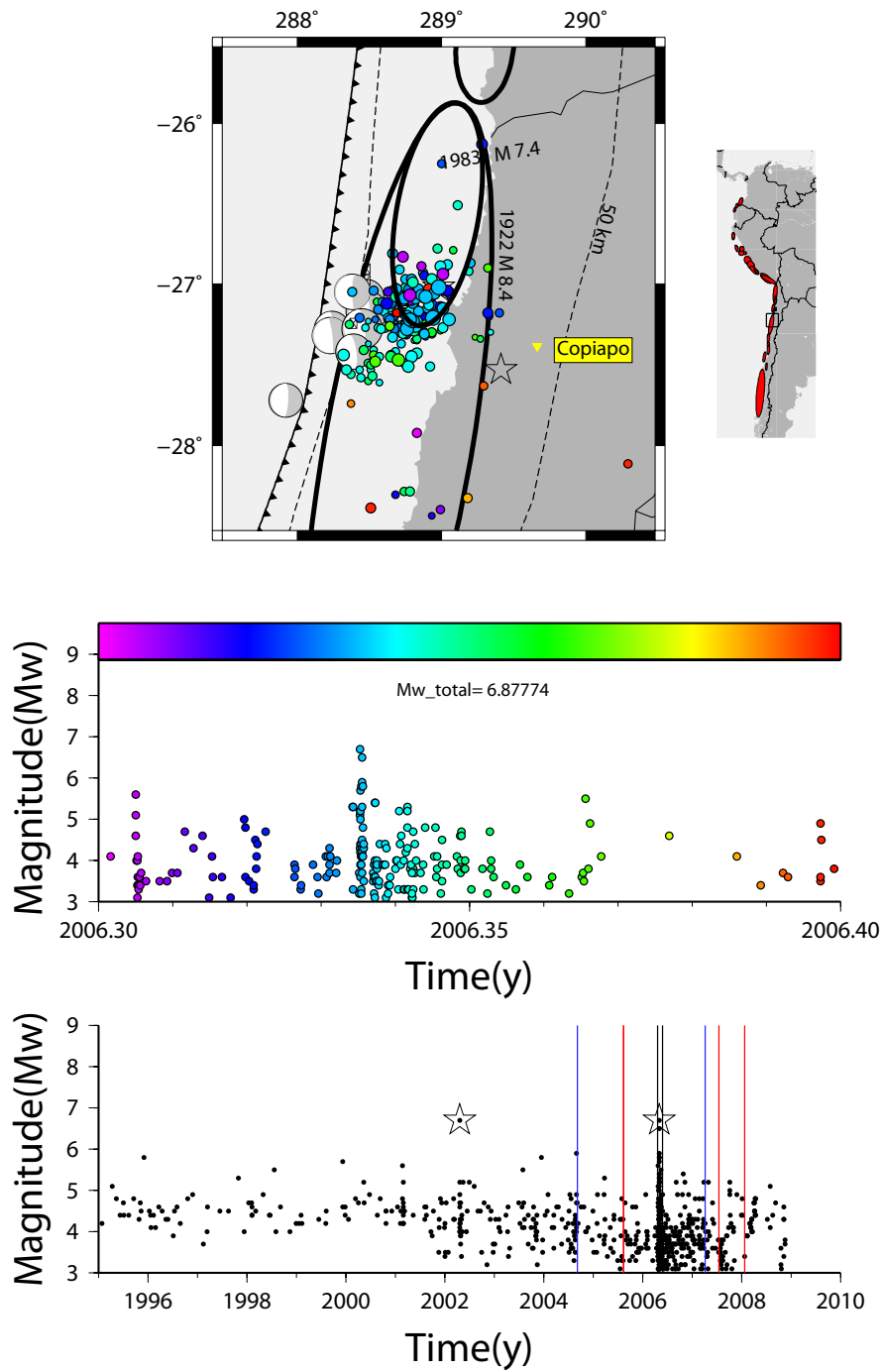


Figure 1.5: 2006 Copiapo Earthquake Swarm. InSAR associated with the swarm is discussed in the text (Table 1.3), colored vertical lines in the bottom panel will show the acquisition dates, with similar colors representing independent interferograms made.

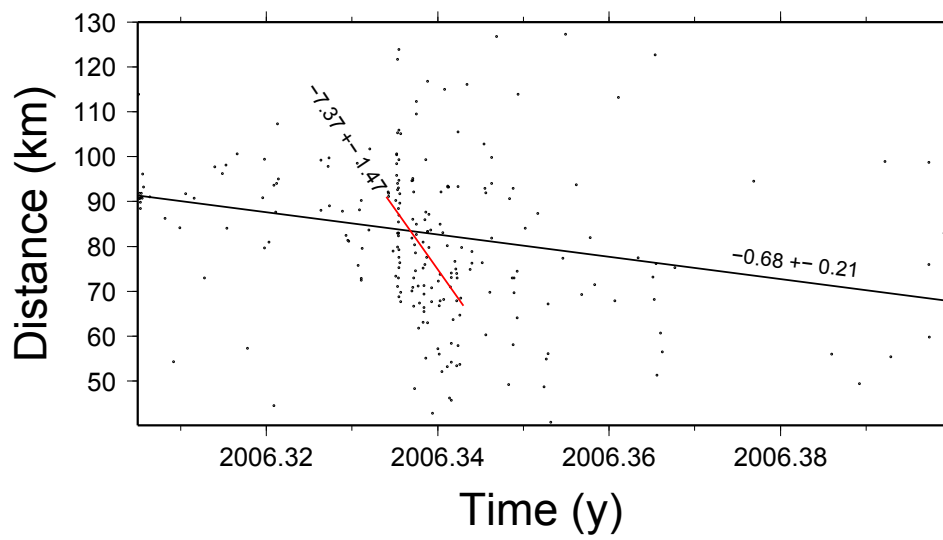


Figure 1.6: Earthquake epicenter propagation for the 2006 Copiapo earthquake swarm.

southern end of an extensive hyper-arid region that extends from central Peru through central Chile along the west coast of South America. The aridity allows for interferograms to remain coherent over periods of several years. Three interferograms were made from track 96 that span the swarm, and the dates of these acquisitions are shown in the bottom panel of Figure 1.5. Our primary goal in performing these inversions is to determine if any aseismic slip component is needed to predict the observed ground deformation. Any disagreement between the seismically and geodetically constrained moments could indicate aseismic slip had occurred.

Since only one track was available that contained this deformation pattern and the rupture plane appears to be offshore, we performed several iterations of the inversion algorithm to arrive at a solution consistent with *a priori* information regarding the seismicity patterns and interface location. We made three interferograms with SAR imagery from Envisat track 96 beam mode 2 that span the swarm - two share a common scene and one is completely independent. All three are used in the inversion scheme in an effort to reduce the noise due to atmospheric or other errors. Atmospheric errors can be on the order of several centimeters, and since the signal we see is  $\sim 6$  cm, using all data in the inversion is necessary.

If allowed to explore all parameter space freely, the inversion arrives at a solution inconsistent with seismicity as located by the EHB catalog or plate dip because only one lobe of the deformation pattern is visible to the radar and the rest of the deformation pattern is offshore. The inversion in this case prefers solutions that are several tens of kilometers further offshore than the seismicity, much steeper dips of  $>45^\circ$  than the approximate  $20^\circ$  dip of the plate interface

[Comte et al., 2002], and with larger magnitude solutions of  $> M_w=7.6$ . Since the primary concern is the event magnitude, this is unacceptable as location, dip, depth, and magnitude all trade off with each other because of the offshore nature of the deformation pattern.

For our next attempt, we added in *a priori* information about the location of seismicity to determine whether the observed deformation could be consistent with the recorded seismicity. First, the location and depth were fixed in space near the seismicity and all other parameters allowed to vary. The first iteration was performed to arrive at the proper strike and dip. The inversion algorithm arrived at a strike of  $15^\circ$  and a dip of  $21^\circ$ . Strikes associated with the swarm in the CMT catalog ranged from  $-27^\circ$  to  $21^\circ$  with a mean of  $-1^\circ$  and standard deviation of  $12^\circ$ . Strikes average out to  $10^\circ$  when they are weighted with the moment of the event. Dips in the CMT catalog average  $21^\circ$  with a standard deviation of  $5^\circ$ . When weighted by the event moments, the mean dip is  $16^\circ$ . Since the inverse solution using the InSAR data for strike and dip are close to the weighted averages of the CMT solutions, these values are assumed to be correct and fixed in future iterations. The strike of the trench at  $\sim 27^\circ\text{S}$  is about  $10^\circ$  [Bird, 2003] and the dip of the interplate contact is determined from local seismicity to be about  $20^\circ$  [Comte et al., 2002].

The second iteration fixes the strike and dip at  $15^\circ$  and  $21^\circ$  and explores location, depth, length and width. The magnitude of the inversion result is very sensitive to depth, and for this particular case deeper fault planes produce smaller residuals. The inversion arrives at a result that is about 15 km deeper than the seismicity reported by the ISC using the Engdahl et al. [1998] location scheme and contains approximately three times the total seismic moment re-

lease. When the location and depth are limited to a very small region (10 km search radius around EHB reported seismicity and down to 25km depth), the inversion arrives at a result that predicts the total seismic moment release exactly. EHB reported seismicity shows events occurring down to ~25km depth in this swarm. Results from the Neighborhood Algorithm inversion and comparisons to seismicity are shown in Figure 1.7. The green stars represent Benioff zone seismicity of the downgoing slab located by a local on and off shore seismic network [Comte et al., 2002] and are not associated with the swarm. The blue dots and red stars represent PDE and EHB reported seismicity for this swarm. Considerable decrease in scatter of hypocentral locations is seen in the EHB events for this swarm and the good comparison between EHB and Comte et al. [2002] seismicity suggests there is little systematic error in these EHB located earthquakes. The second iteration of the inversion forced the fault plane to agree with the *a priori* information of EHB located seismicity. Comparison of data and forward models of deformation are shown in Figure 1.8. This result suggests no component of the observed ground deformation needs to invoke aseismic slip as the seismically radiated energy can account for nearly all of the geodetically observed moment release. While no additional slip is needed to explain the signal, the inversion does not rule out the potential for aseismic slip since small changes in fault locations and size will have a large impact on the apparent moment magnitude of the slip.

For comparison, we also present the best fit model without using the *a priori* information. The inversion algorithm arrives at a moment magnitude of  $M_w=7.22$ , more than three times larger than the seismic moment of  $M_w=6.89$ . This would imply aseismic slip is a necessary component, but we choose not to believe this model because of the *a priori* information mentioned above. Results

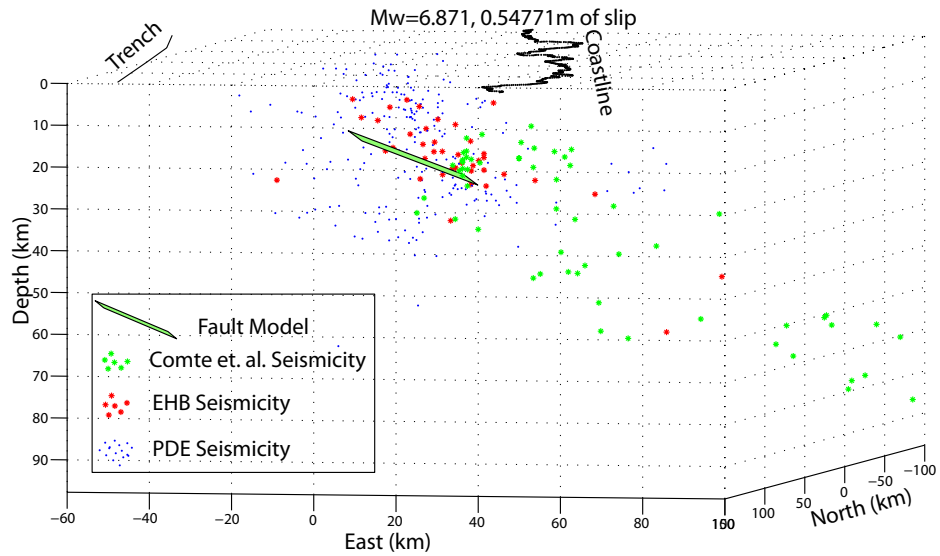
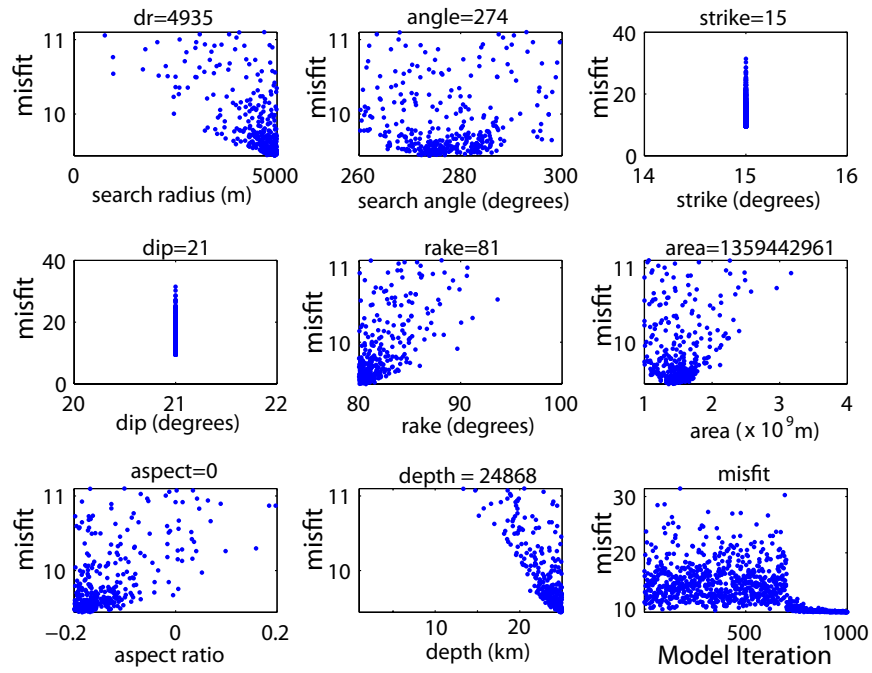


Figure 1.7: Results from the Neighborhood Algorithm for the 2006 Copiapo Swarm. Each panel represents the residual between data and model as a function of the different model parameters explored.

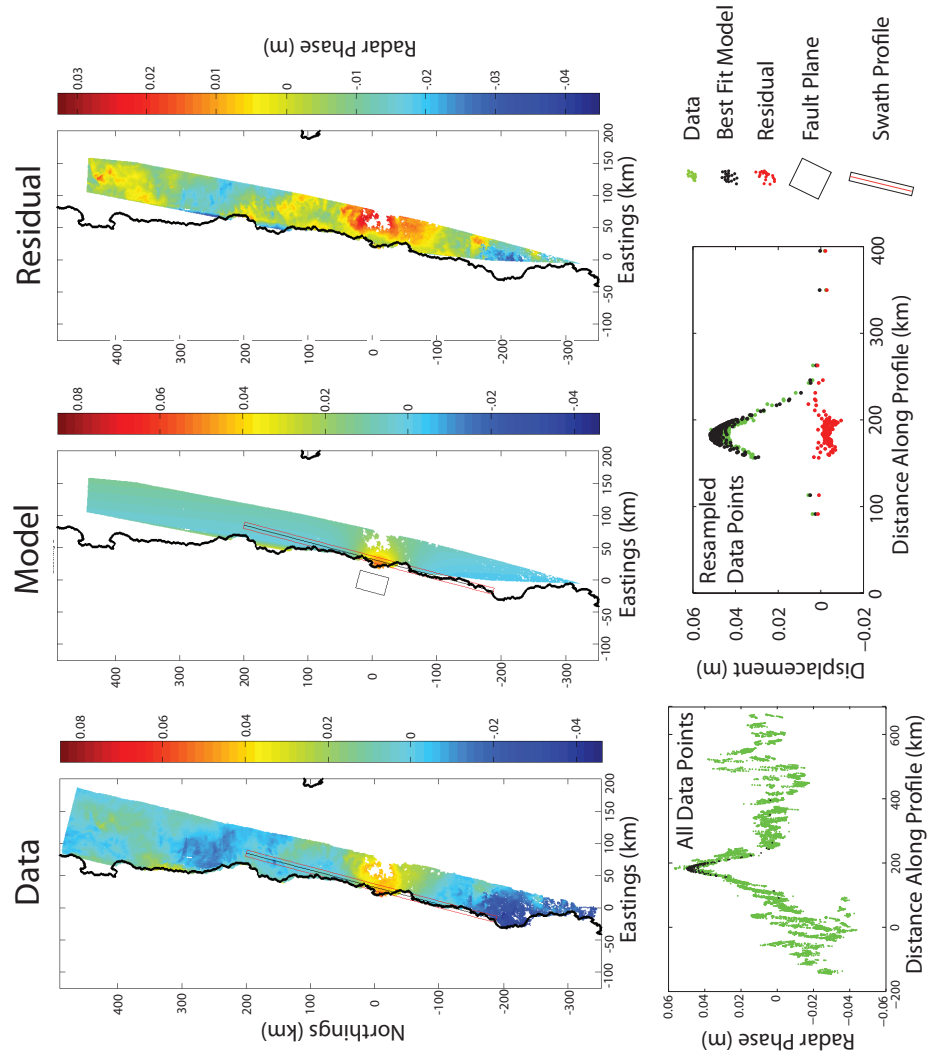
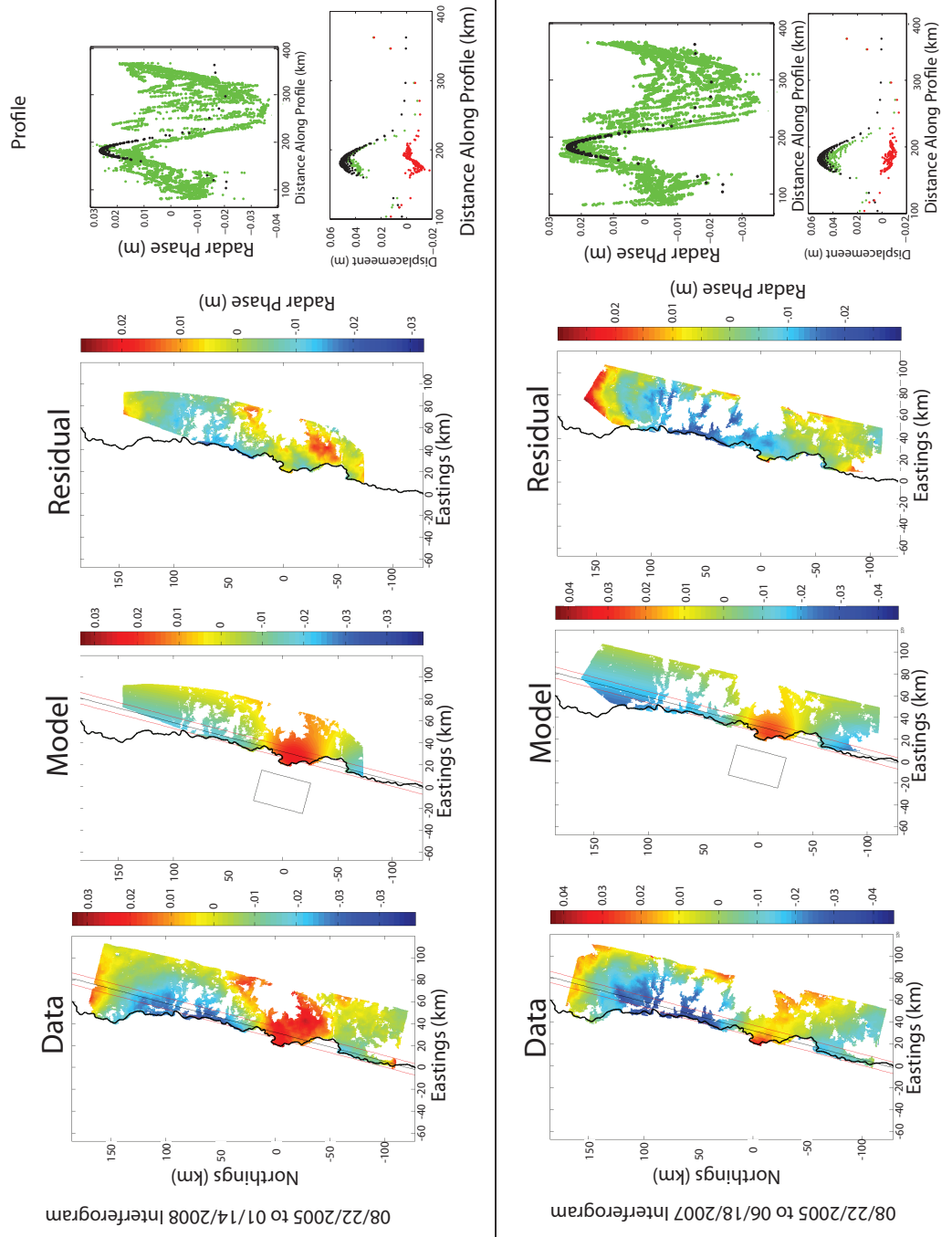


Figure 1.8: Comparison between full resolution data and best fit inverse model after using *a priori* information for the 2006 Copiapo Swarm. All profiles are taken from the same swath profile as shown in the data and residual columns, with the first profile in each case representing all the data and model points and the second profile showing just the resampled data and model points. Model and Residual interferograms are based on linear interpolation of the resampled interferograms onto the full resolution interferogram.

Figure 1.8 (continued)



from the Neighborhood Algorithm inversion and comparisons to seismicity are shown in Figure 1.9 and comparison of data and forward models of deformation are shown in Figure 1.10.

### **Central Chile, July 1997-September 1998 Sequence**

This sequence began in July 6, 1997 with a thrust event with  $M_w=6.7$  and was followed almost a month later by a swarm of over 30 earthquakes with a maximum magnitude of  $M_w=6.3$ . The swarm occurred immediately south of but separate from the initial July 6 earthquake and the large events were relocated by Lemoine et al. [2001] and found to occur on or near the megathrust, here at 15 to 20 km depth. Figure 1.11 shows this entire sequence of earthquakes and 1.12 shows the first earthquake and the subsequent swarm only. The sequence shows a north to south progression of epicenters as indicated in Figure 1.13, indicating that stress transfer may be an important aspect of this sequence, and was studied by Lemoine et al. [2001] and Gardi et al. [2006] for various types of stress interaction within the sequence. The PDE catalog does not have enough resolution to differentiate between smooth propagation or discrete jumps in epicenters, or random scatter in epicentral errors. Lemoine et al. [2001] and Gardi et al. [2006] were primarily concerned with the 15 October 1997 Punitaqui event, which was an intraslab event with a slab push mechanism. Slab push mechanisms show a polarity opposite the regular thrust focal mechanisms and are interpreted to be in the subducting slab due to plate unbending and by definition is indicative of down-dip compression. Slab push mechanisms are relatively rare in this region, especially one of this magnitude. Both studies concluded that the Coulomb stress change due to the amount of slip corresponding to the

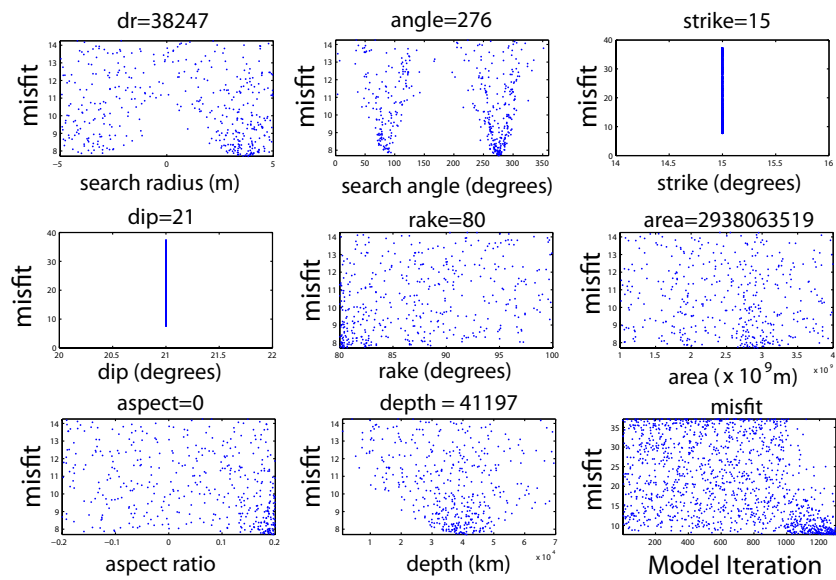


Figure 1.9: Results from the Neighborhood Algorithm for the 2006 Copiapo Swarm when *a priori* information is not used. Each panel represents the residual between data and model as a function of the different model parameters explored.

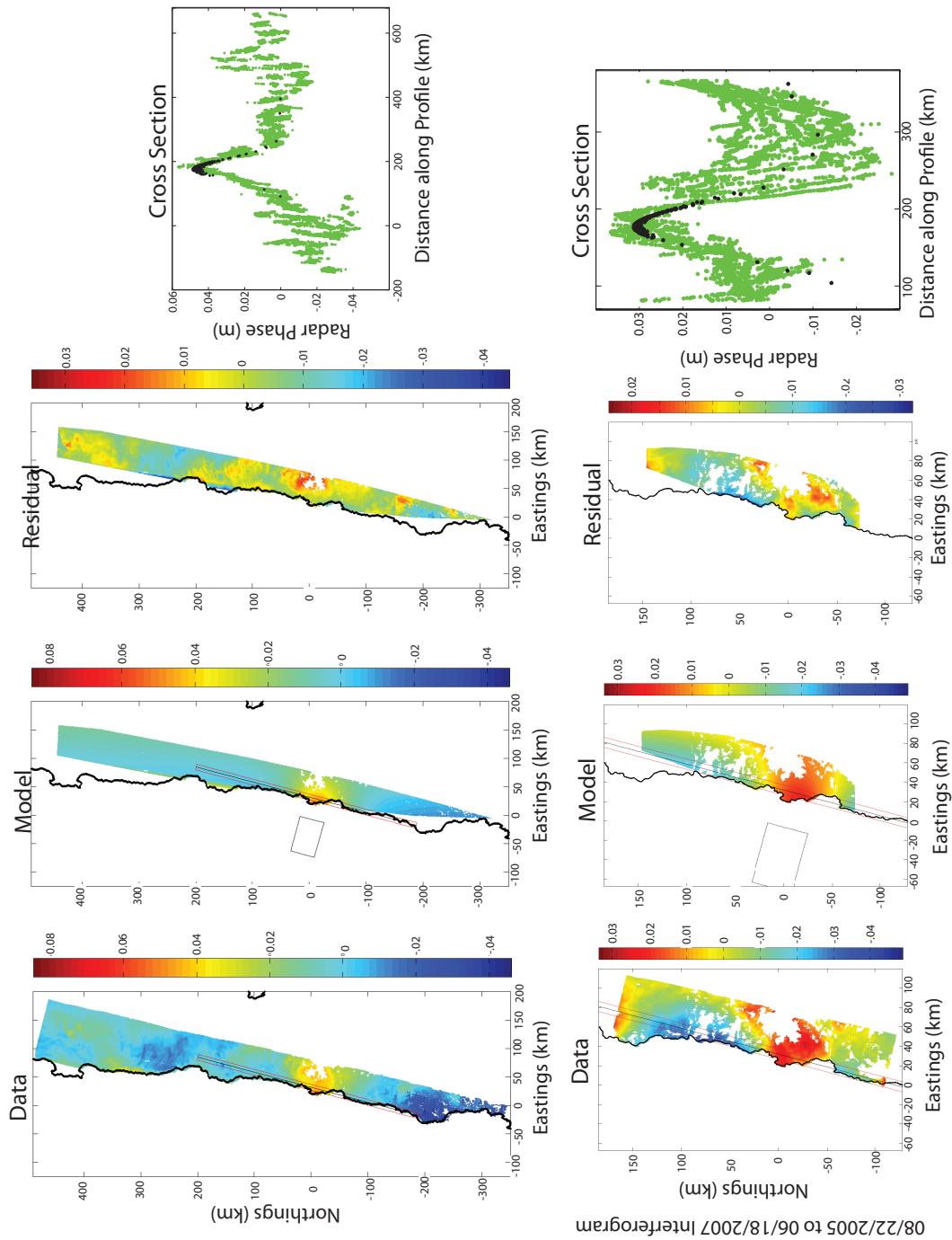


Figure 1.10: Comparison between full resolution data and best fit inverse model for the 2006 Copiapo Swarm. Moment magnitude is  $M_w=7.22$  for this model, more than 3 times greater than the seismically constrained moment.

magnitudes of the July earthquakes was insufficient (hundredths of a bar) to trigger the slab push earthquake.

Figure 1.12 shows that the swarm displays north to south propagation, with the initiation of the swarm closest to the initial July 6 event. All earthquakes are within the rupture region of the Mw=7.9 Illapel earthquake of April 1943 as defined by aftershock sequences, which was a shallow thrust event which ruptured ~100 km of the margin centered at 30°S and displayed relatively low rupture complexity [Beck et al., 1998]. Low rupture complexity may indicate that the fault did not have significant stress or frictional heterogeneity at the time of rupture. If the Punitaqui swarm signifies an area that exhibits stress or frictional heterogeneity, as the occurrence of swarm-like behavior may require, this could indicate stress variations within the earthquake cycle. An additional swarm may have occurred in 2001 in the same region (Figure 1.3.1), but seismicity is very much elevated after the 1997-1998 sequence and so is difficult to distinguish visually. Determination of changes in seismicity rates will require modeling beyond the scope of this thesis, such as comparing seismicity patterns with predicted ETAS models [e.g., Ogata, 2007].

### **Southern Peru and Ticsani Volcano, 2005**

Figure 1.14 shows a swarm that occurred near Ticsani Volcano and Laguna Vis-cacha in the middle of 2005. The swarm begins between the Ticsani and Vis-cacha and experiences a burst of seismicity a couple of months later beneath Ticsani (Edmundo Norabuena, personal communication, 2005). The relationship between the burst of seismicity beneath Ticsani Volcano and the swarm was examined by González et al. [2006] and will be examined in depth here.

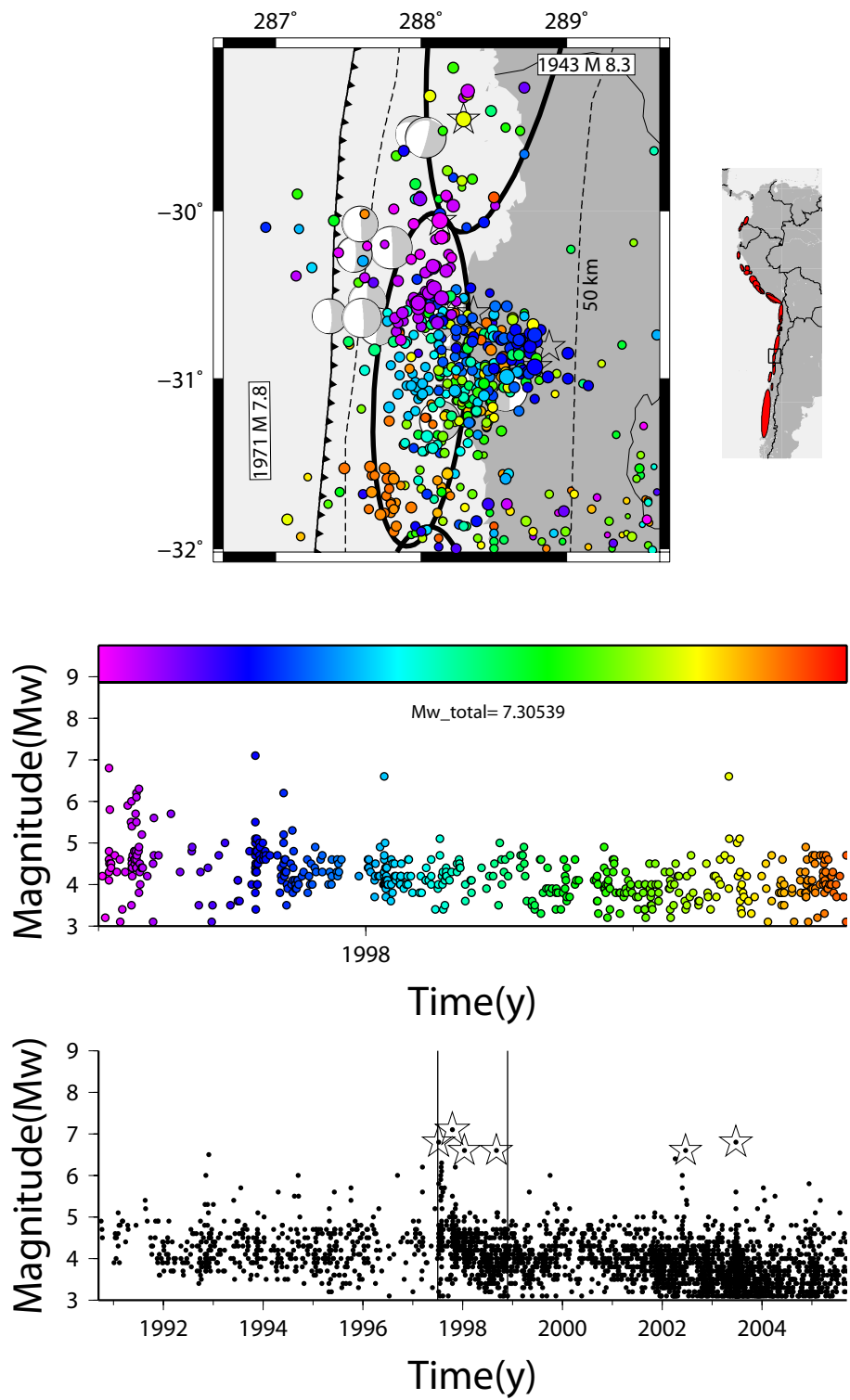


Figure 1.11: 1997-1998 Punitaqui Earthquake Sequence.

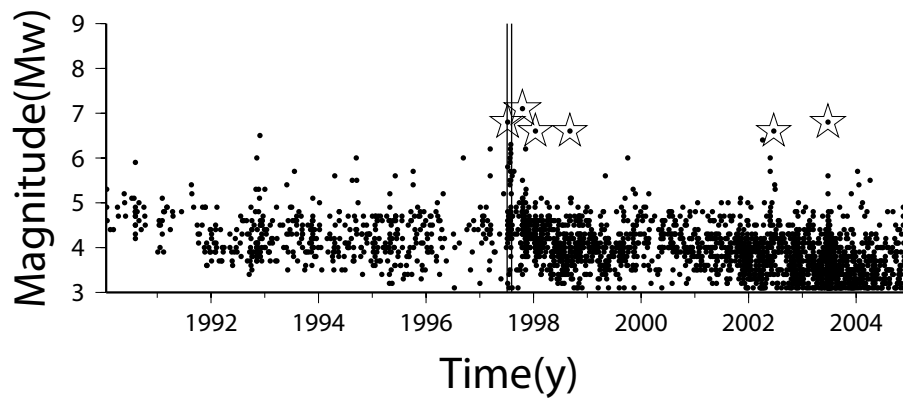
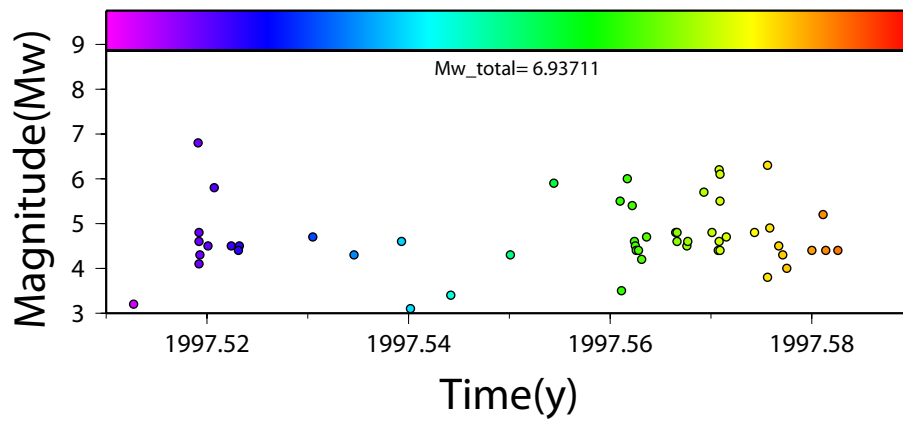
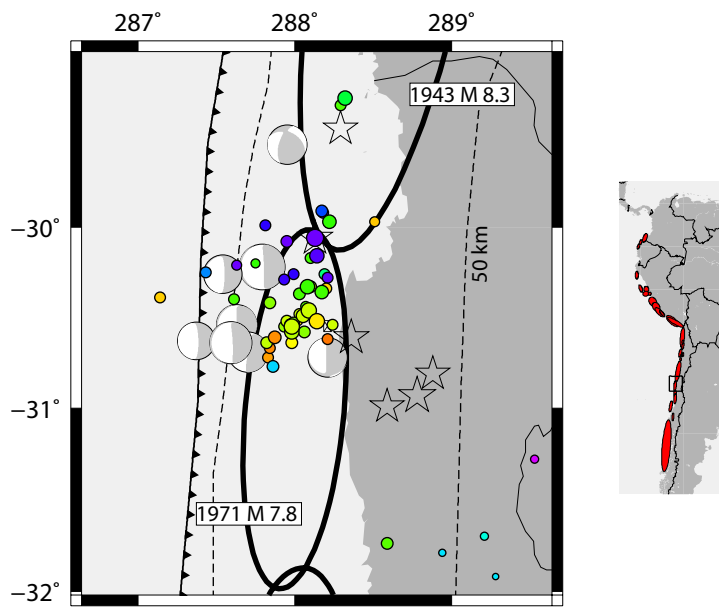


Figure 1.12: Close up of the 1997 Punitaqui Earthquake Swarm.

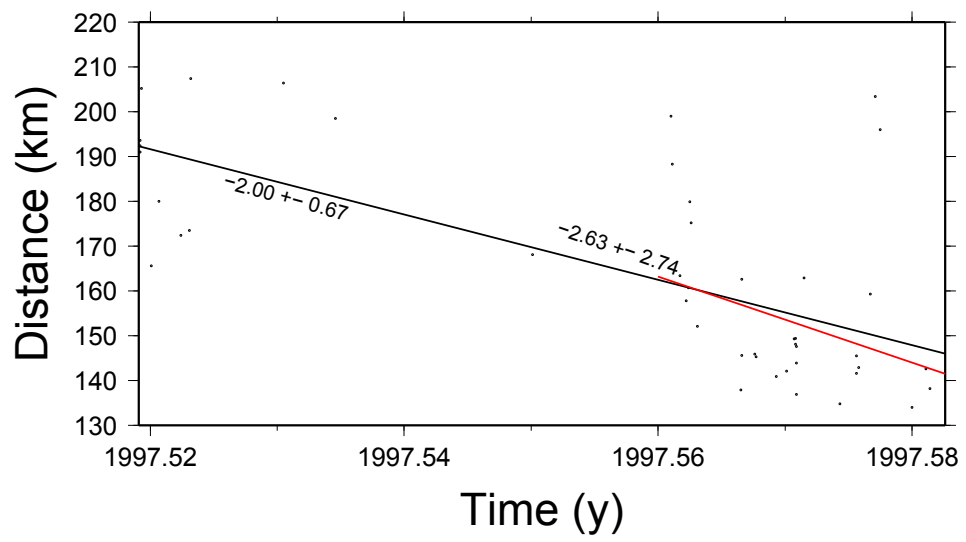


Figure 1.13: Earthquake epicenter propagation for the 1997 Punitaqui swarm.

This swarm highlights possible interaction between different sources in that there appears to be two different types of clustering activity in adjacent regions: the southeastern cluster spans the whole 3 months and is more uniformly distributed in time (Figure 1.14, purple to green events) while the northwest cluster appears as a sudden burst that begins and ends in a short time span (Figure 1.14, yellow events).

Ticsani lies on the Andean plateau in Southern Peru where the altitude and climate of the plateau are conducive to maintaining radar coherence over long time spans. The volcanic regions of the Andes are also extensively sampled by SAR, so there are several different InSAR pairs that document the deformation associated with this swarm. Figure 1.15, compiled by Matt Pritchard, shows 7 interferograms spanning times that do not contain the swarm (panels a-g) and 3 interferograms from times that do contain the swarms (panels h-j). The interferograms appear to contain 3 deformation sources, most clearly visible in panel h. The southeastern source beneath Laguna Viscacha first appeared in interferograms that spanned January of 2003 to March of 2004, well before the seismic swarm took place. No anomalous seismicity exists in the global catalogs during this approximate location and time. The other two sources (in the center and northwest corner of 1.15, panel h) are most likely associated with the swarm activity, although the relationship between the deformation signal and the earthquake times are impossible to tell from these interferograms because of the sampling times.

The source closest to Ticsani Volcano shows two prominent lobes of deformation usually indicative of a double-couple source mechanism (Figure 1.15, panels h-j). This deformation signal is focused on when resampling the three

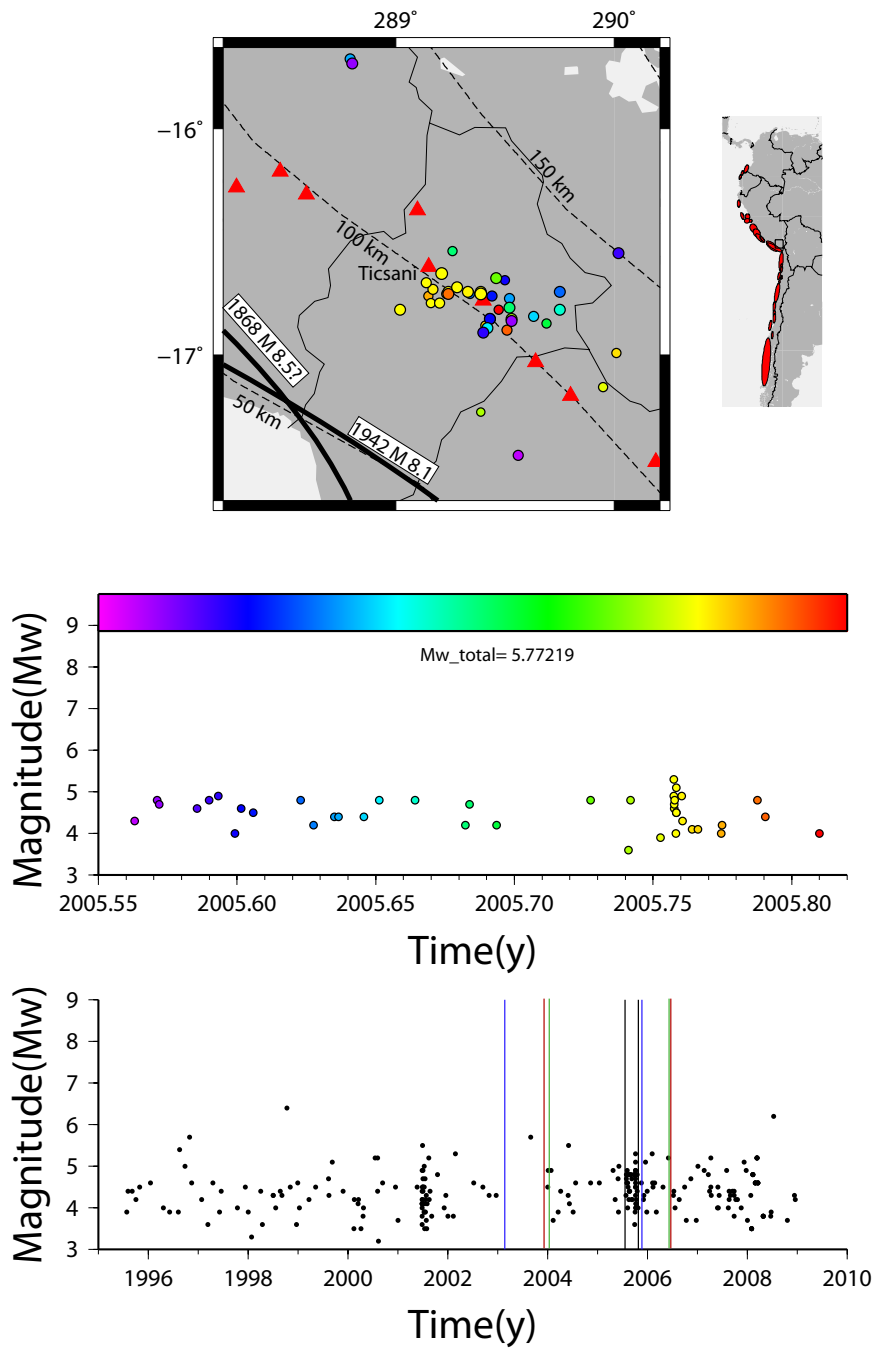


Figure 1.14: The 2005 Ticsani Earthquake Swarm. InSAR associated with the swarm is discussed in the text, and colored vertical lines in the bottom panel will show the acquisition dates, with similar colors representing independent interferograms made.

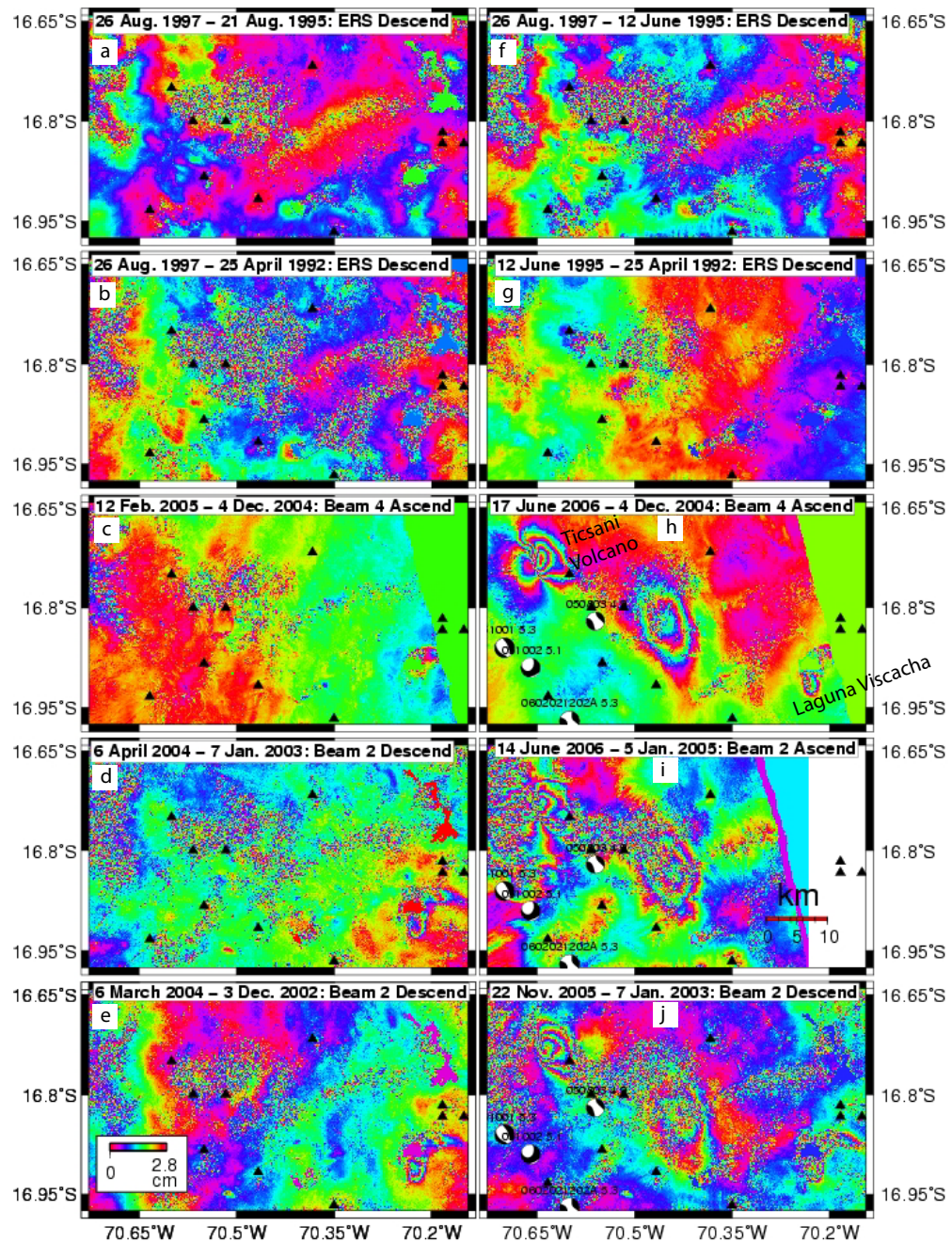


Figure 1.15: Interferograms of the 2005 Ticsani Earthquake Swarm. The first 7 interferograms show no deformation at or near Ticsani but some do show deformation near Laguna Viscacha by at least March 2004.

interferograms that show the signal and inverted with the Neighborhood Algorithm. This deformation signal is sampled by three different Envisat tracks: track 318 beam mode 2, track 411 beam mode 2, and track 361 beam mode 4. Envisat beam modes represent different incidence angles only. It is sampled by two descending tracks and one ascending tracks, so the one dimensional sampling issues encountered for the Copiapo swarms are not encountered during this inversion. Because it was well sampled with multiple tracks and look angles and the entire deformation pattern (both lobes of deformation) is resolved, the inversion was allowed to effectively explore all parameter space at once. The results from the Neighborhood Algorithm are shown in Figure 1.16 with comparisons of data and models given in Figure 1.17. The inversion arrived at a  $M_w=5.7$  event, not significantly greater than the seismic moment suggests, while giving an excellent fit to the InSAR data. This suggests that no additional aseismic moment was released along with this swarm activity.

### **Topocalma Knoll and Subduction of the Juan Fernandez Ridge**

Subduction of the Juan Fernandez Ridge near  $32.5^\circ\text{S}$  (Figure 1.3.1) provides a boundary for subduction angle (flat slab subduction to the north) and sedimentation input to the trench (low input to the north) [vonHuene et al., 1997]. However, it does not appear to be a definitive boundary to earthquake rupture propagation, as the 1730 rupture extended to both sides of this region by hundreds of kilometers [Kelleher, 1972; Comte et al., 1986]. At  $\sim 32.4^\circ\text{S}$  between the trench and the coast, the Papudo seamount has been subducted and is associated with a bathymetric high. The subducted Topocalma Knoll offshore of Valparaiso at  $\sim 33.1^\circ\text{S}$  and the tectonically controlled San Antonio Canyon represent the south-

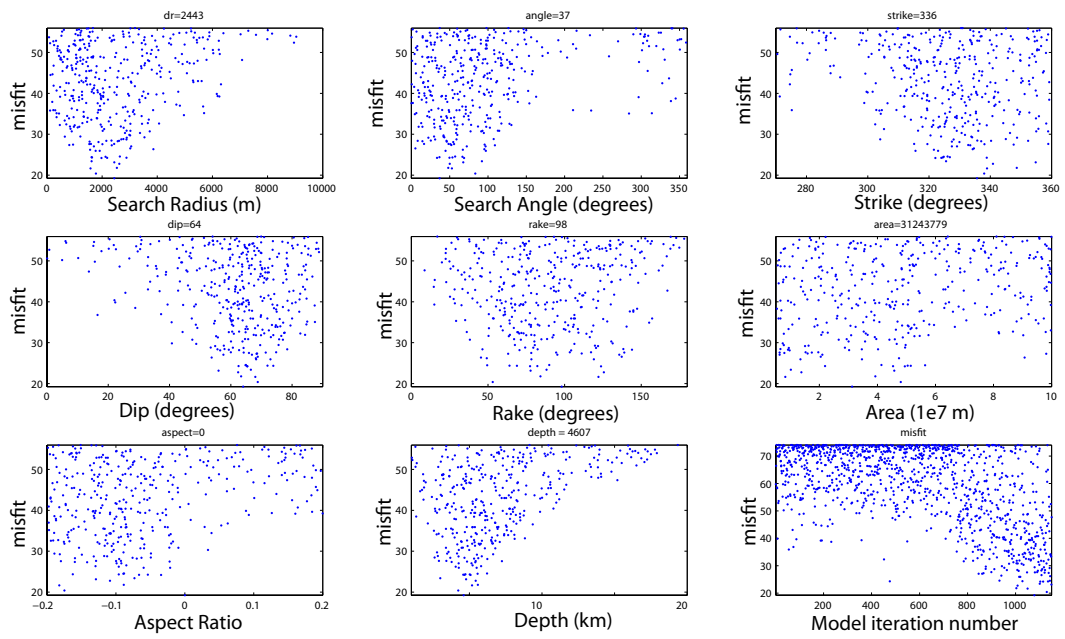


Figure 1.16: Neighborhood algorithm results for the Ticsani Swarm shown in Figure 1.14

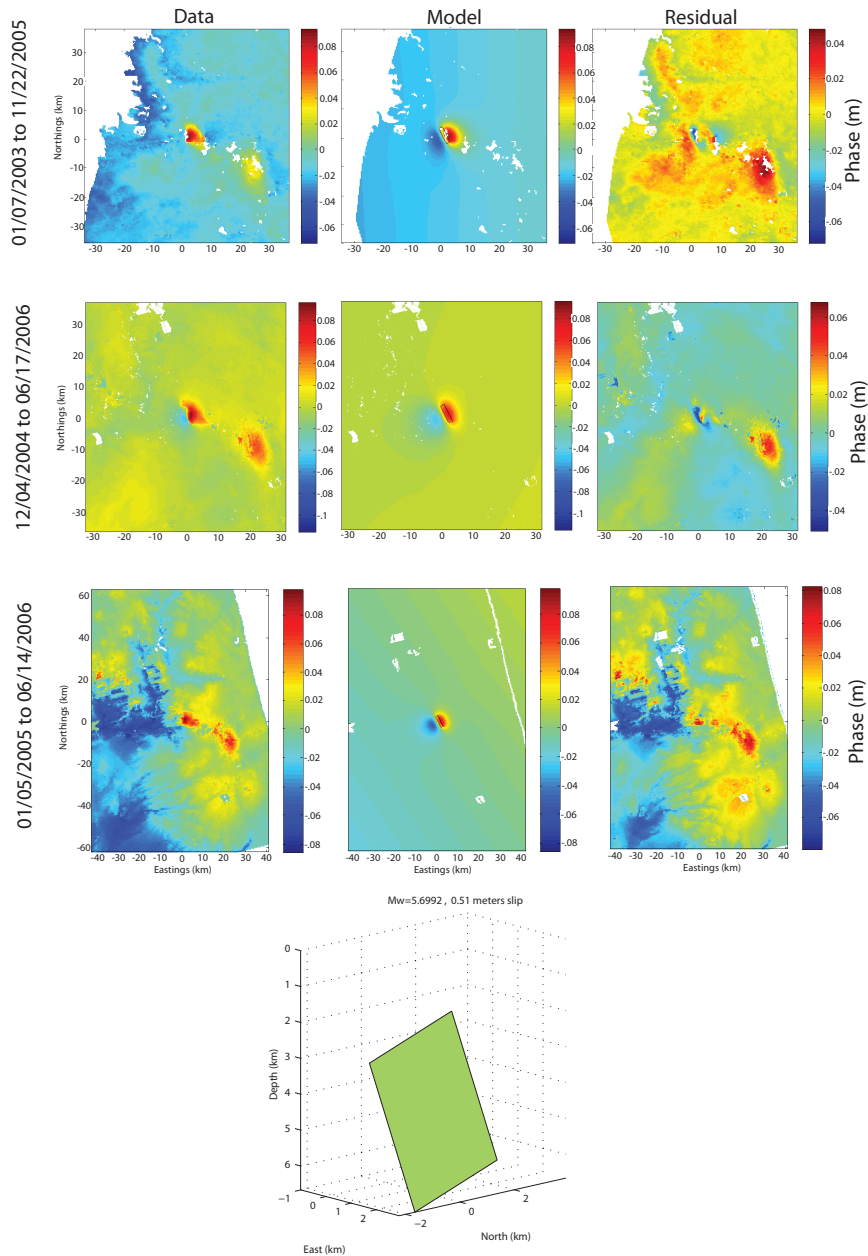


Figure 1.17: Inverse model of the 2005 Ticsani Earthquake Swarm. Red is an increase in LOS displacement or subsidence, blue is uplift. The subsidence-only pattern to the southeast is effectively removed during resampling of the deformation field so is not modeled or removed.

ernmost part of this transitional zone. This is a seismically active area with seismicity located on the plate interface and throughout the overriding plate above it.

A great subduction earthquake ( $M_w=8.0$ ) occurred on March 3, 1985 in this region, dubbed the Valparaiso earthquake. Comte et al. [1986] document intense foreshock activity in the region of the epicenter, and this activity appears to be swarm-like. Foreshock swarms are not uncommon and have been studied extensively in California [e.g., Jones, 1994], New Zealand [Evison and Rhoades, 1993] and documented elsewhere [Zobin and Ivanova, 1994]. The foreshock swarm and aftershocks of the 1985 earthquake are shown in Figure 1.18.

Thierer et al. [2005] document a shallow swarm in October of 2001 in the vicinity of the San Antonio canyon and above the plate interface where the Topocalma Knoll has subducted at near 20 km depth. More than 30 events were recorded by an array of ocean bottom seismometers (OBS), 10 of which were reported to have magnitudes of  $M_L=4.0$  or greater. The main burst lasted only one day but seismicity remained elevated immediately following the swarm [Thierer et al., 2005]. The swarm search presented in this thesis locates this swarm despite having only 10 earthquakes recorded by the global catalog. A similar but significantly more energetic swarm occurred in this region in 1999, and this swarm is shown in Figure 1.19. In addition to the 1999 and 2001 swarm, this search documents six other swarms in the Juan Fernandez-Topocalma region. These other swarms are similar to the documented 2001 swarms in their duration and maximum magnitudes. Swarms in the Topocalma Knoll region appear to occur regularly as six of the seven swarms from 1973 to 2009 occurred in this region, which is near the epicenter of the 1985 earthquake.

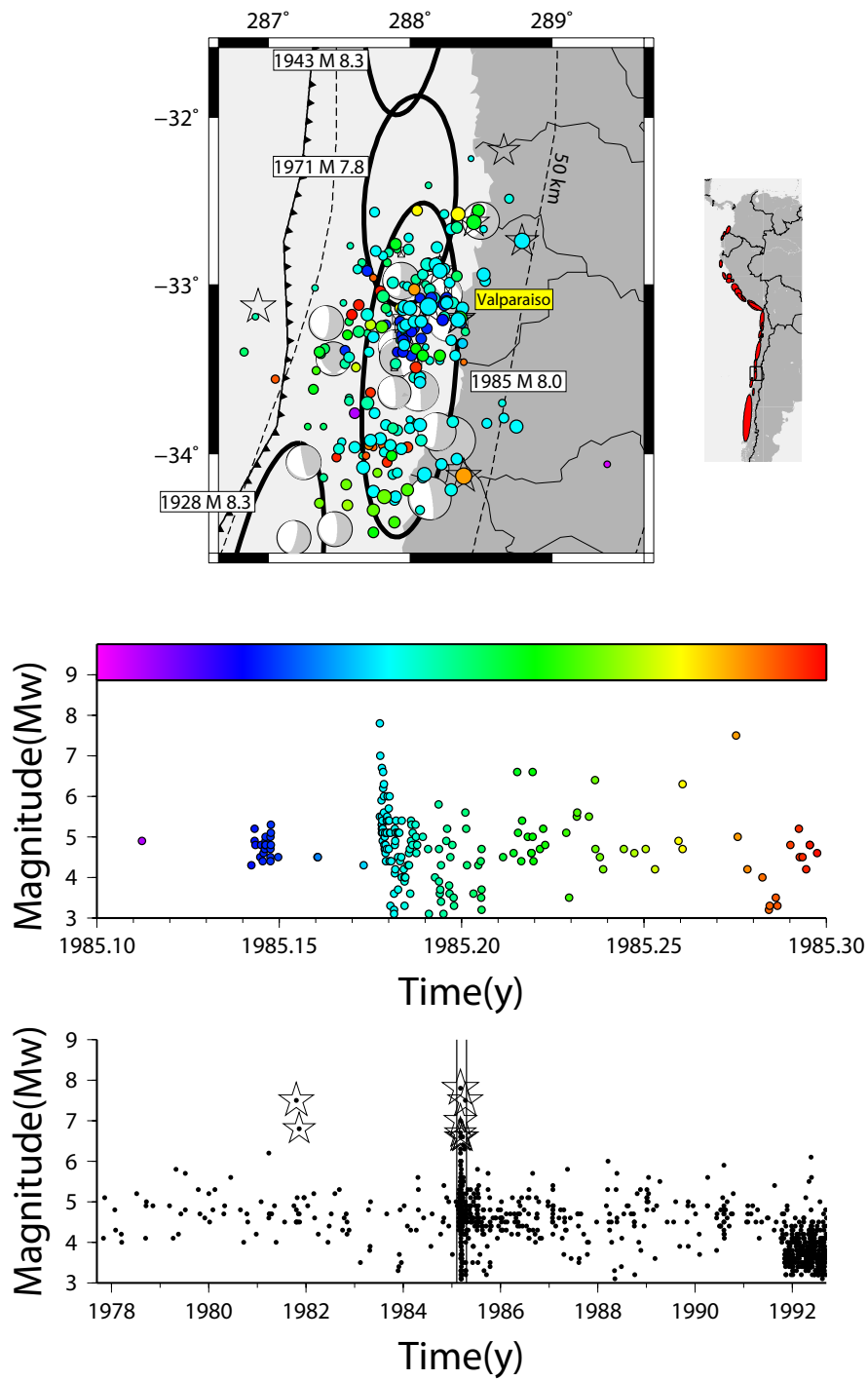


Figure 1.18: 1985 Valparaiso earthquake sequence showing a pre-shock swarm in the vicinity of the mainshock epicenter.

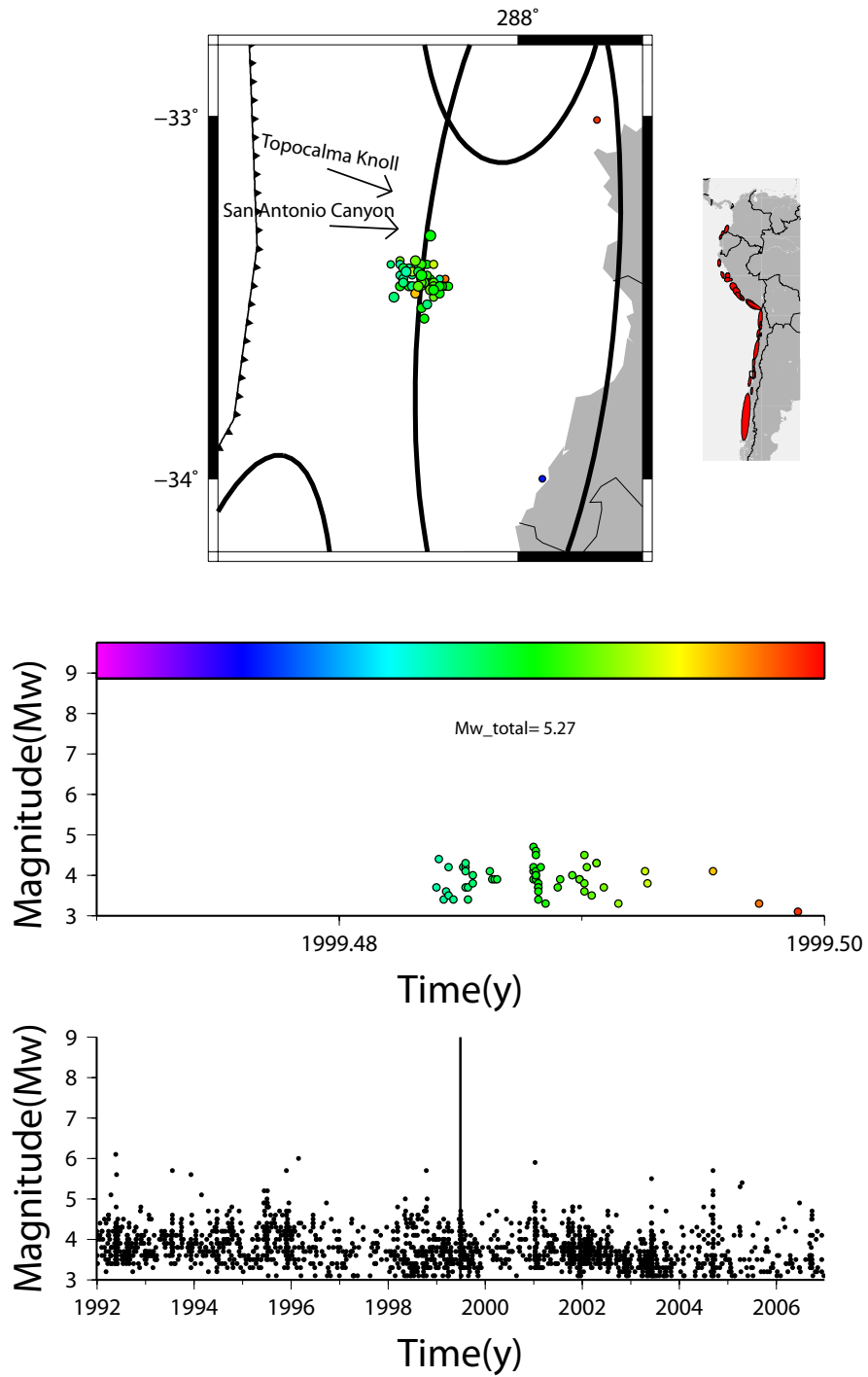


Figure 1.19: This 2001 earthquake swarm at the Topocalma Knoll is similar to the 5 other ones documented in Table 1.1

The other swarm in the region occurred in the vicinity of the subducted Papudo seamount in July of 2003, and is shown in Figure 1.20. The Papudo seamount and Topocalma Knoll are both correlated with positive magnetic anomalies, indicating emplacement by the Juan Fernandez Ridge hot spot [Yanez et al., 2001], ~700 km off the coast of Chile. This swarm was close in time to another cluster of earthquakes to the south, which appears to be a mainshock/aftershock sequence. The mainshock/aftershock sequence, despite releasing over four times as much moment as the Papudo swarm, shows a slightly smaller area of aftershocks. This is indicative of a smaller stress drop during the earthquake swarm. To the south of this region, at ~34°S, a small swarm occurred in mid-2005 and is shown in Figure 1.21. Whether or not this swarm is in some way connected to the subduction of the Juan Fernandez Ridge is unclear.

Multichannel seismic reflection data acquired and presented by Yanez et al. [2001] suggest that the Topocalma Knoll was formed by uplift of a continental crustal block in response to seamount subduction. Laursen and Normark [2002] go further and say the Topocalma Knoll records the location of the subducted San Antonio seamount. They suggest compressional deformation associated with subduction of the Juan Fernandez Ridge seamounts helped form the Valparaiso basin with the formation of trench-ward verging thrusts in the overriding plate above seamounts. Additionally, high pore fluid pressure along the plate interface associated with subducting sediments has been inferred in the region [e.g., Kirby, 2000; Laursen and Normark, 2002], and this fluid pressure may cause hydrofracturing of the base of the overriding plate. A combination of high amounts of fluids and a hydrofractured and heavily faulted overriding plate may provide conditions conducive to generating earthquake swarms (e.g. fluids and fault or stress heterogeneity).

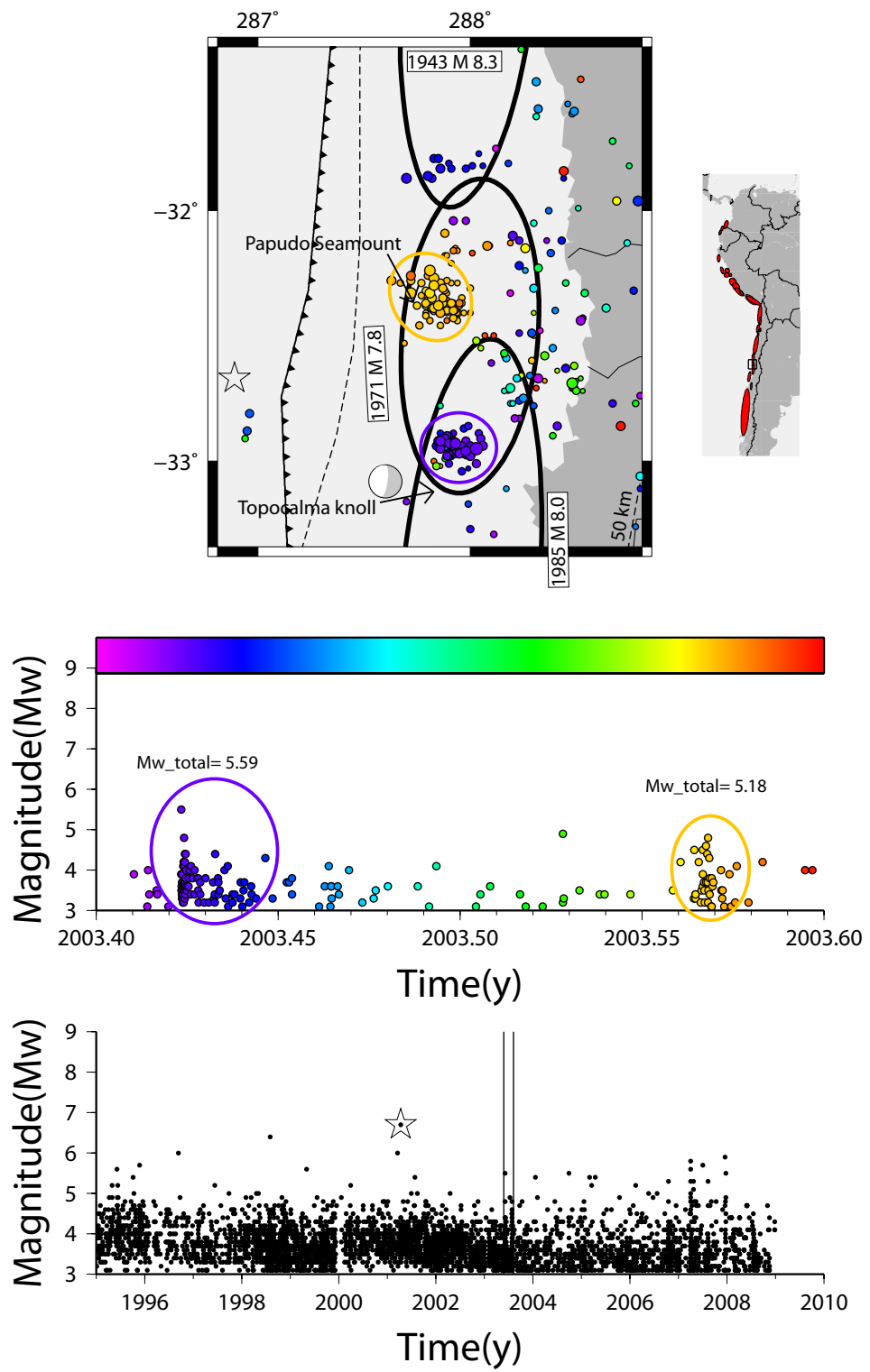


Figure 1.20: The 2003 Papudo Seamount Earthquake Swarm.

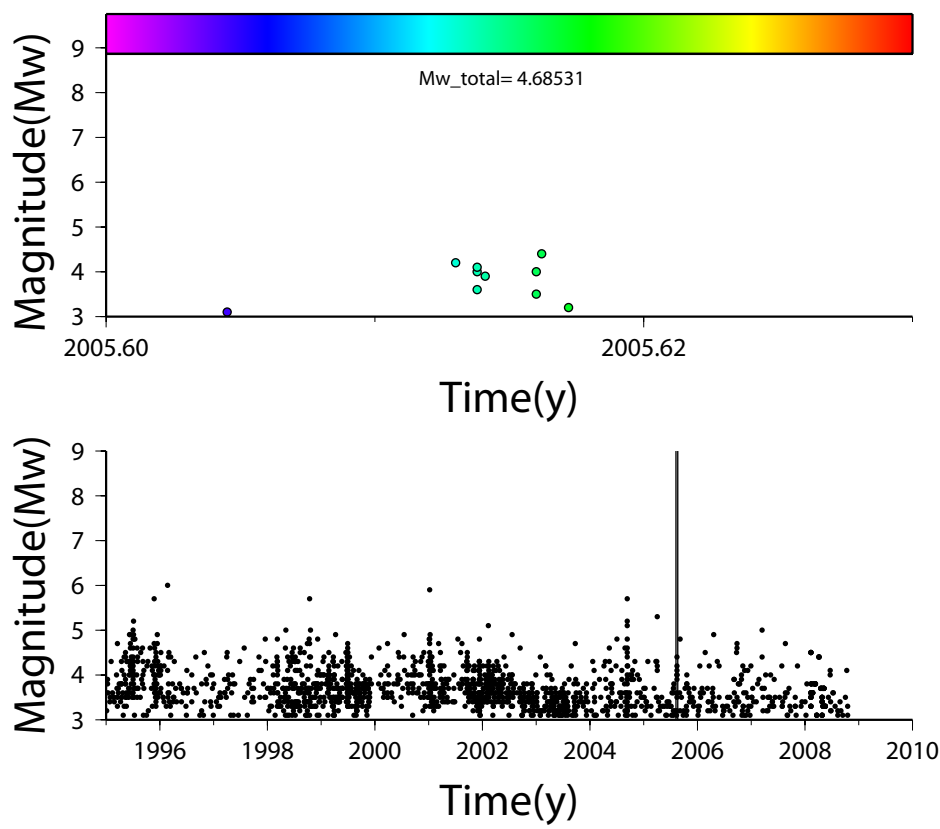
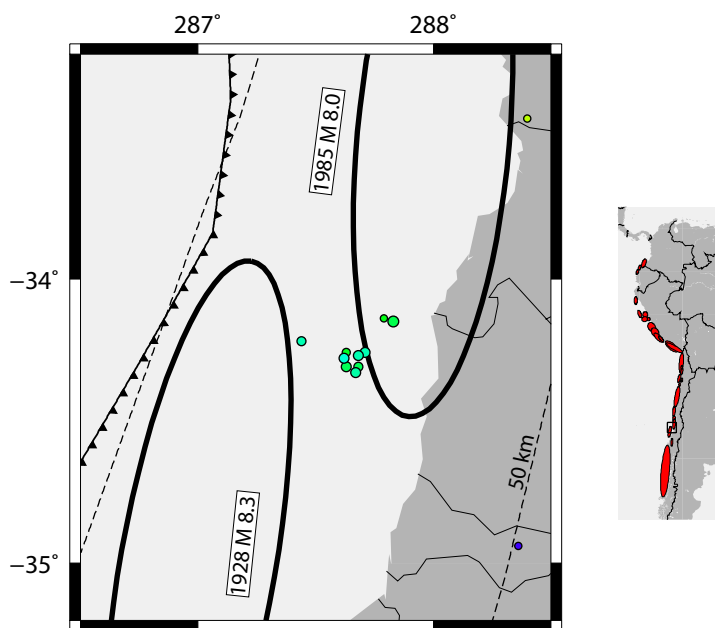


Figure 1.21: 2005 Earthquake Swarm at ~34°S.

## **Puerto Aysen Swarms (45-46°S)**

At 46°S, the Chile Rise active spreading center is subducting beneath South America (Figure 1.3.1). Oblique subduction and the indenting force of the ridge is the suspected cause of strain partitioning accommodated by the Liquine-Ofqui Fault Zone (LOFZ), a dextral intra-arc system that strikes parallel to the trench.

In January 2007, an earthquake swarm began near the Aysen Fjord at ~45.3°S and near the LOFZ. This swarm was recorded by a temporary network of 60 seismometers in the region deployed by the Universidad de Chile and the University of Florida [Mora et al., 2008; Barrientos et al., 2007]. Mora et al. [2008] report over 6000 earthquakes associated with the swarm, and deformation associated with this swarm was examined by Fukushima [2007]. The swarm search conducted for this thesis successfully identified this swarm. 15 earthquakes in the swarm were large enough to be identified by the NEIC (PDE), but this far surpasses the background seismicity average of much less than one per year. The swarm is shown in Figure 1.22. Three earthquakes have focal mechanisms obtained from the global centroid moment tensor (CMT) project. The first shows a slightly oblique strike slip mechanism while the last two show an additional component of opening. Focal mechanisms with sizable isotropic components are often attributed to volcanic sources, such as deflation of a magma dike.

The origin of the 2007 Aysen swarm (tectonic, magmatic, or both) will be difficult to discern as the LOFZ dissects the Andean magmatic arc. However, our search documented an earlier swarm in 1991 from August 8 to September 7. This swarm contained 14 earthquakes and is shown in Figure 1.23. This swarm is directly related to the eruption of Cerro Hudson Volcano. The eruption be-

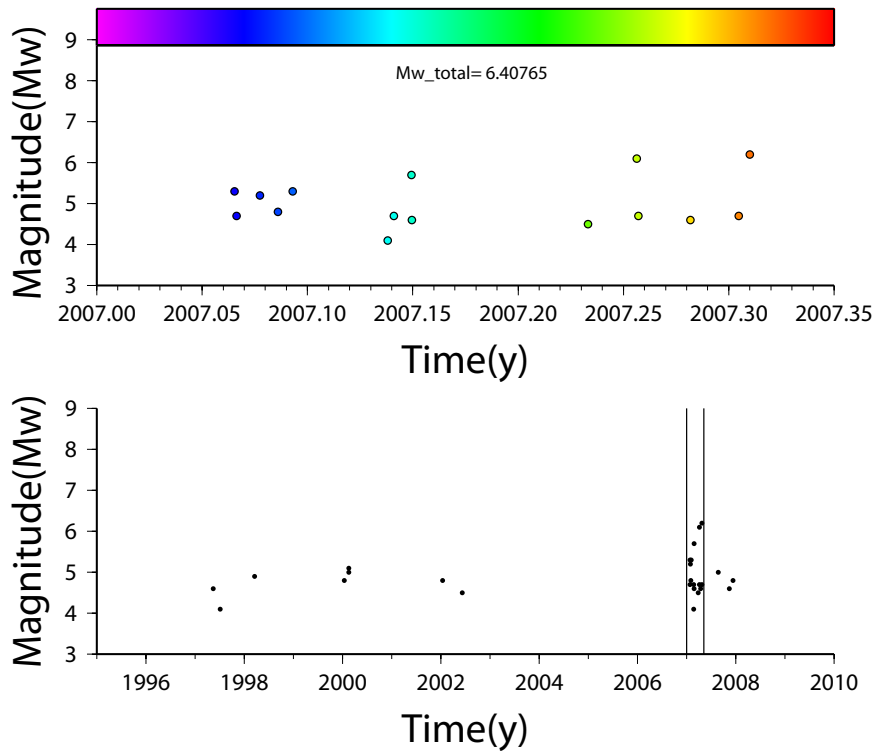
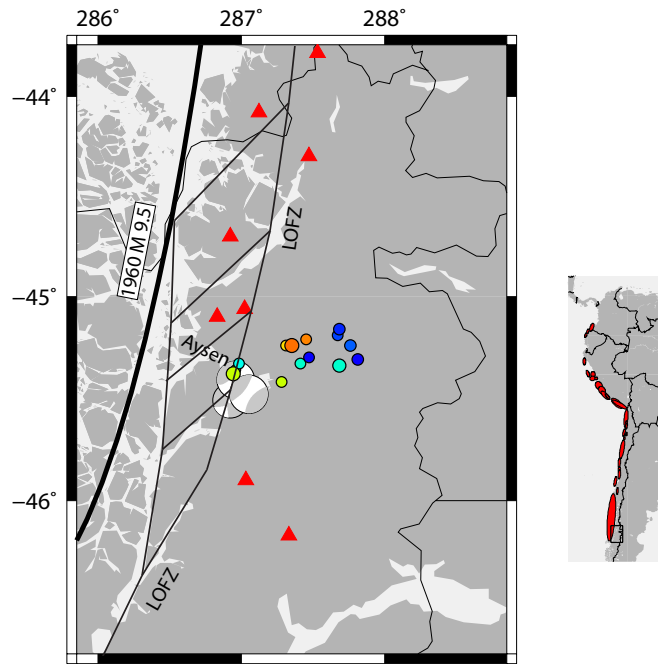


Figure 1.22: 2007 Swarm near the Aysen Fjord in Southern Chile.

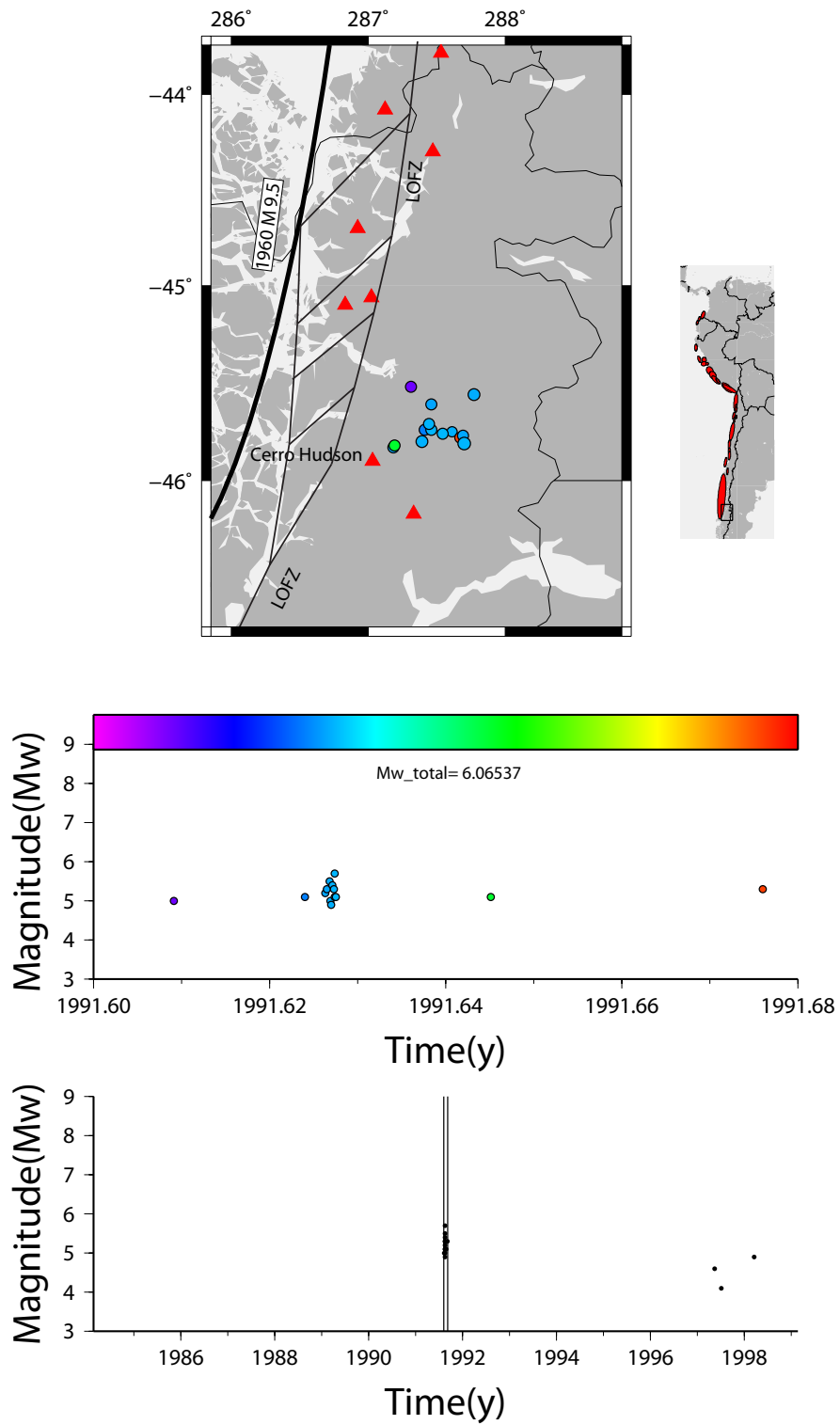


Figure 1.23: 1991 Swarm near the Hudson Volcano in Southern Chile.

gan on August 8 with a basaltic flow and intensified from August 12-15 with an andesitic eruption [Naranjo and Stern, 1998; Venzke et al., 2002]. A seismic station 50 km away recorded a couple hundred earthquakes, but was just a single station so no locations were obtained. In addition to these two swarms, three events were detected at virtually the same location as the 1991 swarm in Jan-Feb 2000 (magnitudes 4.8, 5.1, and 5.0) but three events are too few to confidently suggest swarm activity.

### **Chaiten eruption, 2008 (~43 S)**

The first eruption of Chaiten volcano in almost 10,000 years occurred in April 2008. This eruption was accompanied by seismic activity recorded at nearby stations STAB and PUMA [Venzke et al., 2002; Lara et al., 2008]. Thousands of small volcano-tectonic (VT) and long period (LP) earthquakes were recorded beneath Chaiten volcano, but seismicity was also present on the Liquine-Ofqui Fault Zone. The relation between the earthquakes on the LOFZ and the eruption remains unclear. Seismicity recorded by the NEIC is shown in Figure 1.24.

Seismicity in the early part of the time window in Figure 1.24 reflects seismicity near or beneath Chaiten volcano. Less than a month later, approximately 100 km to the north, a second series of seismicity occurred along the LOFZ. The northern cluster is near Hornopirén volcano, but global catalogs are not precise enough to show the relationship between seismicity and the volcano (Andres Pavez, personal communication). Lange et al. [2008] deployed a temporary seismic network in 2004-5 along the LOFZ from 41.5°-43.5°S. They describe four clusters of crustal earthquakes along the LOFZ, two of which are near the small town of Hornopirén 20 km from Hornopirén Volcano and below Chaiten Vol-

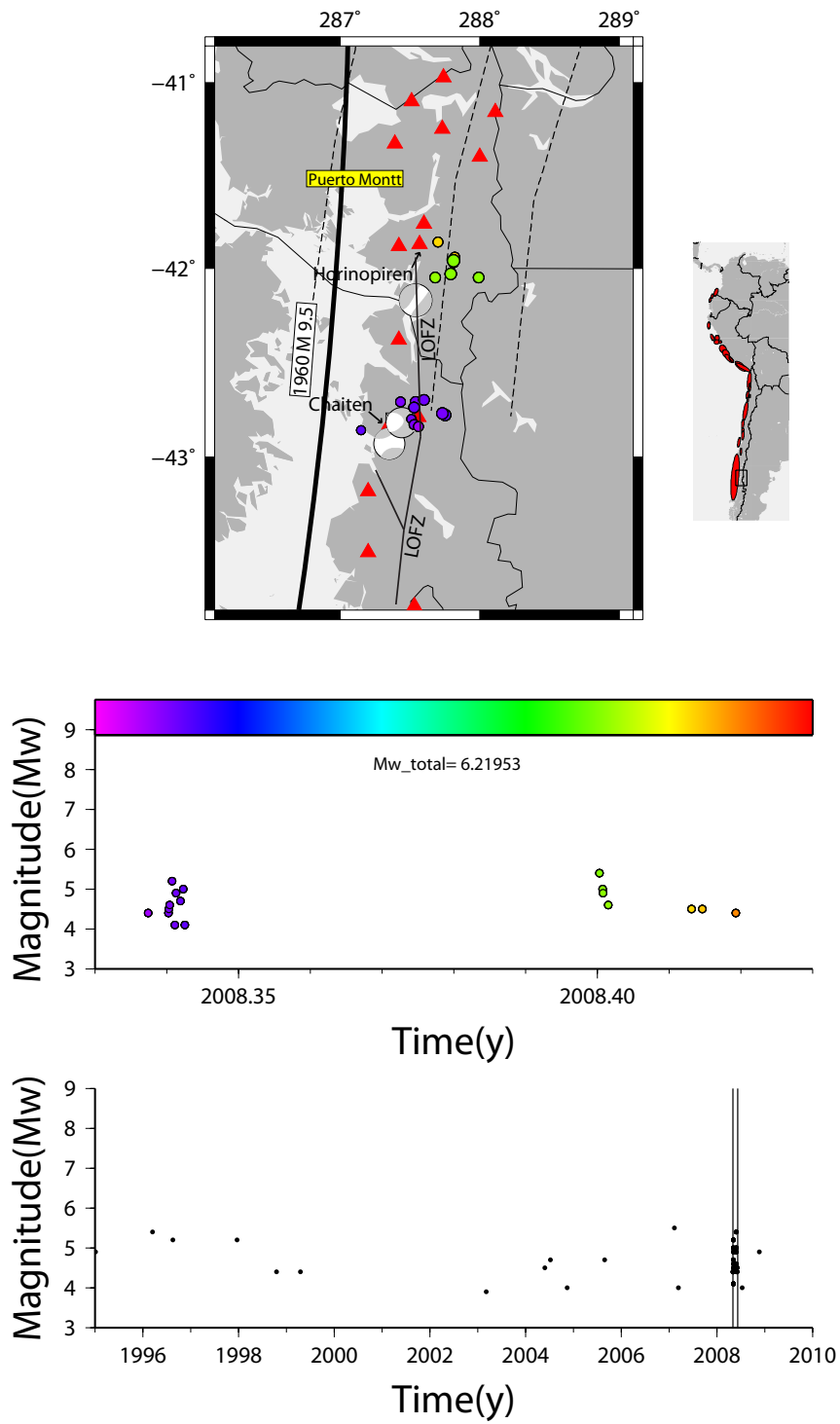


Figure 1.24: 2008 Earthquake Swarm concurrent with the first volcanic eruption at Chaiten Volcano in 10,000 years.

cano. The article was published online 11 days before the Chaiten eruption, and since the deployment was 3 years before the eruption, seismicity was present at least that long prior to the eruption.

Fournier et al. [2009] examine interferograms of this swarm and conclude that geodetically required volume changes cannot account for the large volume of erupted material indicating complex interaction between volcanic and other (e.g. seismic, magma compressibility) deformation sources. Additional deformation sources, such as aseismic slip, could be present but separating volcanic from tectonic sources in such a complex system is difficult. The limiting factor in separating volcanic from tectonic sources is that no continuous deformation histories can be established. No continuous GPS exist in the region and SAR acquisitions were not made during the swarm, so a time series of deformation cannot be constructed.

Both clusters show CMT solutions that contain significant non-double couple components, and since the LOFZ slices through the volcanic arc a magmatic link between the two regions may be considered. Alternatively, an aseismic slip event could have been the cause of both swarms and the eruption. Such a slip event was inferred to occur in Alaska in 1996 when several volcanoes separated by hundreds of kilometers simultaneously either erupted or experienced swarm activity [McNutt and Marzocchi, 2004]. Any model to explain the seismicity should consider that both Hornopirén and Chaiten were seismically active with microearthquake activity from 2004-5 and that the Hornopirén region experienced elevated activity during the Chaiten eruption.

## 1.4.2 Newly Discovered Swarms

In addition to the 8 swarms documented in the literature, 30 additional swarms were found during the search presented in this thesis. The following sections describe these swarms individually. None of the newly discovered swarms had sufficient InSAR coverage for further analysis, motivating the need for denser temporal coverage of SAR acquisitions, particularly in vegetated areas. Newly discovered swarms described hereafter were probably recognized by local populations because most events were large enough to be felt. In cases where swarms occurred near volcanic regions, local populations may have even been alerted to the swarm activity (e.g., by the Sernageomin service of the Government of Chile).

### **Ecuador swarms at Carnegie Ridge intersection**

Historical seismicity for Ecuador shows there is a sizable seismic gap between about  $0^{\circ}$  and  $10^{\circ}\text{S}$  [Swenson and Beck, 1996]. This section of the margin accommodates a large convex bend in the trench and the subduction of the Carnegie Ridge, which records the Galapagos hot spot to the west, from about  $0^{\circ}$  to  $2.5^{\circ}\text{S}$ , both of which have been postulated to produce enough heterogeneity at the plate interface to prevent the propagation of large earthquake ruptures into or throughout the region. The margin north of the Carnegie Ridge has broken two times in the past 300 years, once in 1906 in a large magnitude 8.8 event and later in a  $M_w=7.9$  in 1942. The 1942 earthquake was the first in a series of three large earthquakes that re-ruptured the entire 1906 rupture area, but did so with only  $\sim 15\%$  of the moment release of the 1906 earthquake [Swenson and Beck, 1996].

At the intersection of the aseismic Carnegie Ridge, near the coastal city of Manta and the southern part of Manabi, two earthquake swarms have been found. The first occurred in 1977 and lasted about a month. The maximum magnitude associated with this is small, only  $M_w=5.1$ , and few events were recorded, but it appears to show north to south propagation as shown in Figure 1.25. The second swarm occurred in 2005 and is shown in Figure 1.26. This swarm was much more energetic with moment magnitudes up to 6.2 and the total sum of the moment was equivalent to a  $M_w=6.6$  earthquake. This swarm showed bilateral propagation of epicenters at rates of  $\sim 4.5$  to 10 km per day as shown in Figure 1.28, however the PDE catalog does not have enough resolution to tell if this propagation occurred smoothly or as discrete jumps. An additional potential swarm is shown in Figure 1.27 and occurs about a degree to the north in 1985, but contained only 5 earthquakes in the cluster.

The coast of Ecuador receives a substantially larger amount of rainfall than northern Chile and southern Peru, so InSAR coherence will degrade faster, particularly for the available C-band data. C-band radar systems (ERS, Envisat, Radarsat) operate at a radar wavelength of 5.6 cm. At this wavelength, radar cannot effectively penetrate through vegetation or the uppermost soil, so rainfall and vegetation growth tend to decorrelate the radar signal. Only one track in Ecuador has acquisition spanning the swarm, and we acquired and processed three scenes to test the coherence near the time of the swarm, with the timing of the acquisitions shown in Figure 1.26. Radar coherence associated with two processed interferograms are shown in Figure 1.29 and show that while some coherence is maintained over short time intervals, it is almost entirely lost over longer intervals. The only scenes spanning the swarm are over 1 year apart, so it does not appear that InSAR provides useful geodetic observations of this

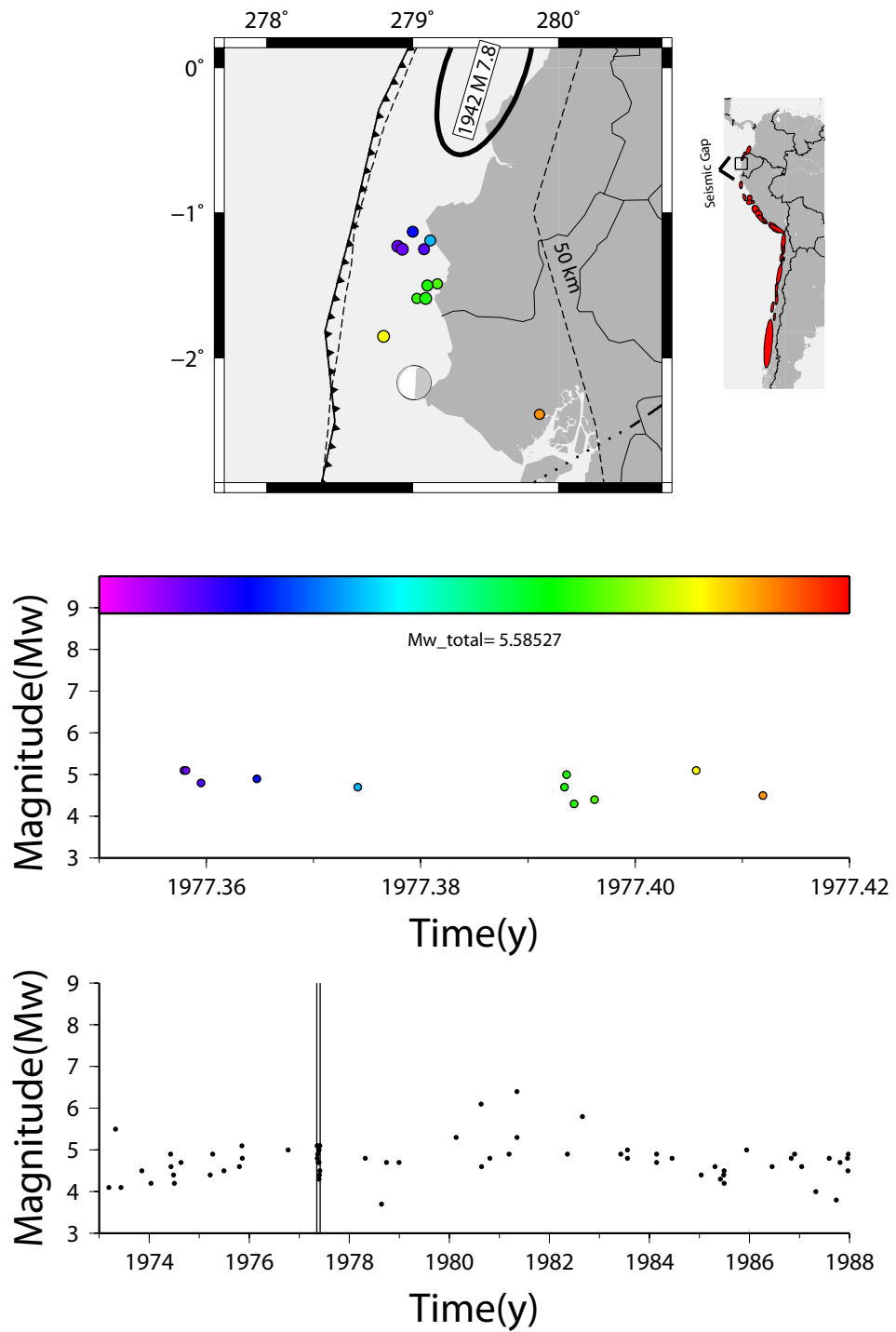


Figure 1.25: 1977 Earthquake Swarm in Southern Ecuador.

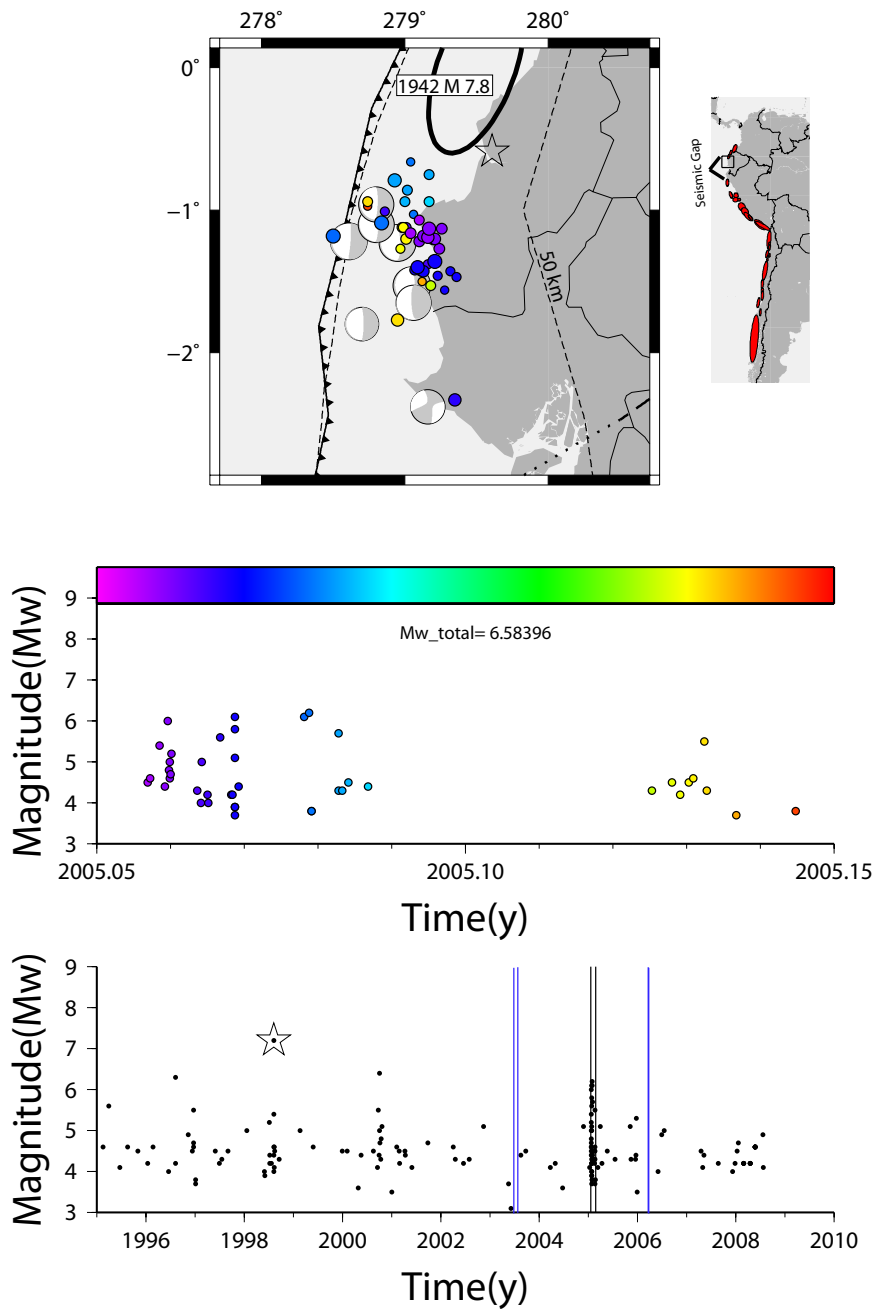


Figure 1.26: 2005 Earthquake Swarm in Southern Ecuador. InSAR associated with the swarm is discussed in the text, and colored vertical lines in the bottom panel will show the acquisition dates, with similar colors representing independent interferograms made.

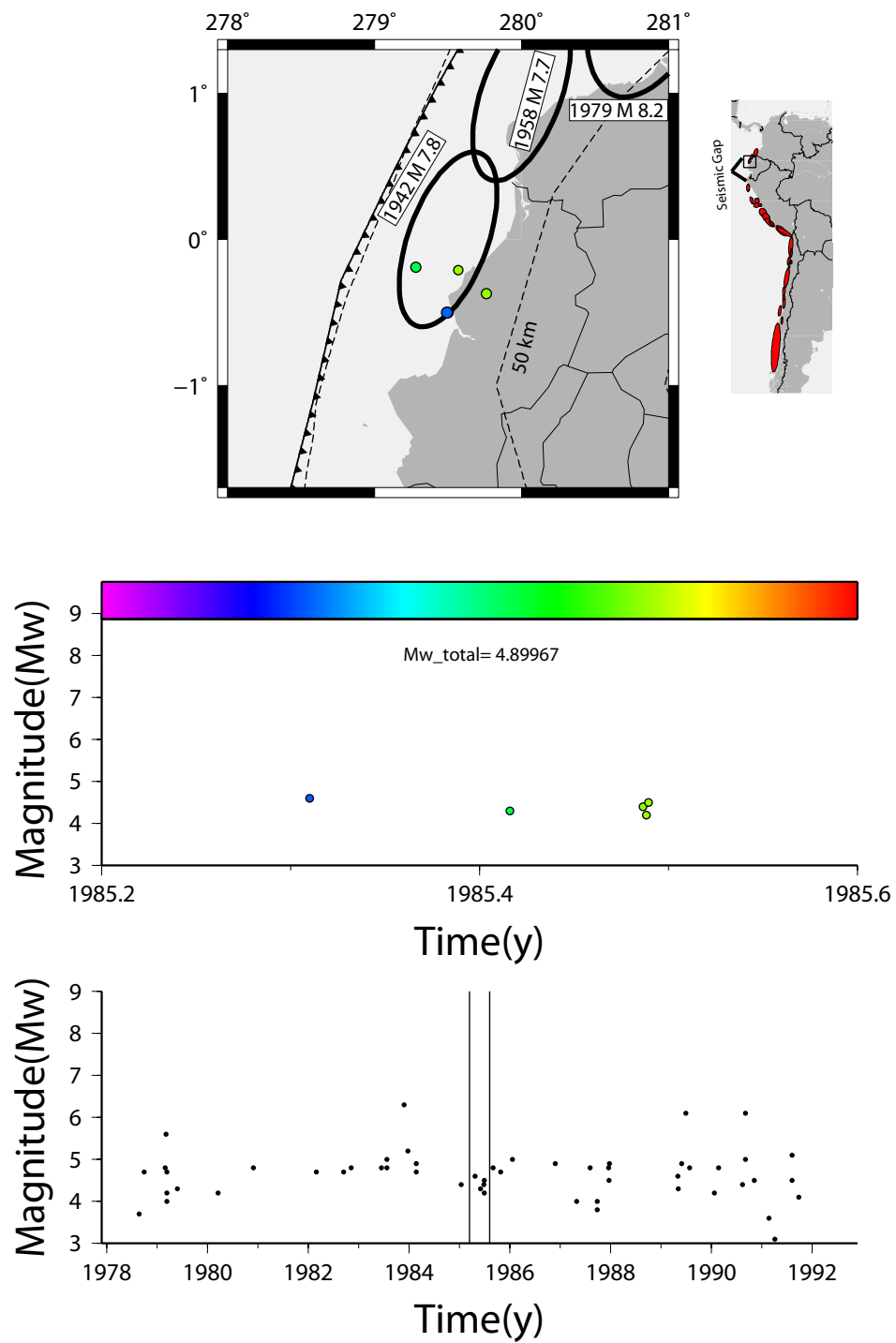


Figure 1.27: Possible 1985 Earthquake Swarm in Southern Ecuador.

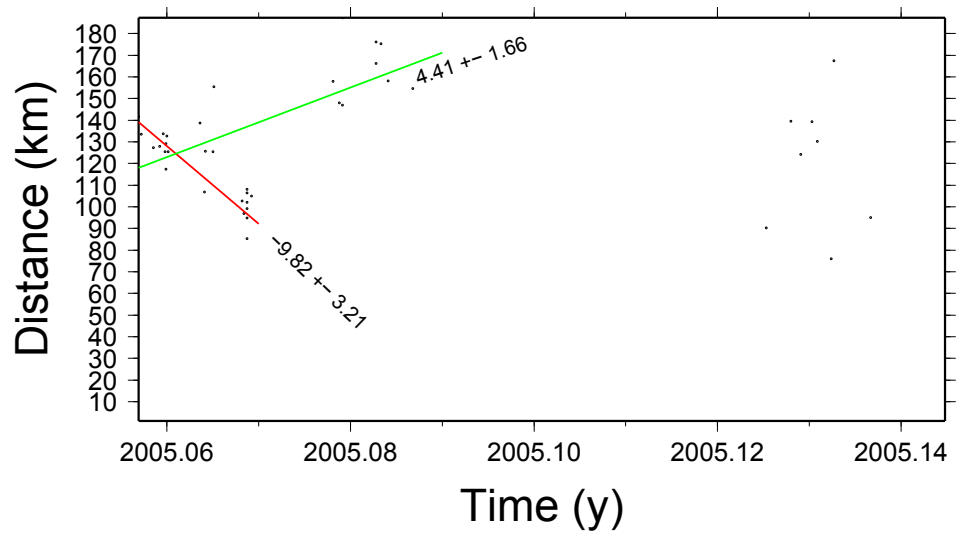


Figure 1.28: Earthquake epicenter propagation for the 2005 Ecuador swarm.

swarm.

### **1977 and 1980 Central Peru Swarms**

Subduction of the Nazca plate beneath central Peru is noted for flat slab subduction which occurs between about 3°S and 15°S. One of the predominant characteristics of flat slab subduction is a disruption of arc volcanism [e.g., Barazangi and Isacks, 1976]. In 1977 and again in 1980, two small swarms occurred on the plateau above the Peruvian flat slab segment, and are shown in Figures 1.30 and 1.31. The Peruvian flat slab segment is noted for an absence of volcanoes, but both swarms occur directly above the 100 km depth contour (Figure 1.3.1) near where volcanism would occur in a normal subduction system [Syracuse and Abers, 2006].

### **1986 Sub-Andean zone in Bolivia**

In 1986 a small cluster of earthquakes occurred in the sub-Andean zone near the Main Andean Thrust of the Eastern Cordillera in Bolivia. This potential swarm is shown in Figure 1.32 but there are too few globally located events to be definitive about the details of the earthquake sequence. The decollement below the eastern edge of the Cordillera is sub-critical within critical taper theory [Davis et al., 1983], and high pore fluid pressure at the base of the wedge has been prescribed to explain the sub-critical angle and structural coherence seen in the main thrust sheet [Roeder, 1988]. This high pore fluid pressure could help explain the occurrence of swarms by reducing the normal stress and allowing for the lower stress drops during events often seen during earthquake swarms.

06/07/2003 to 07/12/2003 Coherence on Google Earth Imagery

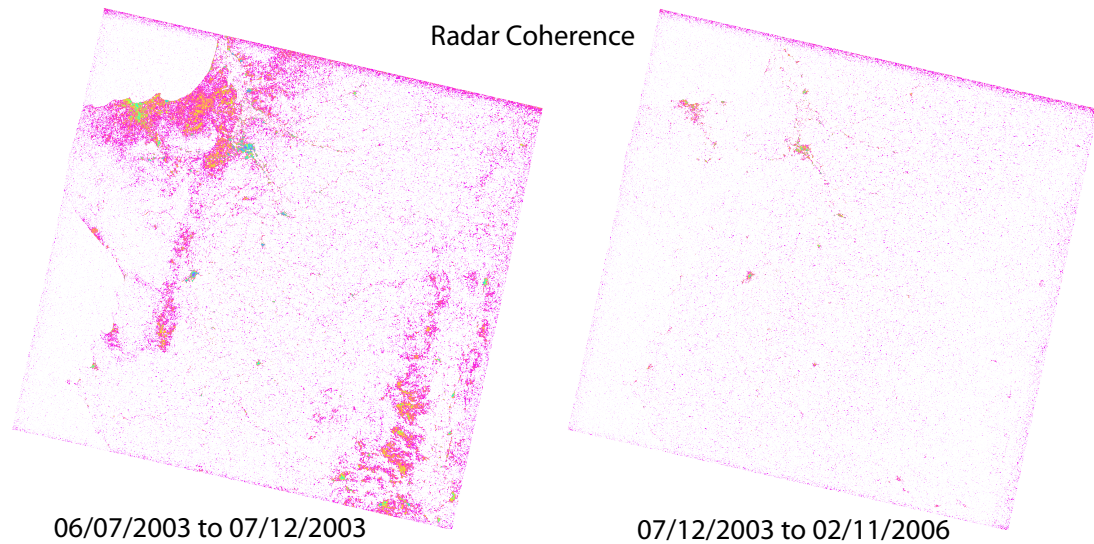
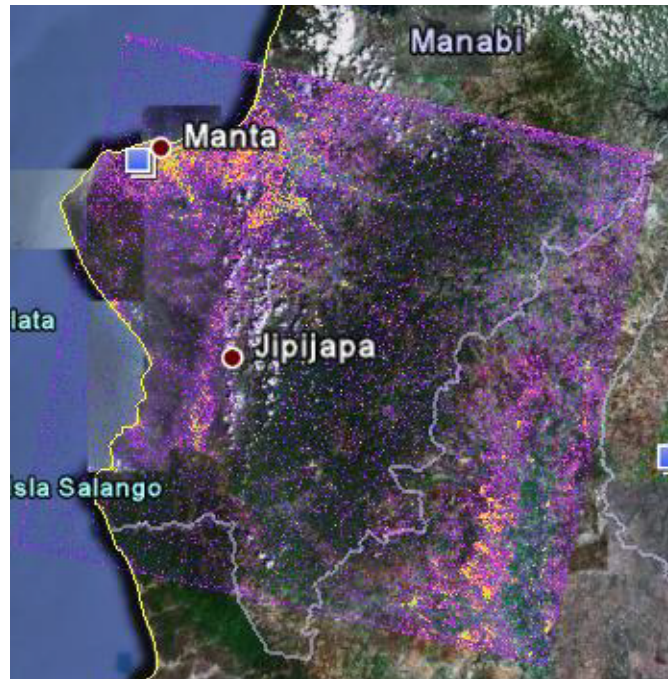


Figure 1.29: Radar Coherence in Southern Ecuador. The 1 month interferogram coherence in the bottom right is overlain on Google Earth Imagery in the top panel. The 2.5 year interferogram that gives the coherence shown in the bottom right panel is the only one which spans the Earthquake Swarm.

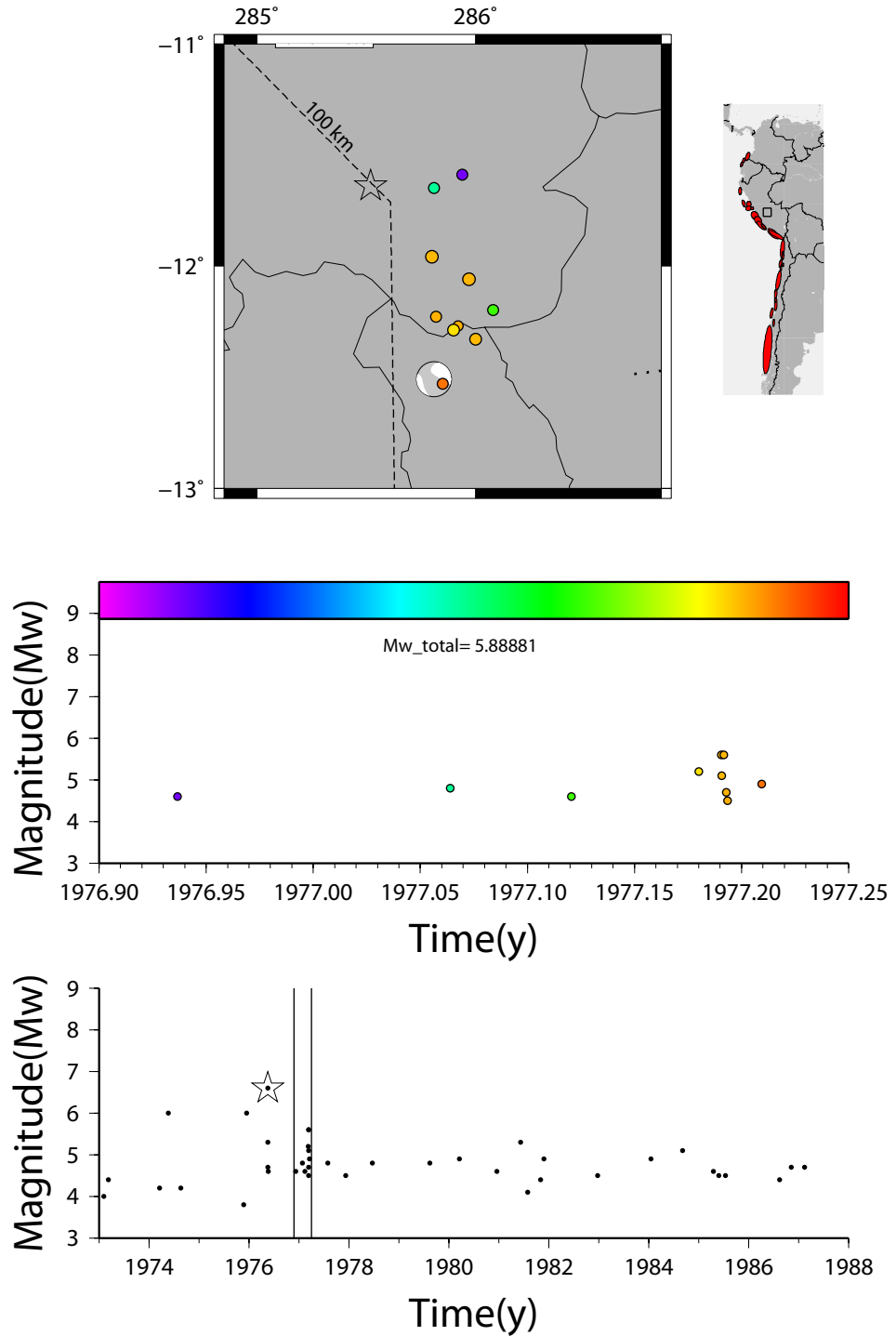


Figure 1.30: 1977 Central Peru Earthquake Swarm.

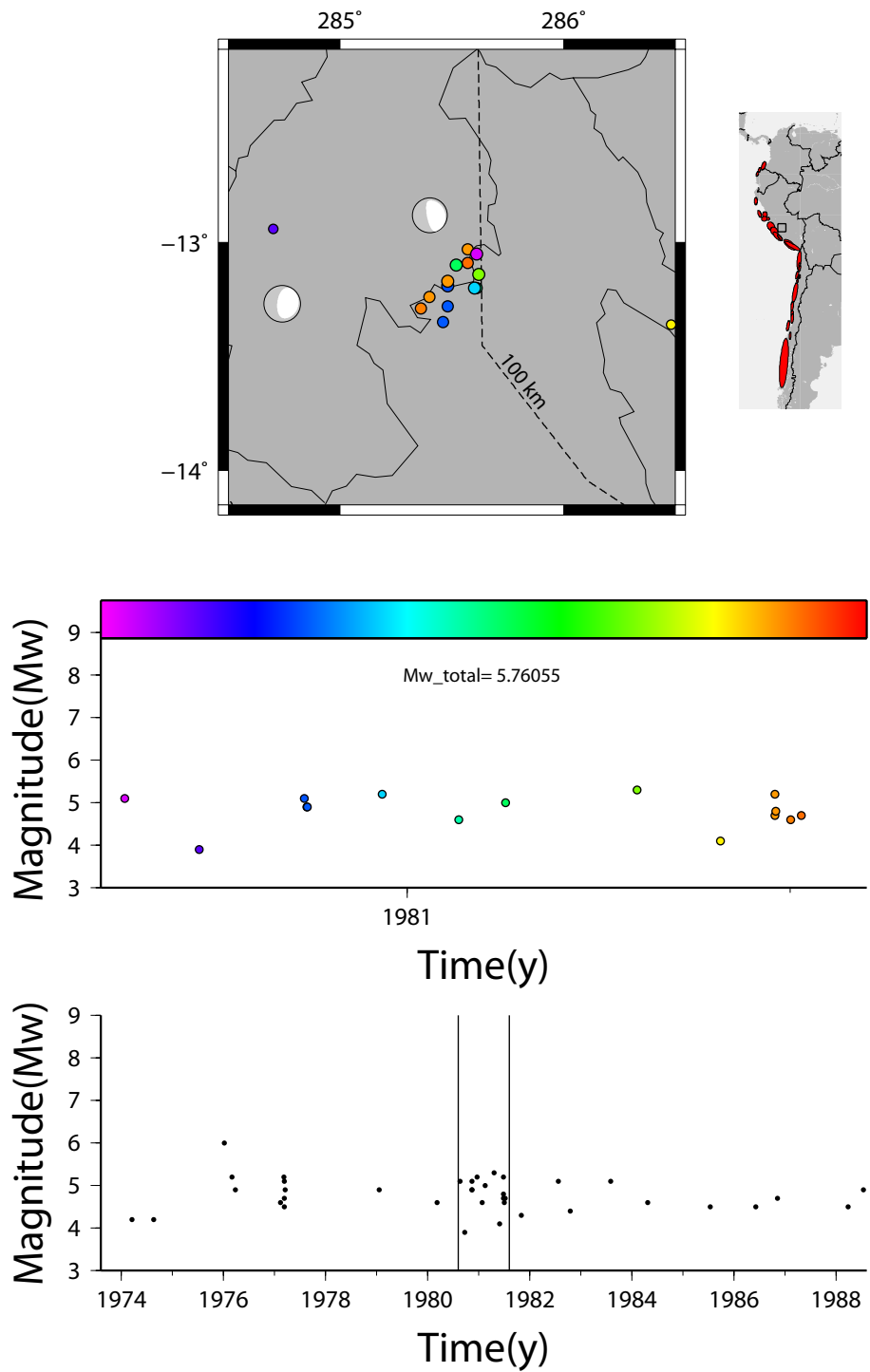


Figure 1.31: 1980 Central Peru Earthquake Swarm.

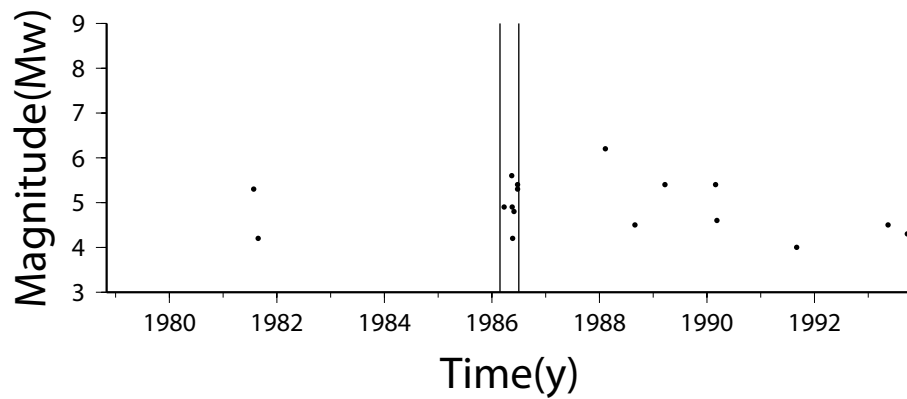
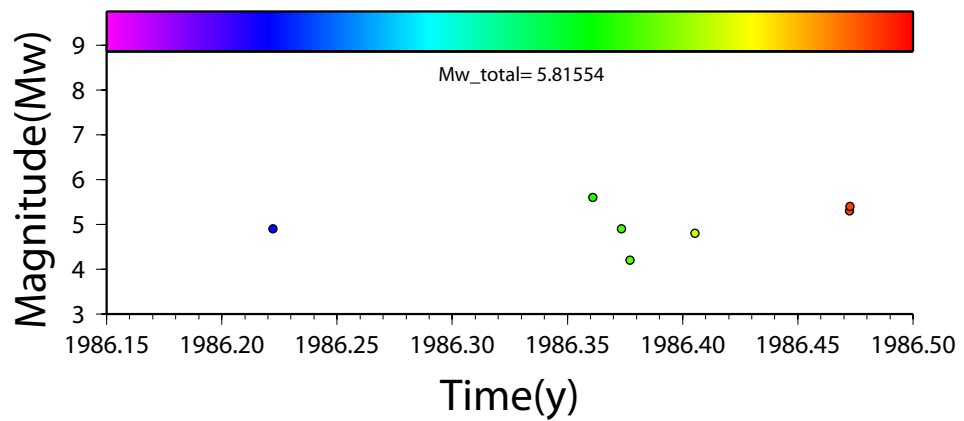
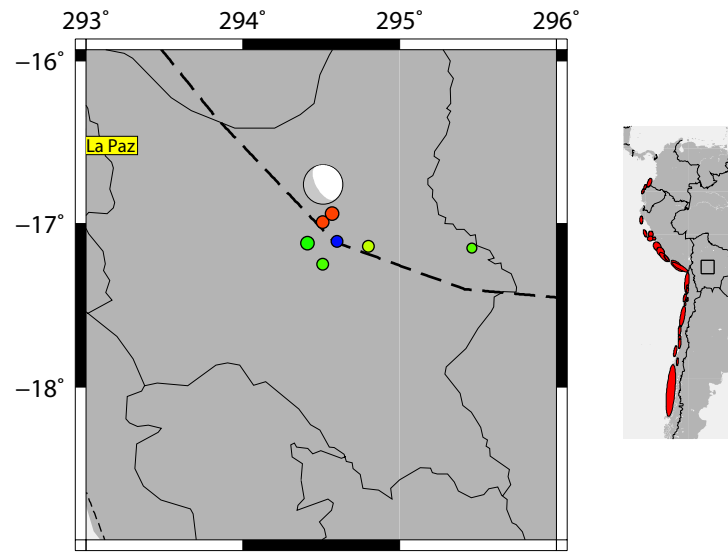


Figure 1.32: 1986 Bolivian Earthquake Swarm

### **1991 Colombia Swarms**

In 1991 two swarms occurred that covered a huge area in Colombia. These two swarms and a mainshock-aftershock sequence that occurred immediately after the second swarm are shown in Figure 1.33. The two swarms each lasted a month or two and had cumulative magnitudes of  $M_w=5.15$  and  $M_w=5.05$  respectively. Each swarm appeared to occupy an area at least a couple hundred of kilometers wide, although the second swarm also contained a tightly clustered group of events near Buenaventura Bay. For comparison, the sequence at the end of this time interval contained cumulative magnitude of  $M_w=7.2$ , over 1000 times as energetic as each of the swarms, but occupies an area no more than 50km by 50km. This large area to moment release ratio implies an extremely low stress drop, on the order of  $1e-5$  bars. Low stress drops are often observed in earthquake swarms.

### **Central Chile at $\sim 38^\circ S$**

One swarm in late 1999 was discovered offshore to the south of the Arauco peninsula and is shown in Figure 1.34. This swarm is immediately south of and adjacent to the aftershock zone of a  $M_w=6.6$  earthquake that struck the region in 2004 and is shown as a star in Figure 1.34. The earthquake was not the subject of any detailed studies, probably because it was not an energetic or damaging earthquake.

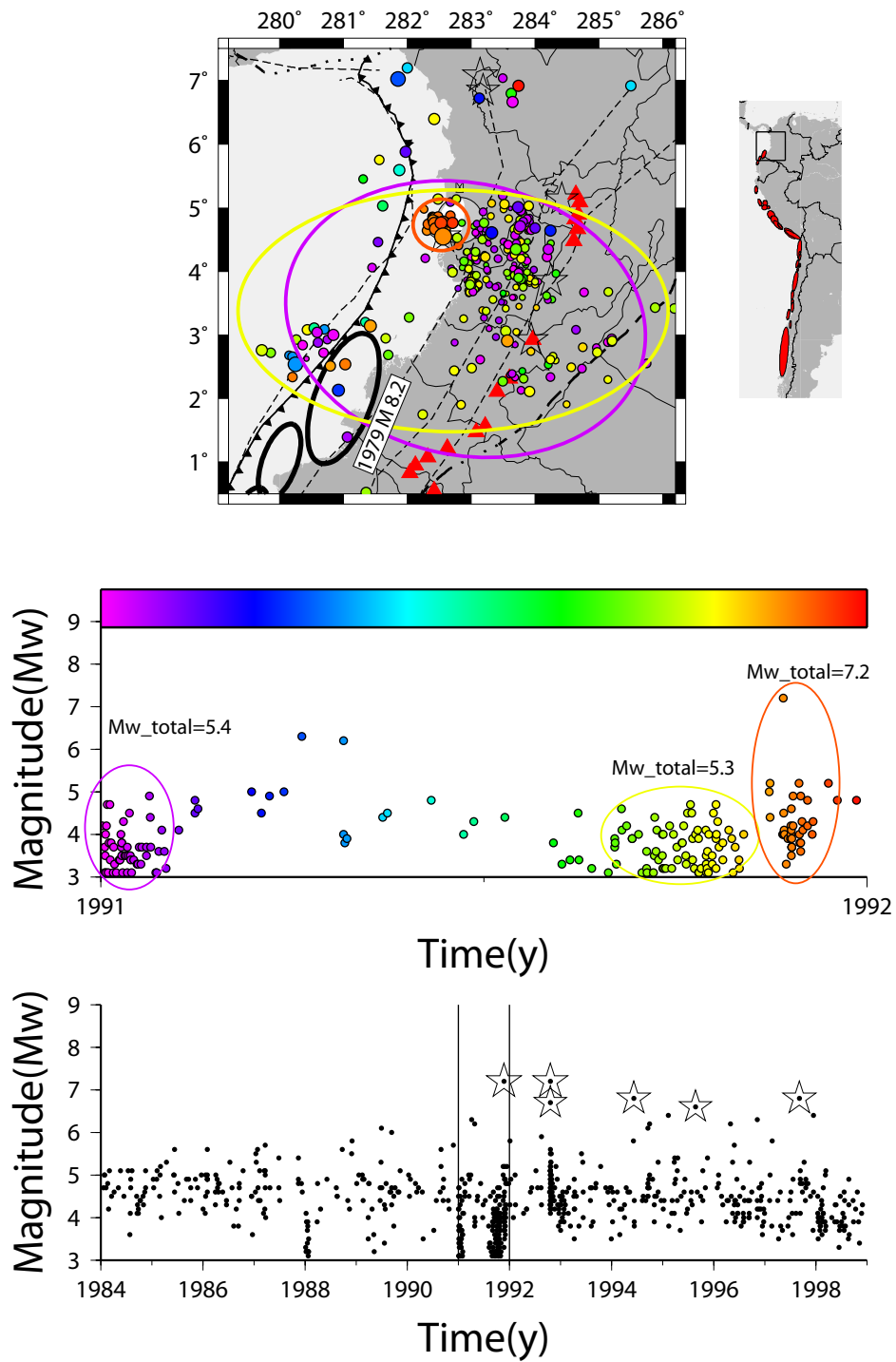


Figure 1.33: 1991 Colombia Earthquake Swarms.

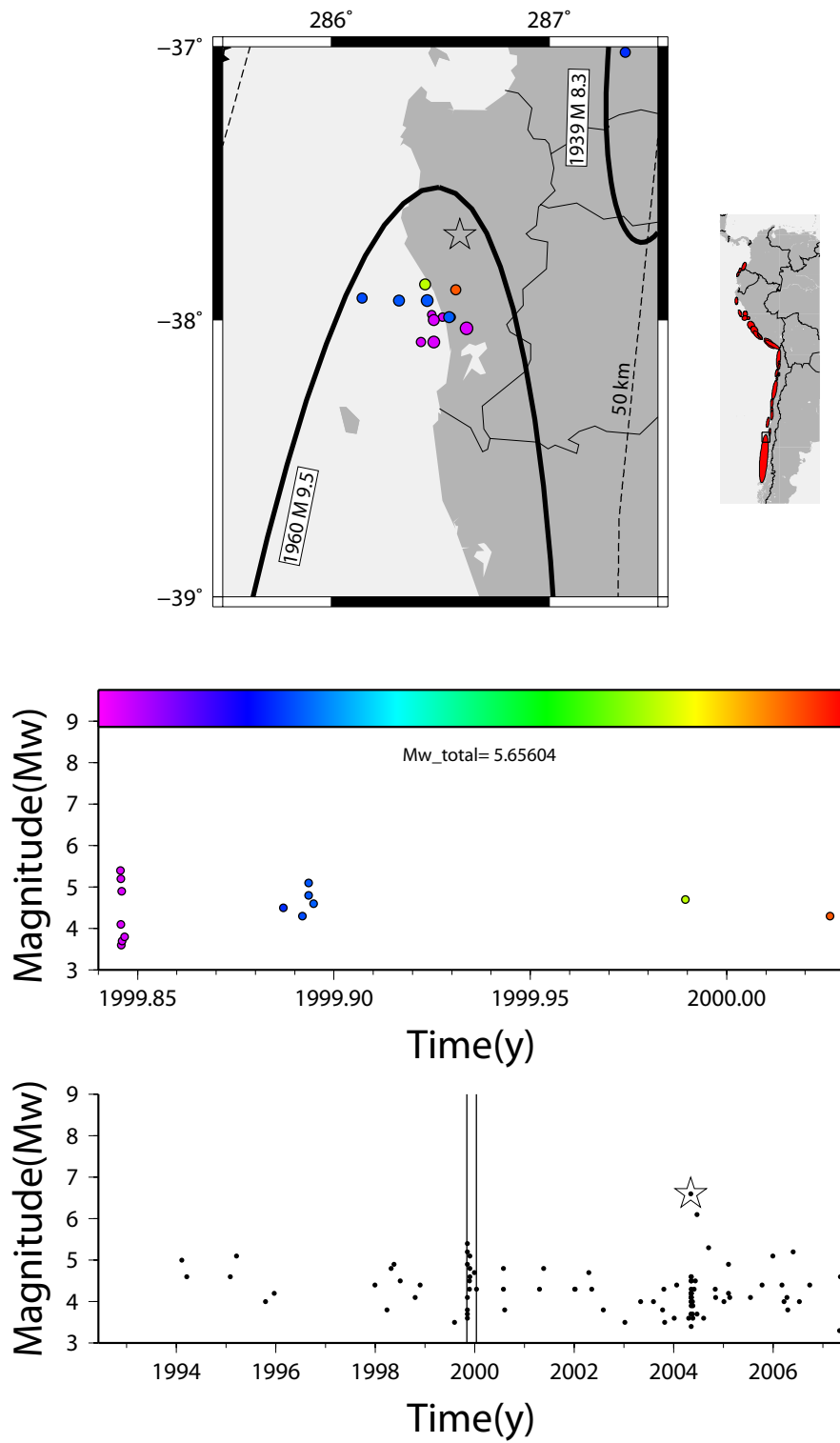


Figure 1.34: 1999 Arauco Peninsula Earthquake Swarm.

## **Northern Peru at $\sim 5^{\circ}\text{S}$**

In 2001-2002 a pair of small clusters of earthquakes (2001.2 and 2002.5) occurred in Northern Peru at the eastern edge of the Eastern Cordillera in Northern Peru. There are less than 10 earthquakes in both clusters, so definitively labeling this as a swarm or otherwise is not absolute. This potential swarm is shown in Figure 1.35. Each of the earthquakes shown here were either near the plate interface (106-117 km depth) or were assigned the default depth in the region of 33km. If all of the events did occur near the plate interface at  $\sim 100$  km depth, this swarm would be the only one found that was not either on or near the shallow megathrust or in the upper plate crust.

## **Triggered seismicity after the 2001 Peru earthquake**

The  $M_w=8.5$  2001 Southern Peru earthquake seems to have triggered seismicity up to several hundred kilometers away from the rupture zone [Devlin, 2008], as shown in Figure 1.36. Several large earthquakes around the world have been documented to trigger seismicity at great distances [e.g., Hill et al., 1993; Husen et al., 2004]. Three of these triggered clusters of seismicity were identified as swarms in this thesis. The first swarm contained two distinct bursts of seismicity oriented beneath Coropuna volcano and to the southeast of Coropuna volcano. [Pritchard et al., 2007] show deformation associated with Coropuna volcano and the swarm shown in Figure 1.37. The second swarm occurred to the west of lake Titicaca and the third occurred to the southwest of lake Titicaca near Tutupaca volcano. The second and third are shown in Figures 1.38 and 1.39.

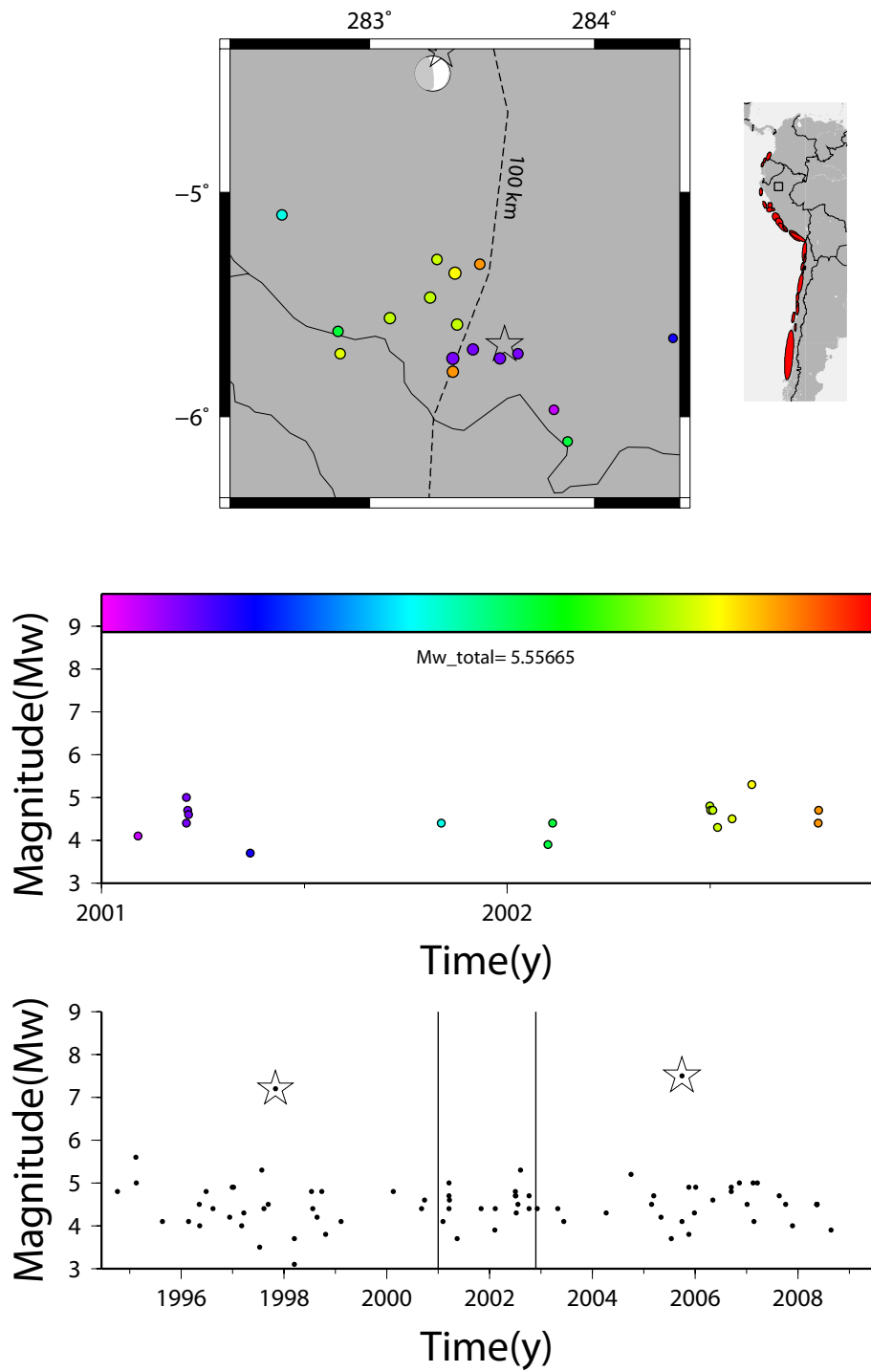


Figure 1.35: 2001 Northern Peru Earthquake Swarm.

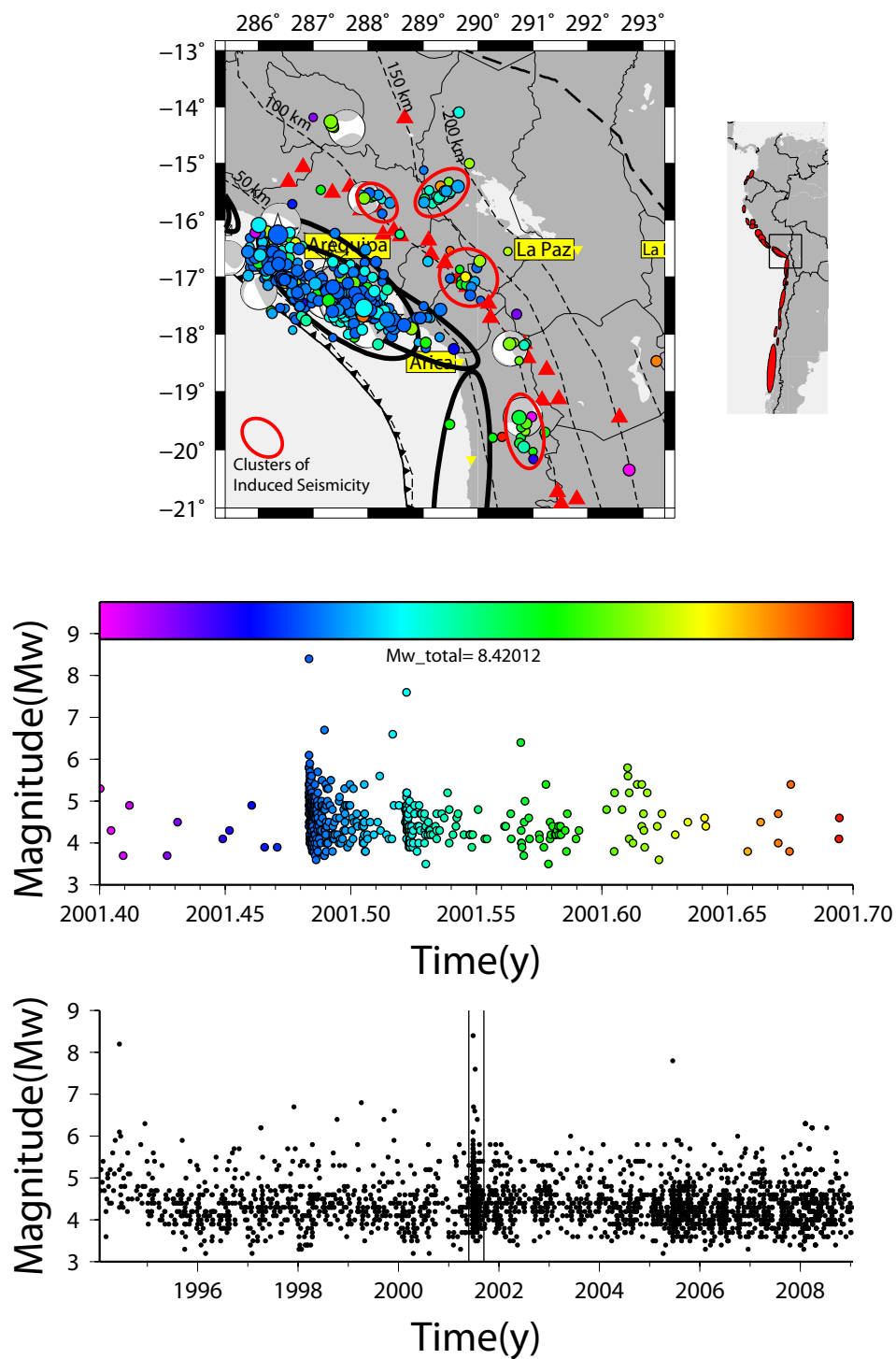


Figure 1.36: 2001 Peru Earthquake and Triggered Seismicity, with triggered seismicity shown in red circles.

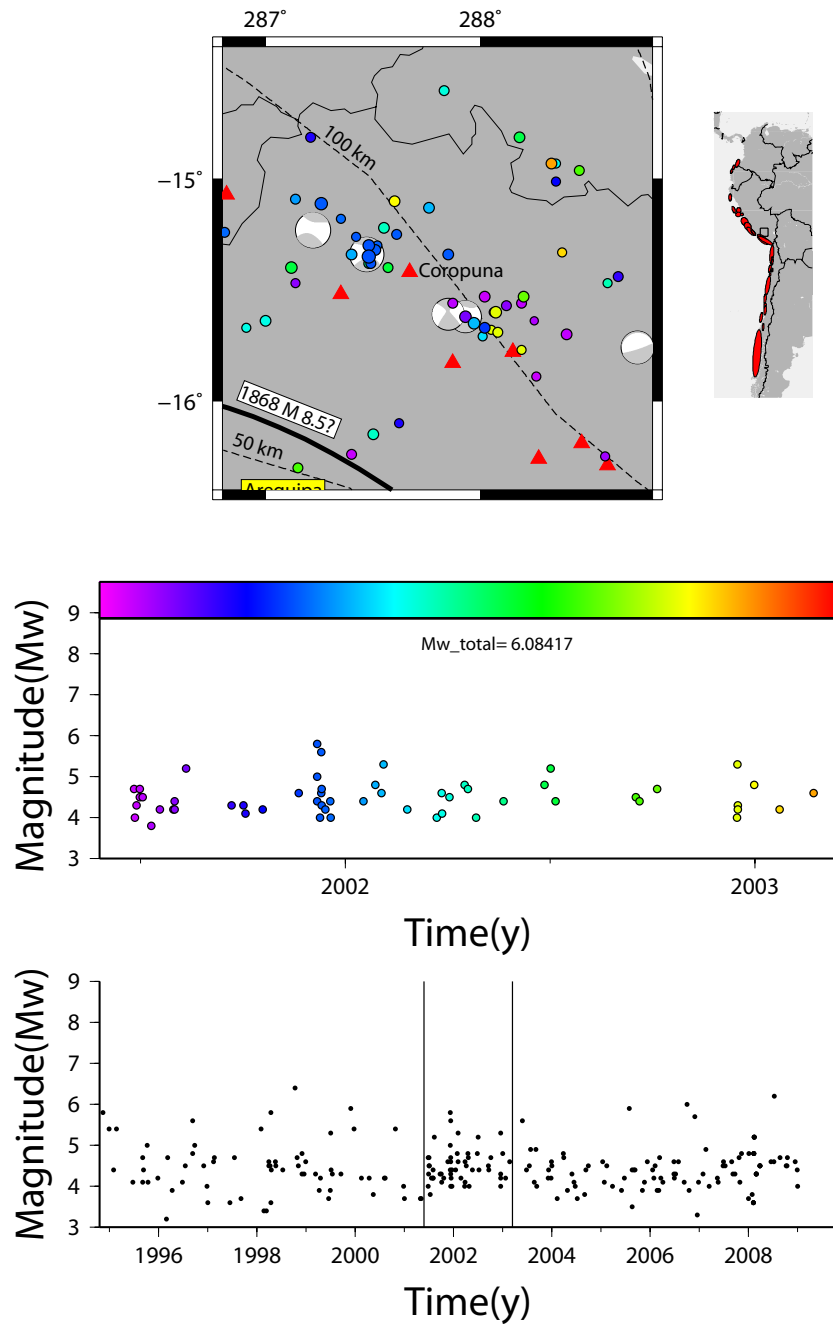


Figure 1.37: 2001 Triggered Swarm at Coropuna Volcano. InSAR associated with the swarm is discussed in the text, and colored vertical lines in the bottom panel will show the acquisition dates, with similar colors representing independent interferograms made.

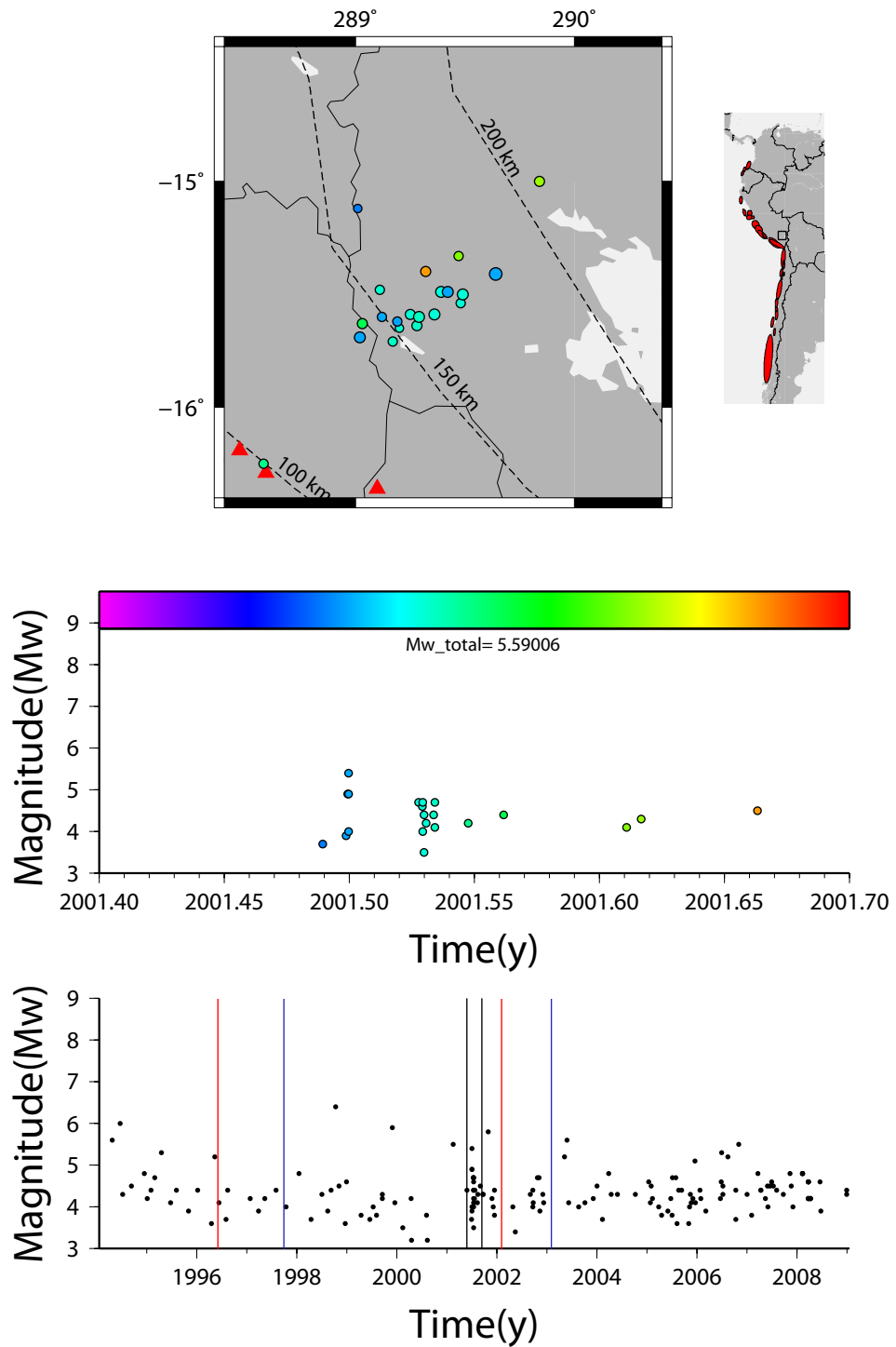


Figure 1.38: 2001 Triggered Swarm near Lake Titicaca.

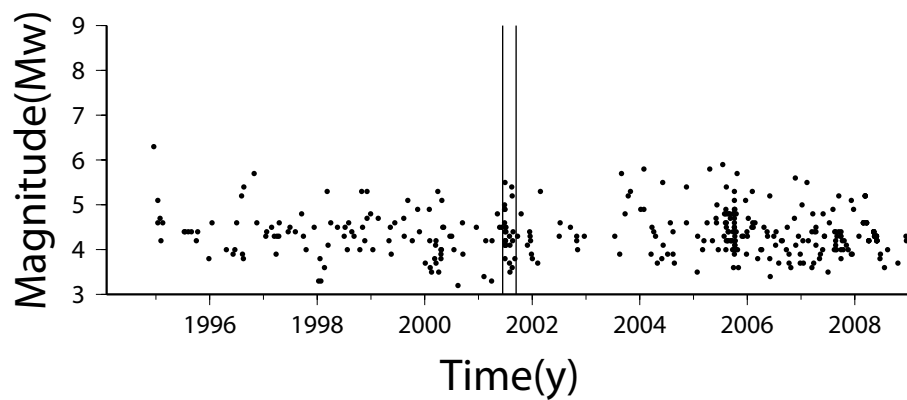
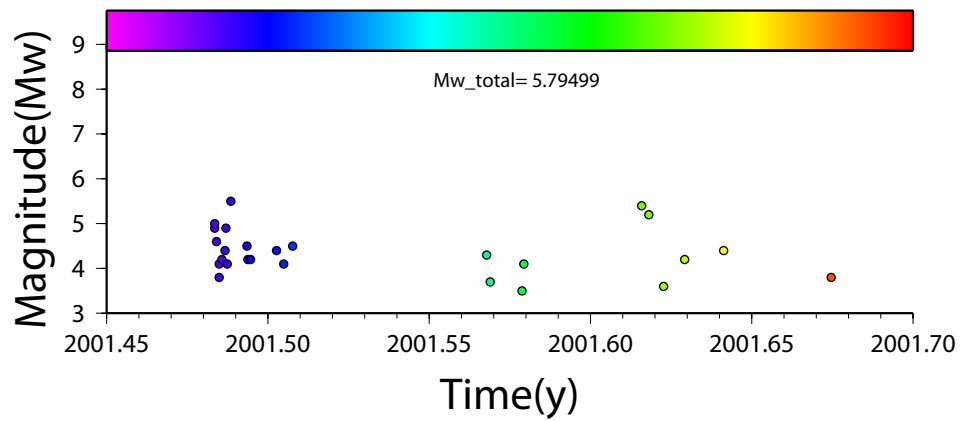
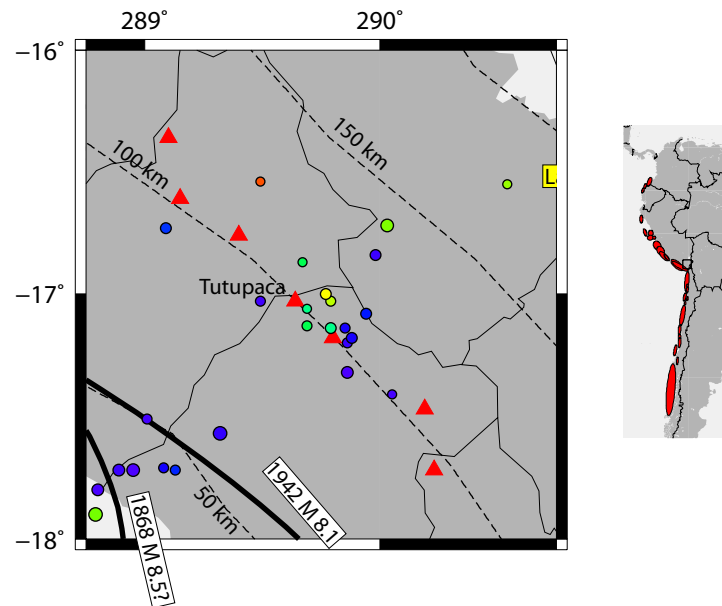


Figure 1.39: 2001 Triggered Swarm at Tutupaca Volcano.

## Prior to the 2007 Peru Earthquake

A  $M_w=8.1$  earthquake struck off Pisco Peru on 15 August, 2007. This earthquake was preceded a year earlier by a  $M_w=6.7$  foreshock with an epicenter very close to the 2007 epicenter. Several interferograms of this earthquake were made by Pritchard and Fielding [2008]. Both the foreshock and the mainshock were near the northern edge of the rupture zone of the  $M_w=8.1$  earthquake [Pritchard and Fielding, 2008; Motagh et al., 2008; Biggs et al., 2009]. South of the epicenter of the 2007 event, a pair of swarms in early 2005 and early 2006 occurred south of Pisco, Peru. The 2007 rupture propagated to the south, and the swarms shown in Figure 1.40 mark the southern terminus of the aftershock sequence of the large Peru earthquake.

To test whether or not the 2005-2006 swarm was accompanied by aseismic slip, we examine interferograms formed from acquisitions made before and after the earthquake. Figure 1.41 shows interferograms made from both acquisitions before the Earthquake in panel 1 and an interferogram spanning both the swarm and the earthquake with the best fit joint InSAR-seismic model for the earthquake removed [Pritchard and Fielding, 2008]. Residuals in both cases are on the order of several centimeters. This is a small swarm, with most earthquakes occurring offshore and with depths of several tens of kilometers. Because of the depth and offshore nature of the swarm, it appears that any slip associated with the swarm is below the observation threshold for InSAR. Nevertheless, the location of the swarm at the southern terminus of the mainshock rupture highlight a potential relationship between the two processes, and will be discussed in section 1.5.

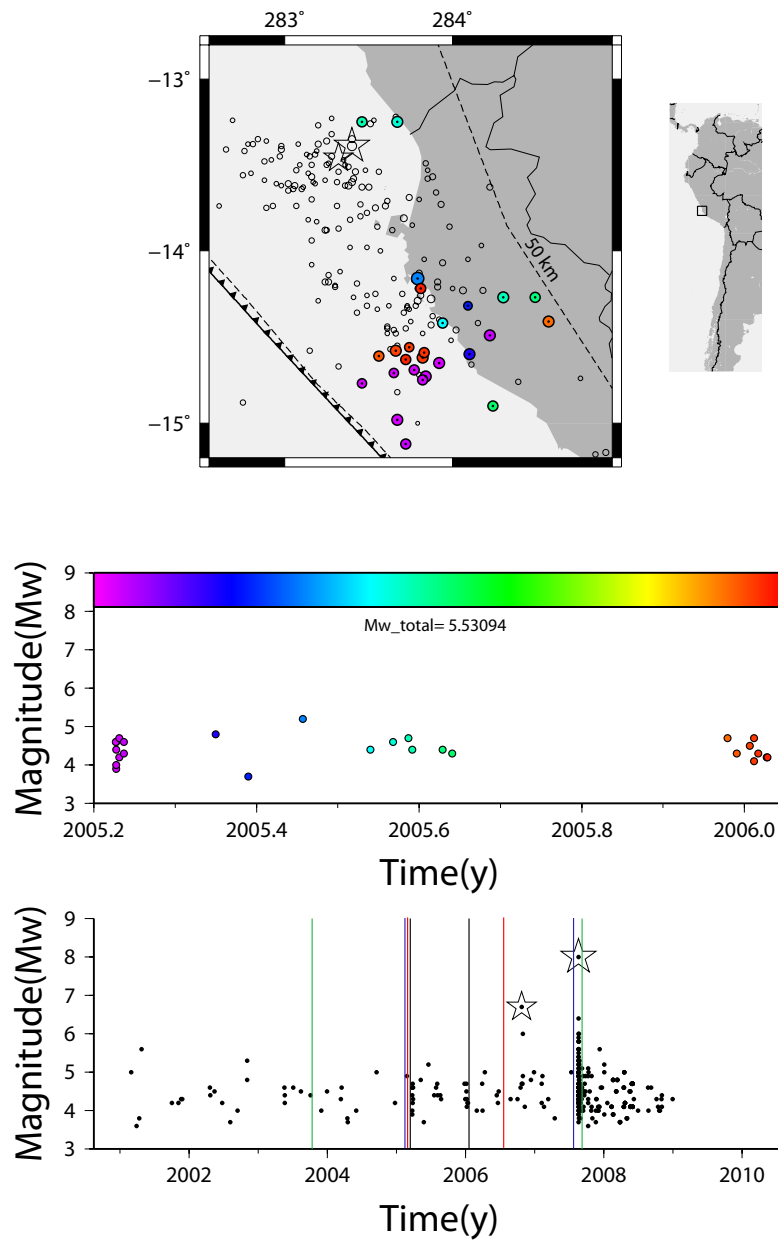


Figure 1.40: 2005 Pisco, Peru Earthquake Swarm preceding the 2007 Pisco Earthquake. The epicenter of the Mw=8.1 Pisco earthquake is shown as a star and the aftershocks of this earthquake are hollow circles. InSAR associated with the swarm is discussed in the text, and colored vertical lines in the bottom panel will show the acquisition dates, with similar colors representing independent interferograms made.

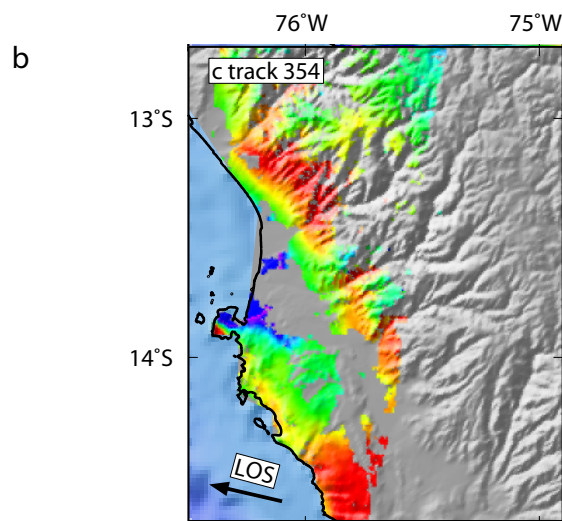
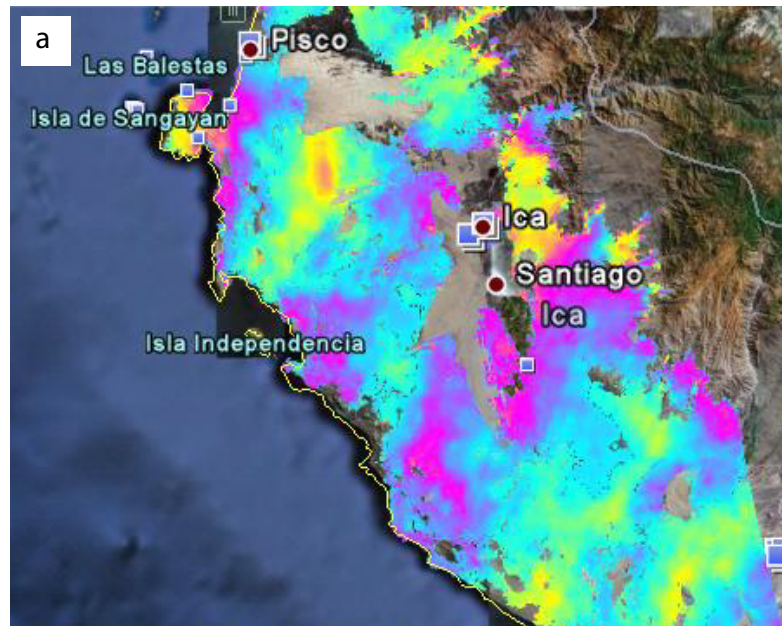


Figure 1.41: (a) Pre-Earthquake Interferogram of the Pisco Region showing no noticeable ground deformation associated with the 2005 earthquake Swarm. (b) Inteferogram containing earthquake and pre-shock swarm with best fit joint InSAR/Teleseismic model removed [Pritchard and Fielding, 2008], also showing no noticeable ground deformation associated with the 2005 earthquake swarm.

## Central American Swarms

As a consequence of downloading all data within a rectangle over South America, earthquakes from Panama and Costa Rica were also analyzed. Three swarms in Panama and one on the Panama-Costa Rica border were found. The first occurred in 1991 along the Costa Rica border and is shown in Figure 1.42, near the North Panama Deformed Belt. The North Panama Deformed Belt marks the northern edge of the Costa Rica-Panama microplate and accommodates the motion of the microplate to the west and north. This region also lies above the subducting Cocos Ridge and marks a volcanic gap between the Panama and Costa Rica volcanoes. The events in this swarm were located by the global catalogs as shallow events with depths less than 20 km.

A second swarm event occurred in 1993 and is shown in Figure 1.43. This event occurred to the south of the North Panama Deformed Belt but still appears to be offshore. This area became active again in 1998 in a widespread pulse of earthquake activity. This pulse or swarm, shown in Figure 1.44, started in 1998 with activity that spanned several degrees and three major tectonic plates and lasted a few months. This pulse marks the beginning of a swarm in northern Panama that is shown in Figure 1.45 and appears to be similar to, although south of, the 1993 swarm. A few months after that, a swarm in southern Panama, shown in Figure 1.46, occurs to the north of the Southern Panama Deformed Belt along the Rio Flores Fault Zone up to the Azuero-Sona Fault Zone. The 1998 swarms were composed of earthquakes with smaller magnitudes than had previously been reported, so further study will need to eliminate the possibility that these swarms are an artifact of a temporarily decreased magnitude reporting threshold.

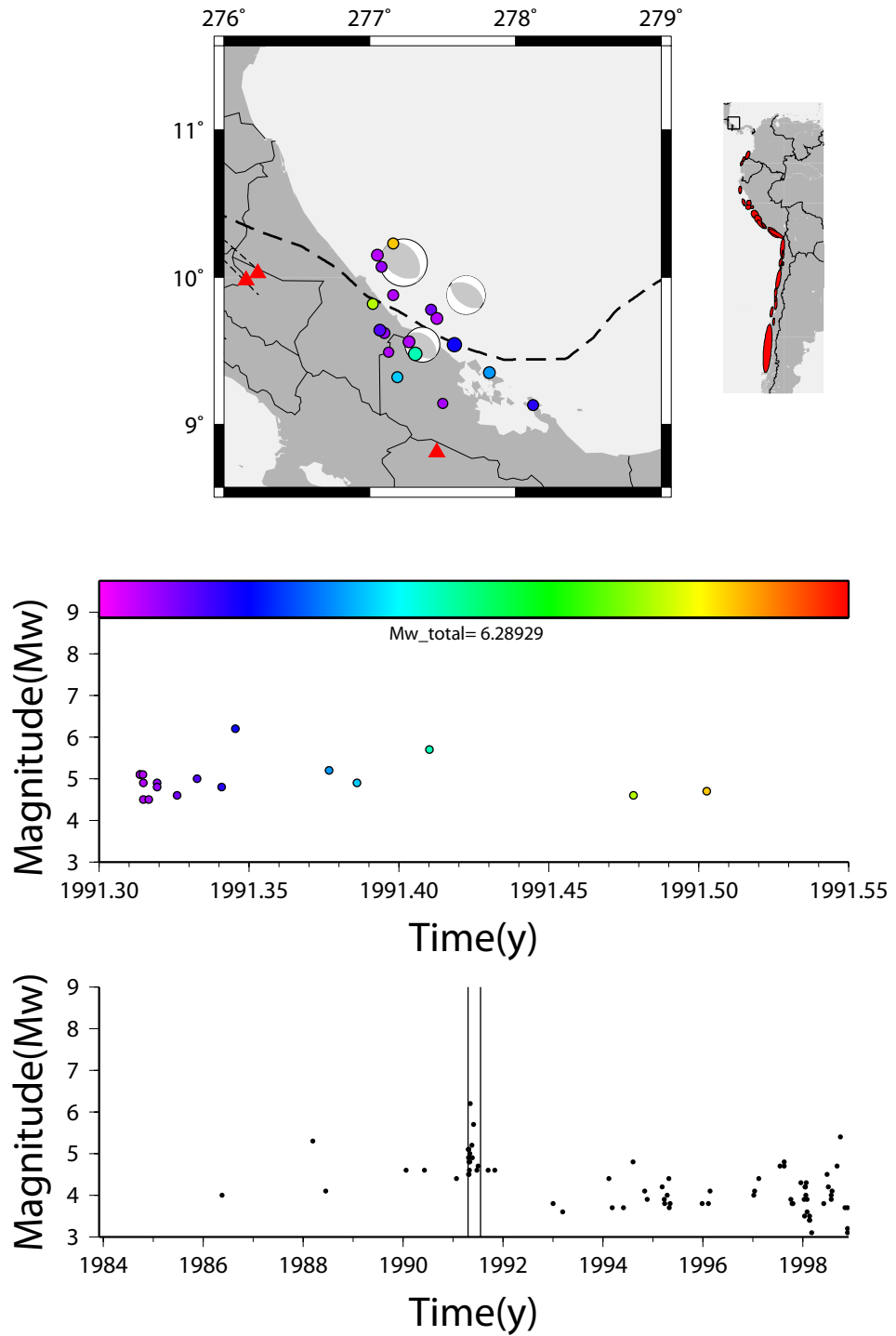


Figure 1.42: 1991 Costa Rica Earthquake Swarm.

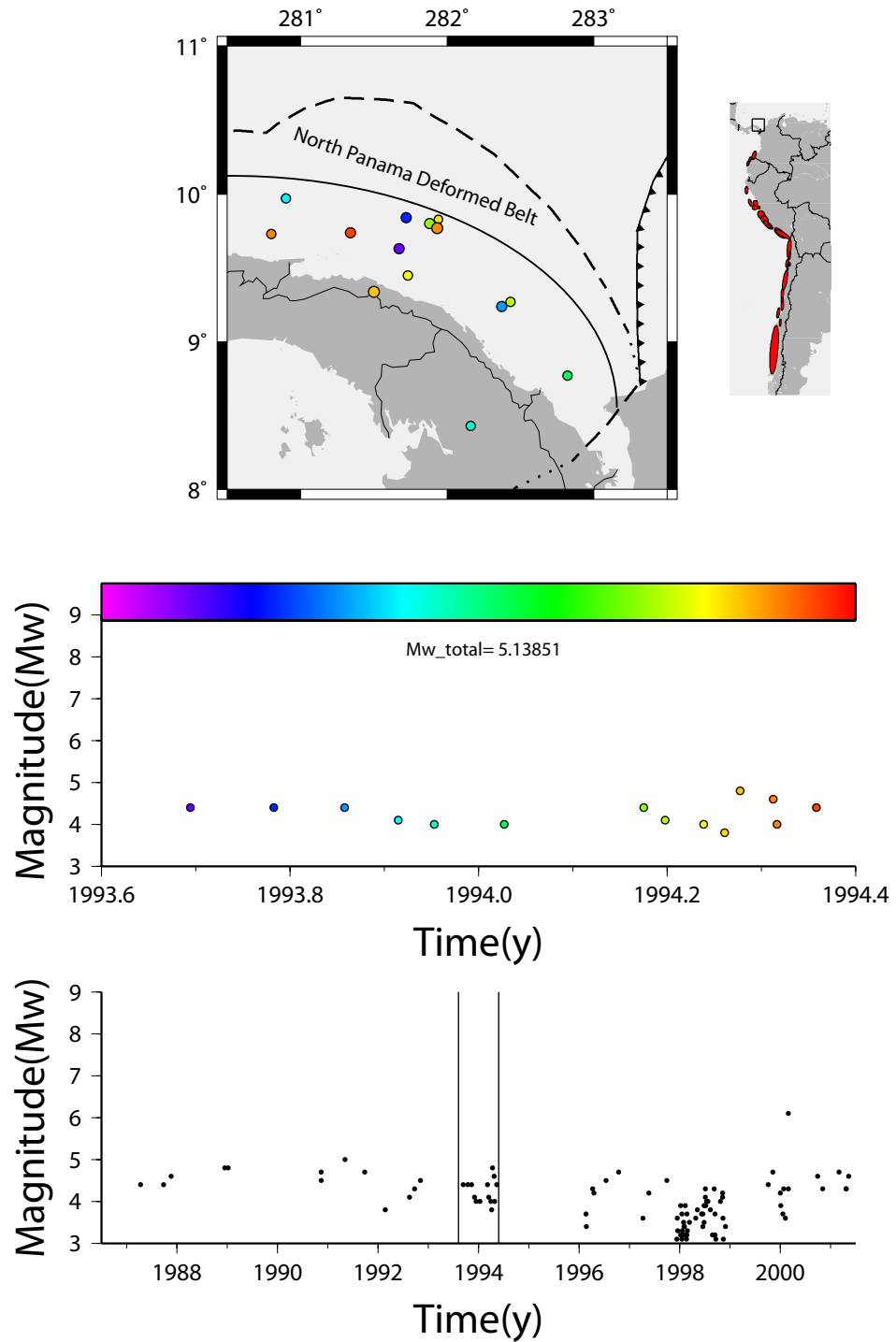


Figure 1.43: 1993 North Panama Earthquake Swarm.

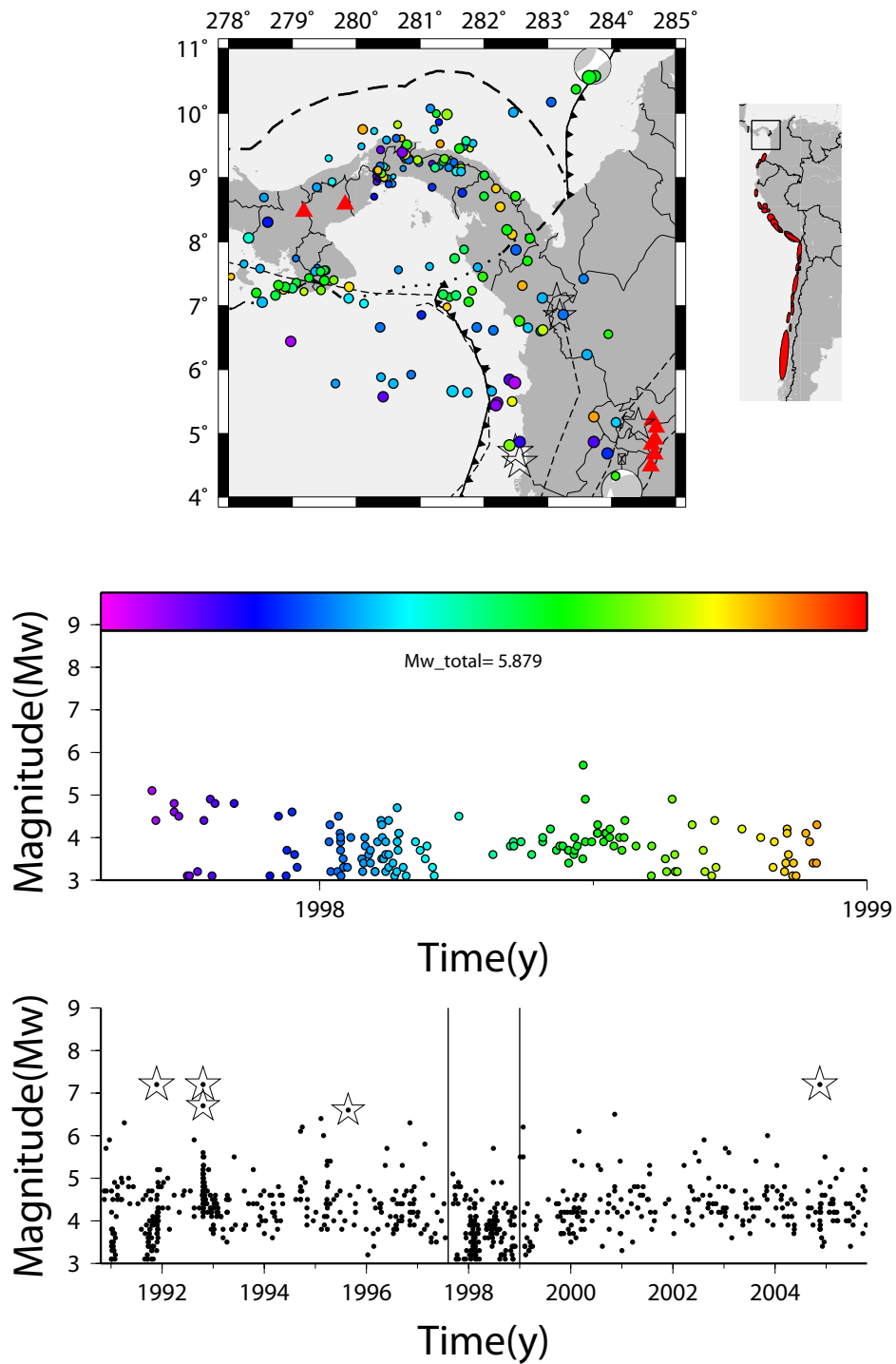


Figure 1.44: 1998 Swarm Activity in Central America.

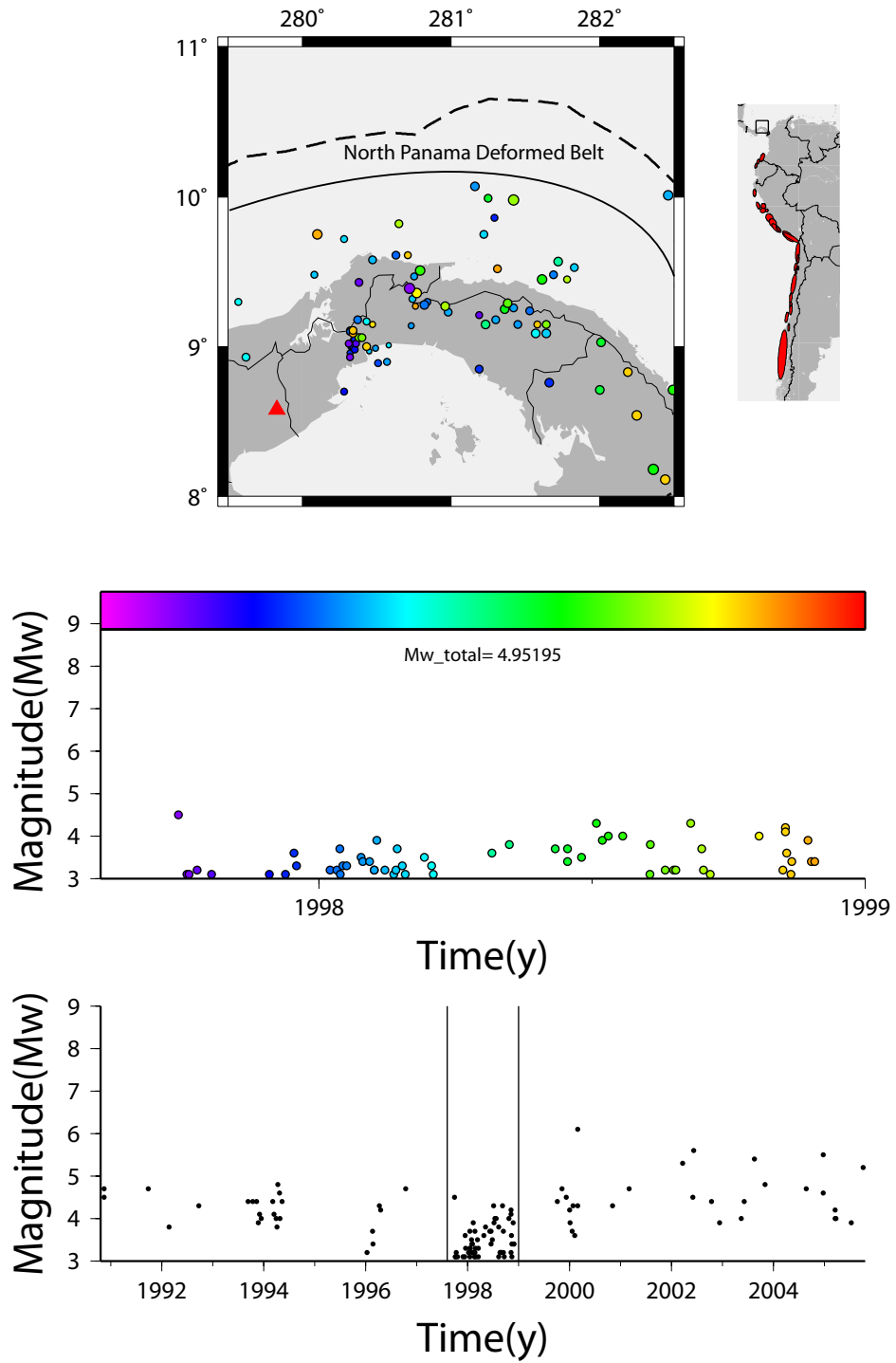


Figure 1.45: 1998 Northern Panama Earthquake Swarm

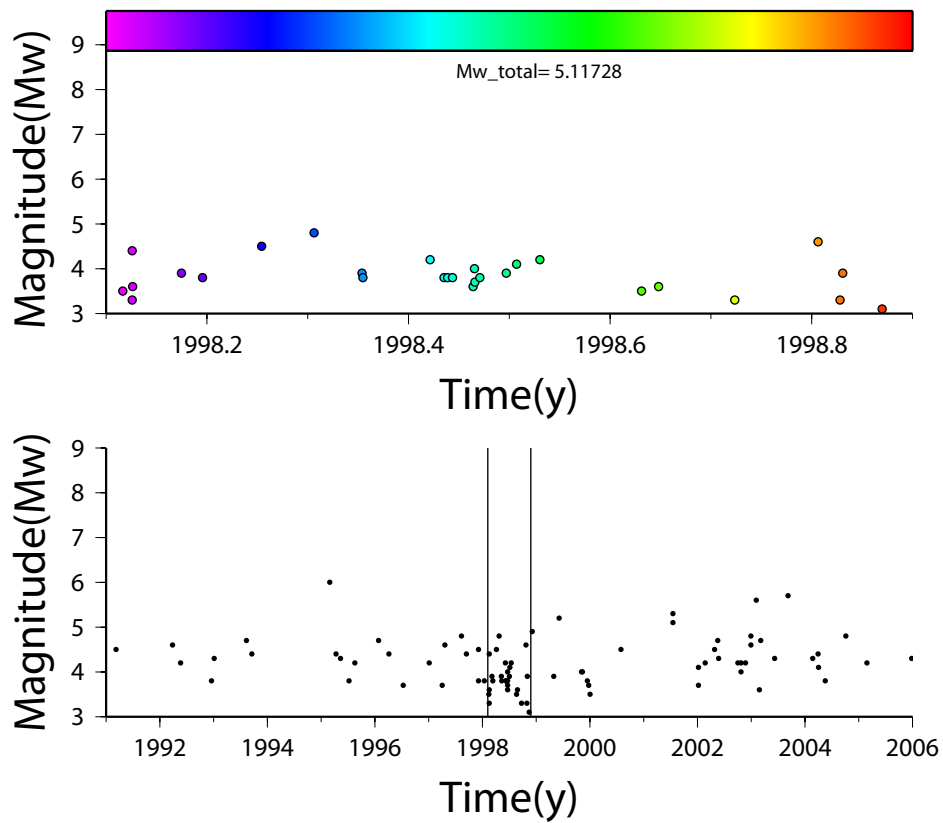
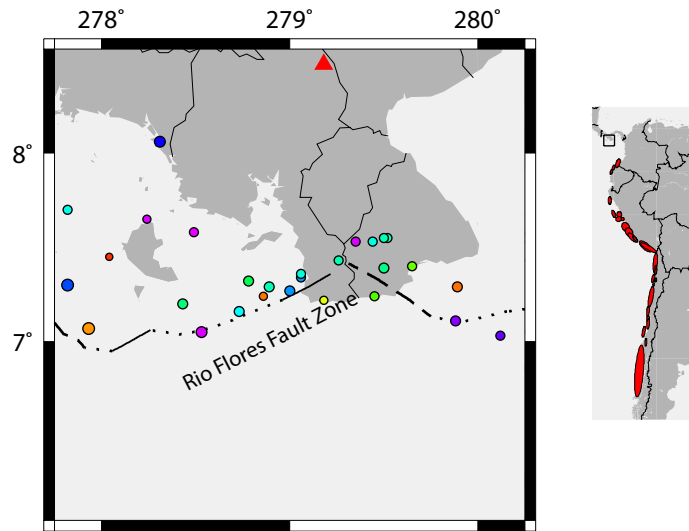


Figure 1.46: 1998 Southern Panama Earthquake Swarm.

## 1.5 Discussion

The role of aseismic slip in plate boundary processes is a key motivation for this thesis as the number of aseismic slip observations has greatly increased due to high precision geodetic techniques (e.g. GPS and InSAR) [Heki et al., 1997]. Studies have focused on potential interaction between aseismic slip events and earthquakes as any advancement could potentially help with earthquake hazard mitigation. Slow or aseismic slip has been observed in association with earthquake swarms [Lohman and McGuire, 2007], non-volcanic tremor (NVT) [Rogers and Dragert, 2003; Hirose and Obara, 2006], or not correlated with any seismic observation [Ozawa et al., 2002]. NVT is a weak, long duration and slowly emergent seismic signal prominent in the 2-10 Hz range and is often inferred to have some relation to fluid release or movement. When NVT is observed in correlation with slow slip, the process is characterized as episodic tremor and slip (ETS) and has been observed in Japan [Hirose and Obara, 2006], Costa Rica [Brown et al., 2005], Cascadia [Rogers and Dragert, 2003], Mexico [Payero et al., 2008], and Alaska [Peterson et al., 2005].

Recently, Shelly et al. [2007] has shown evidence that NVT in Japan during GPS detected slow slip events is actually a swarm of low-frequency earthquakes (LFE) and that tremor in the Parkfield region of the San Andreas Fault also consist of identifiable low frequency earthquakes [Shelly et al., 2009]. Low frequency earthquakes differ from regular earthquakes in that they are enriched in  $\sim 1-5$  Hz and depleted at higher frequencies. Shelly et al. [2006] show evidence that LFE's represent fluid-enabled shear slip on the megathrust. Preliminary work also suggests LFE's are abundant within Cascadia NVT (Mike Brudzinski, personal communication, 2009), so the observation of NVT anywhere may

be observation of an earthquake swarm manifested in a manner that is not detectable by traditional seismic deployments or teleseismic data. In Japan and Mexico, tremor and LFE's locate adjacent to the region of aseismic slip, but the relationship between aseismic slip and megathrust earthquakes remains unknown in these regions because observations have not been occurring for a long enough time to sample any possible interaction. Earthquake afterslip has been shown on several occasions to occur immediately adjacent to mainshock slip asperities [e.g., Heki et al., 1997; Hsu et al., 2006] suggesting that aseismic slip and afterslip are intimately related. Slow earthquakes or aseismic slip, either postseismic or as independent slow slip events, may indicate that the fault is exhibiting velocity strengthening characteristics since the rupture is not allowed to reach shear wave speeds [Segall and Rice, 1995; Segall et al., 2008].

The search presented in this thesis identifies swarms on or near the megathrust in some interesting and unique regions of the South American margin. There are three main aseismic ridges currently subducting beneath South America: the Carnegie Ridge in Ecuador, the Nazca Ridge in Peru, and the Juan Fernandez Ridge in Chile. All three of these ridges have had earthquake swarms in the past 40 years (most easily seen in Figure 1.3.1). The Carnegie and Nazca ridges have been characterized by prominent seismic gaps [Swenson and Beck, 1996, 1999], and the 2007 Pisco earthquake was shown to only partially fill the Nazca gap [Pritchard and Fielding, 2008]. There are two end-member models for why seismic gaps occur. Either (1) the fault is fully locked and accumulating strain to be released in a great earthquake, or (2) the fault is unable to accumulate strain and will never rupture in a great earthquake. If the swarms in Ecuador are associated with significant aseismic moment release [e.g., Lohman and McGuire, 2007; Ogata, 2007] this could possibly explain part of the seismic

gap in the southern Ecuador region as frequent aseismic strain release could prevent the fault from loading.

The 2007 Peru Earthquake was studied using InSAR by Pritchard and Fielding [2008]. Pritchard and Fielding [2008] demonstrate that a seismic gap still remains, particularly at the crest of the incoming Nazca Ridge to the south of the 2007 rupture zone. This marks the area of the 2005-2006 earthquake swarm. Pritchard and Fielding [2008] solve for approximately 10 m of maximum slip during the earthquake. Since the last earthquake in the region occurred in 1746, this earthquake ruptured approximately half of the ~20m slip deficit accumulated since then. This deficit may be made up in future earthquakes or the deficit may be accommodated aseismically. Additionally, this earthquake exhibited very low rupture velocity ( $<1.5\text{km/s}$ ). Such a low rupture velocity indicates that not enough seismic energy is being radiated to propagate the rupture efficiently along strike. Conceptual models for slow or aseismic slip events require that rupture is inhibited in some way so rupture propagation does not reach shear wave speeds. If a relationship between the low earthquake rupture velocity during the 2007 earthquake and aseismic slip associated with the swarm above the Nazca Ridge exists (aseismic slip is just really slow rupture velocity), these observations could be documenting a transition in fault properties associated with the subduction of the Nazca Ridge from velocity weakening to velocity strengthening.

There is at least one other example of prior swarms occurring at the spatial edge of coseismic rupture, which took place in Kamchatka. Slavina et al. [2007] reported a preshock swarm before the  $M_w=7.8$  Kronotskii earthquake on December 5, 1997. This swarm was at the northernmost edge of the rupture zone,

as shown in Figure 1.47. Zobin [1999] report 23 swarms as having occurred off the peninsula of Kamchatka in the past, so we applied our swarm search to this region as well. There are several areas of repeating earthquake swarms as reported by Zobin, but there are also two swarms that seem closely tied to the rupture zone of 1997. We found a swarm in 1973, shown in Figure 1.48, which marks the southern edge of the 1997 rupture zone. We also found that a swarm in 1983, shown in Figure 1.49, as well as the 1997 preshock swarm detailed in Zobin [1999], mark the northern edge of the 1997 rupture zone.

The swarms before the earthquakes in Kamchatka and Peru could be affecting coseismic rupture in two ways: releasing slip deficit aseismically so that rupture cannot propagate through the swarm area, or signifying an area of the plate interface that has mechanical properties conducive to swarm generation and provides a barrier to rupture propagation (i.e. an area of stable sliding, heterogeneous, wet). It does not appear as though the Peru swarm of 2005-2006 released much moment aseismically, but the period from 1746 to 1973 will remain undocumented so distinguishing between these two end members is impossible.

We explored the magnitude-frequency content in our earthquake swarm catalog to test whether there is any indication of how frequent swarms in South America may be and if South American swarms are similar in frequency to swarms in Japan or Southern California. Vidale and Shearer [2006]; Vidale et al. [2006] use local catalogs to constrain types of earthquake bursts in Japan and Southern California, but the sizes of the events and duration of the catalogs are different than our swarm search. Vidale et al. [2006] shows swarms in Japan with total magnitudes ranging from 2 to 4 and a catalog length of 2.9 years. In

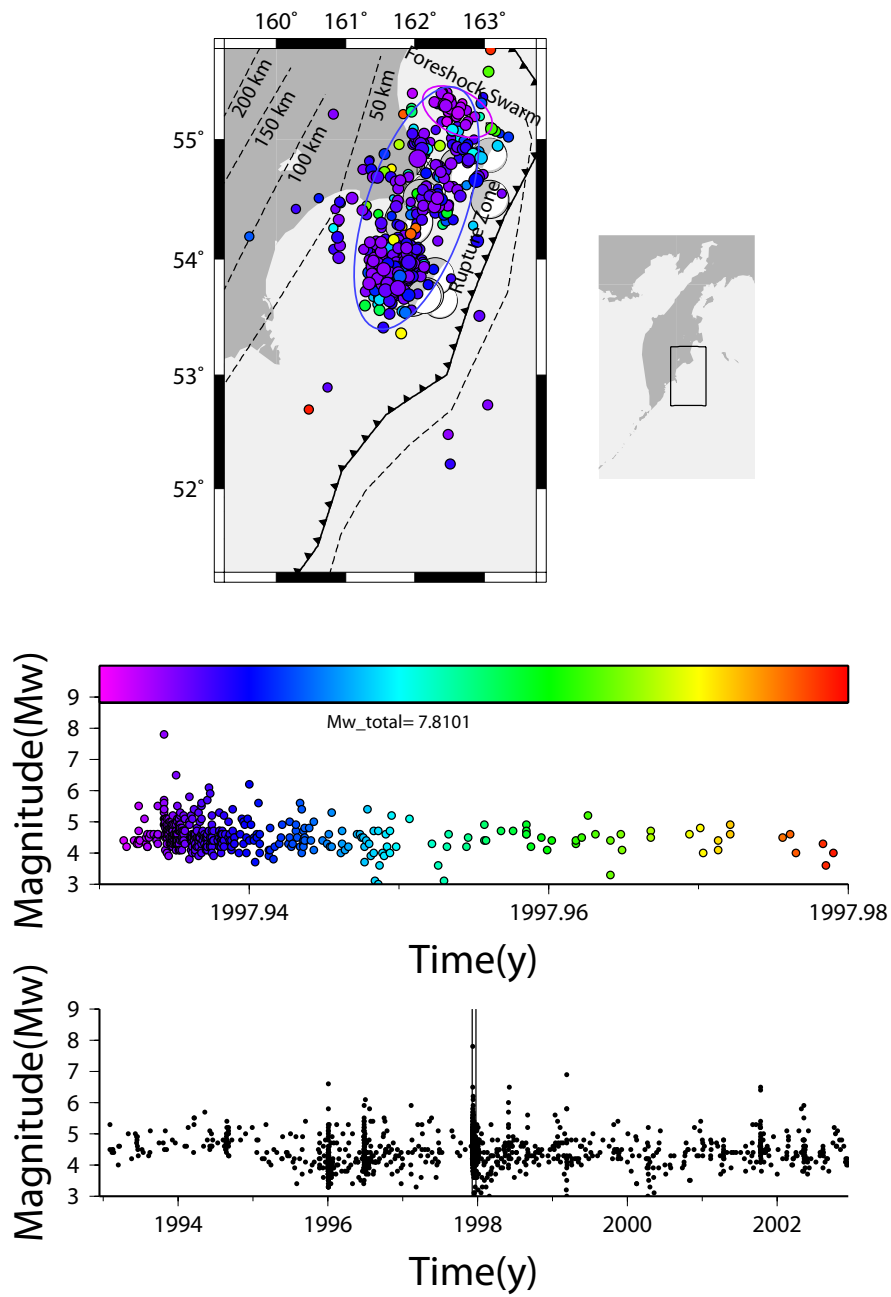


Figure 1.47: 1997 Kronotskii Earthquake and pre-shock Earthquake Swarm at the northern edge of the rupture zone.

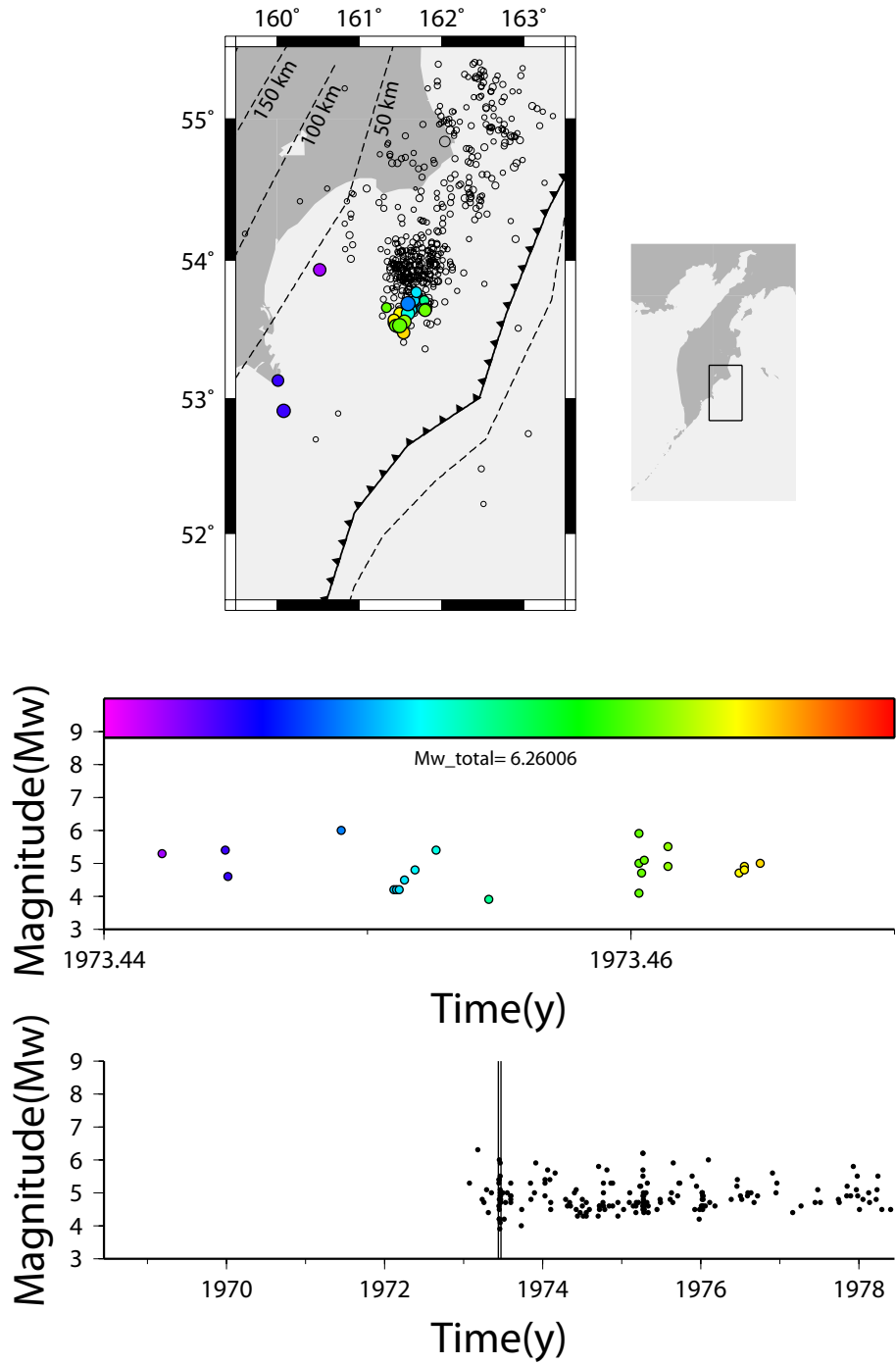


Figure 1.48: 1973 Kamchatka Earthquake Swarm. Open circles represent the 1997 Kronotskii earthquake aftershocks.

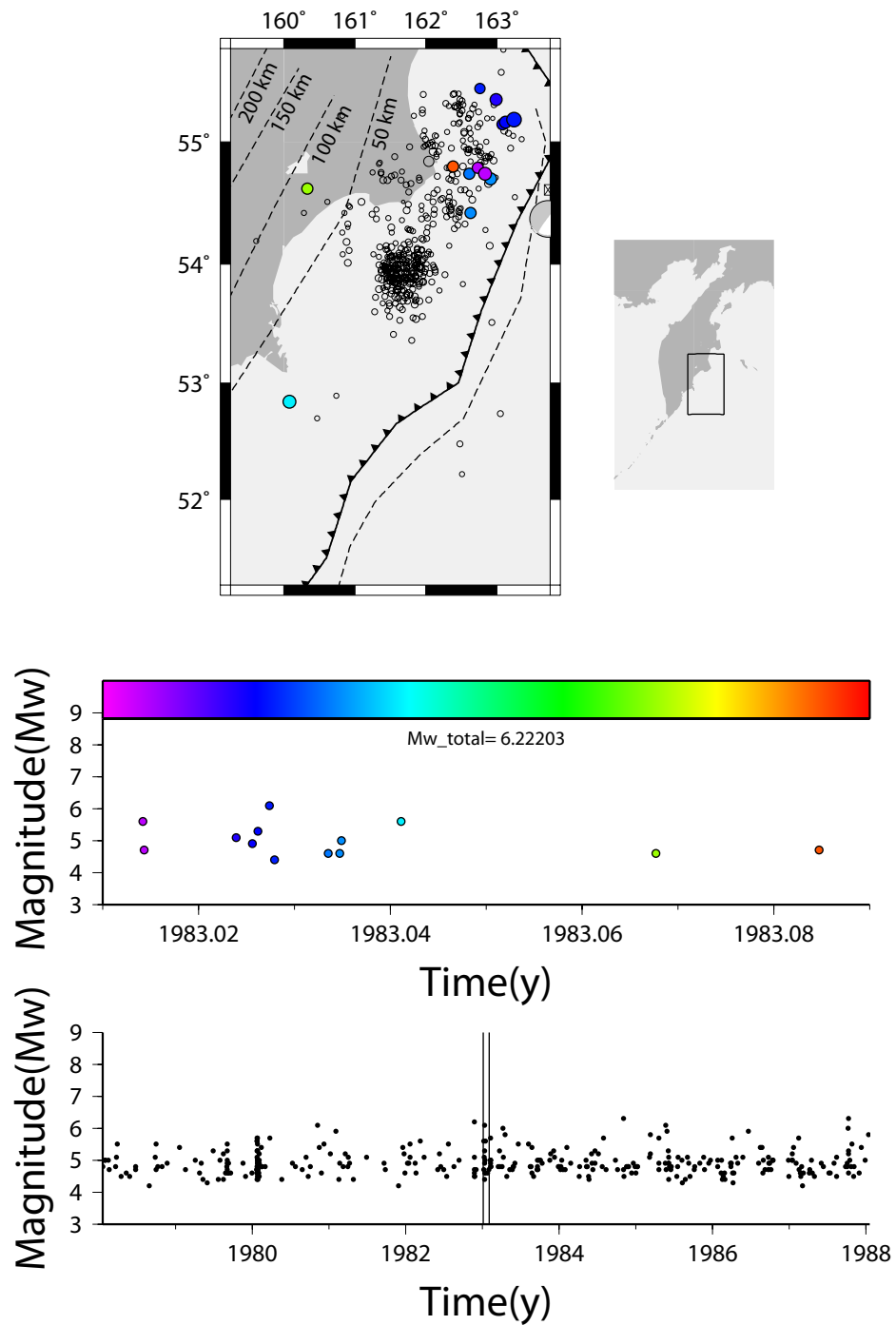


Figure 1.49: 1983 Kamchatka Earthquake Swarm.

order to compare South American swarms with the local catalog of Japanese swarms, we examine the frequency of swarms per unit of margin length and time. We did not include Southern California in this analysis because the different tectonic environments don't allow the frequency to be normalized correctly (normalizing by margin length). Figure 1.50 shows that when normalized this way, both swarm catalogs are similar with respect to how frequent swarms of a given magnitude should be. We grouped the magnitudes into 0.4 Mw bins to attempt to accommodate for the small catalogs available. Extrapolating the inverted values of frequency for the length of the South American margin shows that a Mw=4 swarm should occur about every year and we estimate there should be 7 Mw=2.5 (near the observable completeness limit when dense seismic networks exist) swarms per year. Some swarms of this magnitude have been reported, at Cordon Caulle for example. A Mw=8 swarm should occur every 50 years, and a Mw=8.5 swarm every 90 years, but it is important to keep in mind that events this large may not be physically possible. A barrier to the size of the swarm will result in the best fit line in Figure 1.50 to become vertical at the barrier magnitude (since 0 swarms will occur at magnitudes larger than the barrier magnitude). Volcanic earthquake swarms, which are included in this analysis, likely have a barrier much before swarms on the megathrust because there isn't enough fault area in the vicinity of a volcano to produce large magnitude events. This could be skewing the results in the range which volcanic earthquake swarms occur but its influence on Figure 1.50 is not clear.

We also used our catalog to explore relationships between different properties of swarms. For example, Ide et al. [2007] has presented a scaling law between moment and duration for slow earthquakes. Figure 1.51 explores different properties of swarms for all swarms in this catalog, but no clear signals

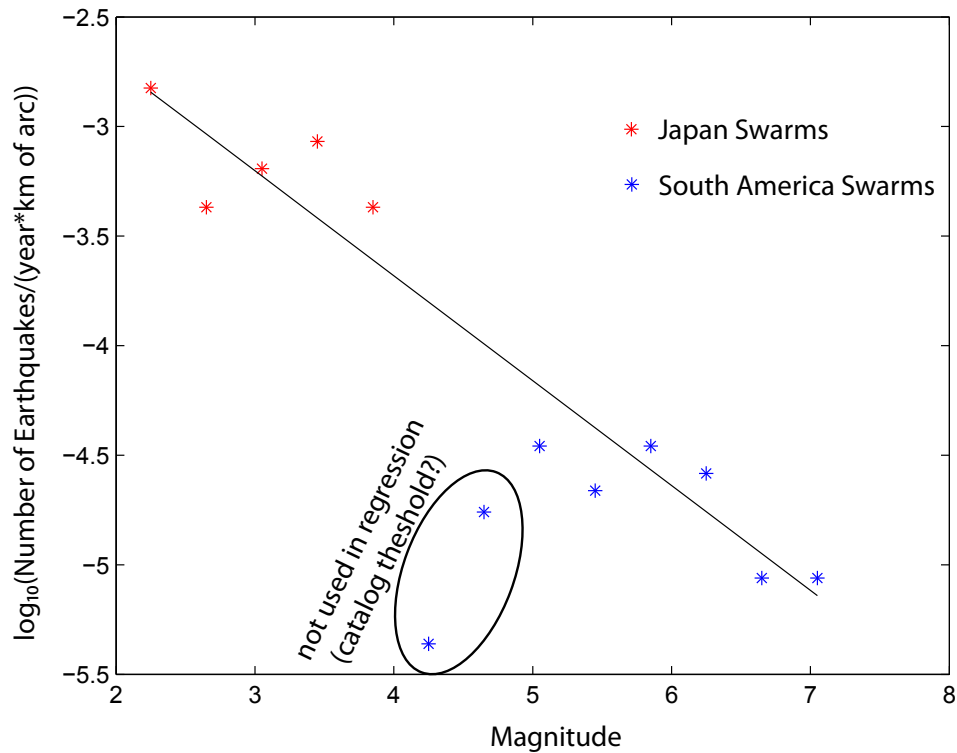


Figure 1.50: A comparison of South American and Japanese earthquake swarms shows that both areas agree on the frequency of swarms at a given magnitude, suggesting these are observations of the same phenomenon at different time and size scales. The two South American data points circled are not included in the linear regression because the downturn is most likely caused by these magnitudes being below the completeness threshold (e.g. in Figure 1 the threshold for the PDE catalog is  $\sim M_w=4.4$ )

emerge. This may be an artifact of combining megathrust swarms and volcanic swarms, so Figure 1.52 shows the same relationships except only for swarms near or on the megathrust (between the trench and 50 km depth to slab contour). Figure 1.52 shows that several of the swarms fit within the scaling law presented by Ide et al. [2007], particularly the ones with larger moment magnitudes.

When possible, we calculated apparent along strike epicentral propagation velocities. Table 1.4 shows a brief comparison of velocities associated with aseismic slip and epicentral propagation rates found in this study. All studies show along strike propagation of epicenters on the order of 5-10 km/day. As this propagation velocity seems to be common for aseismic transient events, any model to explain slow slip should explain this velocity.

Both swarms studied with InSAR in this thesis show no need for an aseismic slip component within the resolution of our data. Both, however, contained inset bursts of seismicity that accounted for a large amount of the seismic moment. Toda et al. [2002] and Llenos et al. [2009] have argued to remove such bursts of seismicity from the analysis because they may indicate a separate process, such as a triggered MS-AS sequence that is not directly related to the aseismic slip. The 2006 Copiapo swarm had two main bursts while the 1973 Copiapo swarm did not show any such bursts within the main swarm area. The 1973 Copiapo swarm did show bursts of seismicity after the main swarm activity, but they were separated from the swarm region by a few tens of kilometers while bursts during the 2006 swarm were within the swarm region. Inversions for the 2006 Copiapo swarm show a stress drop of 0.68 bars, which is over an order of magnitude lower than the average of  $\sim 10$  for interplate contacts Lay and Wallace

Table 1.4: Comparison of along strike epicentral propagation velocities.

Location	Propagation Velocity	Reference
Copiapo 1973	3.5 km/day	This study
Copiapo 2006	7.5 km/day	This study
Ecuador 2005	2.5 km/day	This study
Punitaqui 1997	5-10 km/day	This study
Salton Trough	3-20 km/day	Lohman and McGuire [2007]
West Moreland	3-10 km/day	Lohman and McGuire [2007]
N. Cascadia	5-15 km/day	Wech and Creager [2008]
C. Cascadia	5 km/day	(Brudzinski, personal com., 2009)
Shikoku Japan	12 km/day	Shelly et al. [2007]

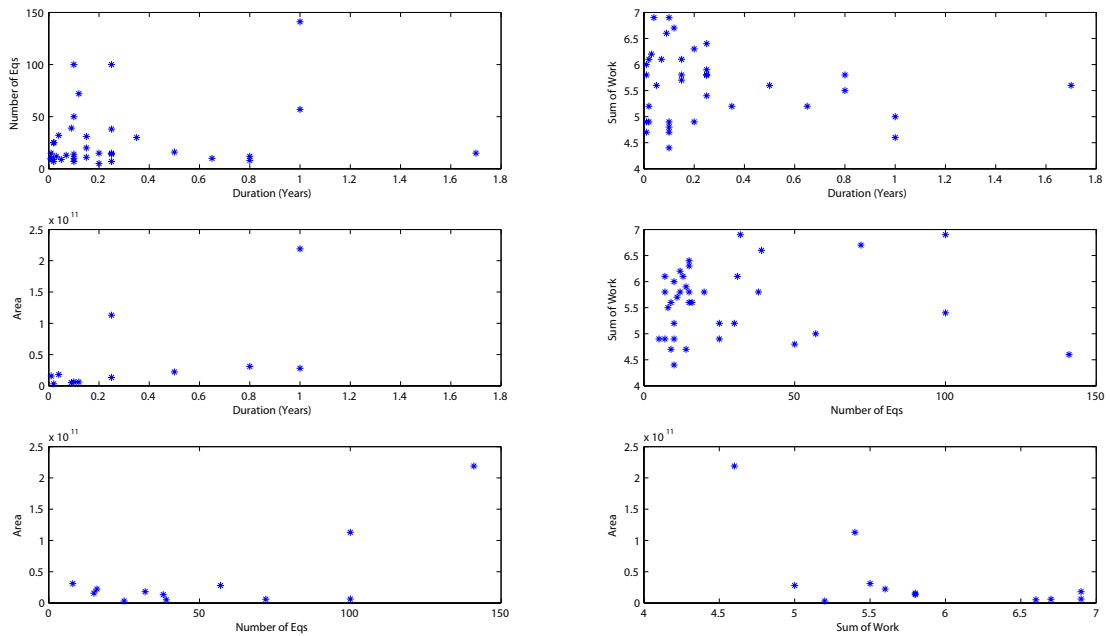


Figure 1.51: A comparison of different swarm properties compiled in this swarm catalog reveals no clear relationships between different swarm properties.

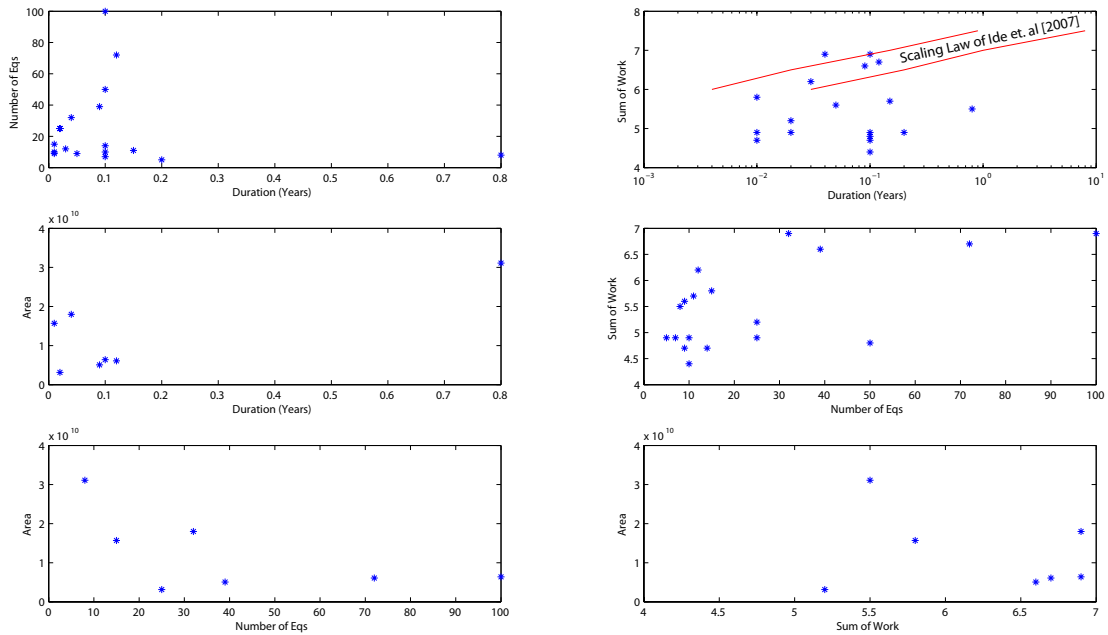


Figure 1.52: A comparison of different swarm properties for swarms on the megathrust compiled in this swarm catalog shows several intriguing possibilities. First, several of the swarms fit within the moment vs. duration scaling law presented by Ide et al. [2007]. Also, this catalog may show an increase in the number of earthquakes with decreasing area, perhaps opposite to what would be expected.

[1995], although this solution is very poorly resolved. Since inversions with single fault patches tend to over-estimate the fault area and under-estimate the slip (leading to a lower apparent stress drop), we also inverted for distributed slip using the solution described in Figure 1.7 as a starting point. For this inversion, we discretized the fault into a 10 by 10 grid of patches and then allowed the length and width of the whole system to vary by a small amount. This allows the inversion to explore the up-dip, down-dip, and along-strike directions by a couple of tens of kilometers. This inversion was run for several different values of smoothing and the final solution was taken off of an L-curve. Picking a solution visually with an L-curve attempts to resolve model smoothness and the misfit norm. The final solution is shown in Figure 1.53 and shows a magnitude of  $M_w=7.08$ , somewhat larger than with the single fault patch. The slip near the trench is not well resolved due to its distance from the deformation pattern and is likely an artifact of noise. We then calculate the stress drop in two different ways. First, we calculate the average stress drop for all patches that slipped more than 0.2 meters which results in a stress drop of 0.54 bars. Second, we calculated the stress drop of the largest slipping fault patch (which slipped 0.77 meters), which results in a maximum stress drop of 0.84 bars. Both of these values still agree with the solution for the single fault patch. There is no discrepancy between the larger magnitude and similar stress drops because this solution has a total fault length and width greater than that of the single fault patch solution.

Both the 1973 and 2006 Copiapo swarms show what appear to be periodic bursts of seismicity within the swarms. Since NVT, which is associated with slow slip events, has been shown to be tidally modulated, we modeled tidal displacements at Copiapo to determine if any tidal forcing was apparent. Fig-

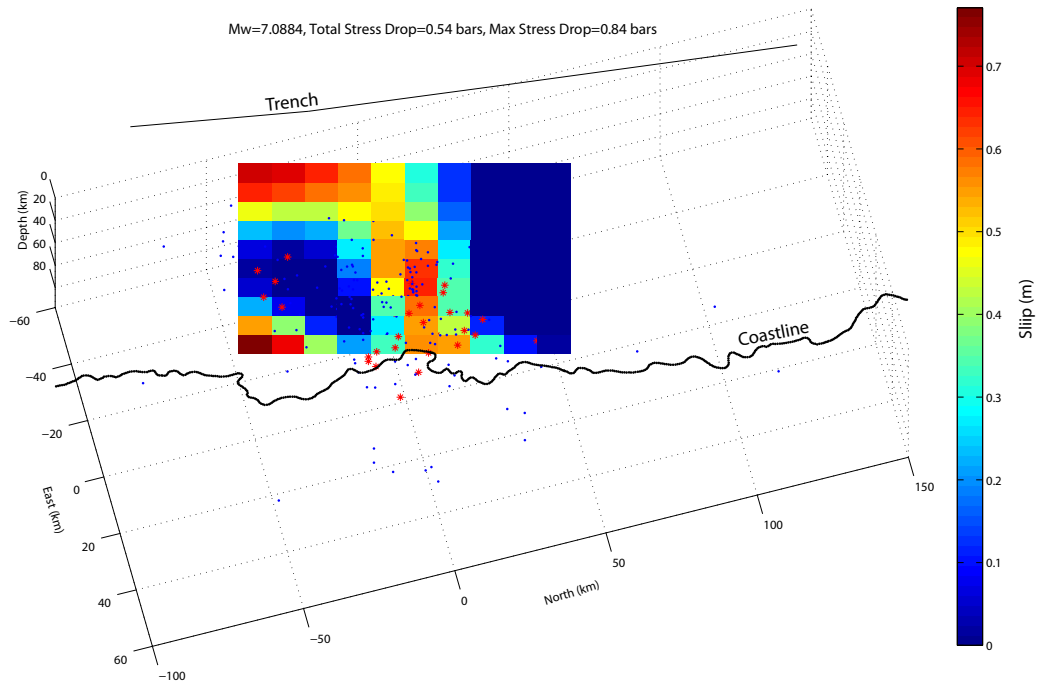


Figure 1.53: A distributed slip solution is arrived at by discretizing the solution from Figure 1.7 and inverting for multiple fault patches. The solution shows a slightly larger magnitude event and similar stress drop (with this magnitude discrepancy accommodated by a larger area)

ures 1.54 and 1.55 show the output of this modeling, but do not show any obvious relation between the tides and the bursts of seismicity. To compute tidal loads, a program at <http://www.oso.chalmers.se/~loading/> by M.S. Bos and H.G. Scherneck was used. The program computes surface displacements (for use on GPS monuments) using the GOT00.2 ocean tide model. This model is a hydrodynamic model on a finite element model with high resolution near the coast that is tuned to fit tide gauges and adjusted to fit TOPEX/Poseidon and ERS1/2 data altimetry data.

Geodetic inversions are sometimes unable to differentiate between single low stress drop events and many smaller but higher stress drop events and this swarm appears to be at least dominated by higher stress drop events that came as a burst within the swarm. Low stress drops are common for slow earthquakes and maybe ubiquitous for aseismic or slow slip events [Ide et al., 2007]. Allmann and Shearer [2009] compiled stress drops for 1759 earthquakes using the corner frequency approach [Boatwright, 1984] and found that the stress drops of the two largest events in the 2006 Copiapo swarm were 19 bars and 14 bars.

One possible explanation for why the Ticsani cluster did not show significant aseismic moment release is that it was not a swarm but rather an statically induced cluster of seismicity due to deformation associated with the swarm to the southeast. Seismicity can be induced in a dog bone-shaped pattern near dike activity with induced seismicity containing mainshock-aftershock sequences not associated with the swarms [e.g., Toda et al., 2002]. The geodetic solution for the Ticsani earthquake shows a stress drop of 35 bars, which is much greater than expected if it were part of the swarm as swarms are generally very low stress drop [Vidale and Shearer, 2006]. Studies such as Llenos et al. [2009]; Ogata

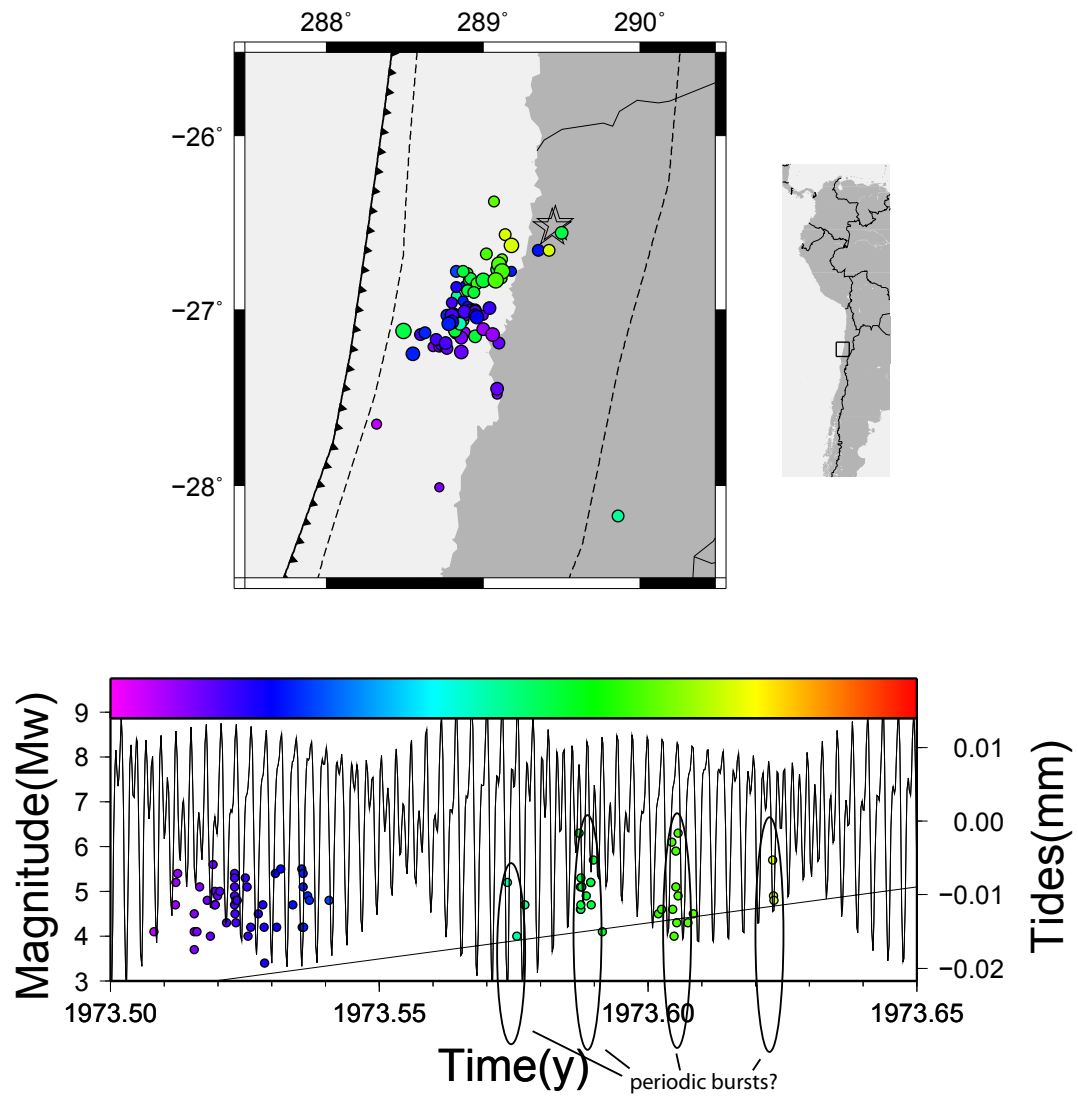


Figure 1.54: 1973 Copiapo Earthquake Swarm and comparison to tidal loading models.

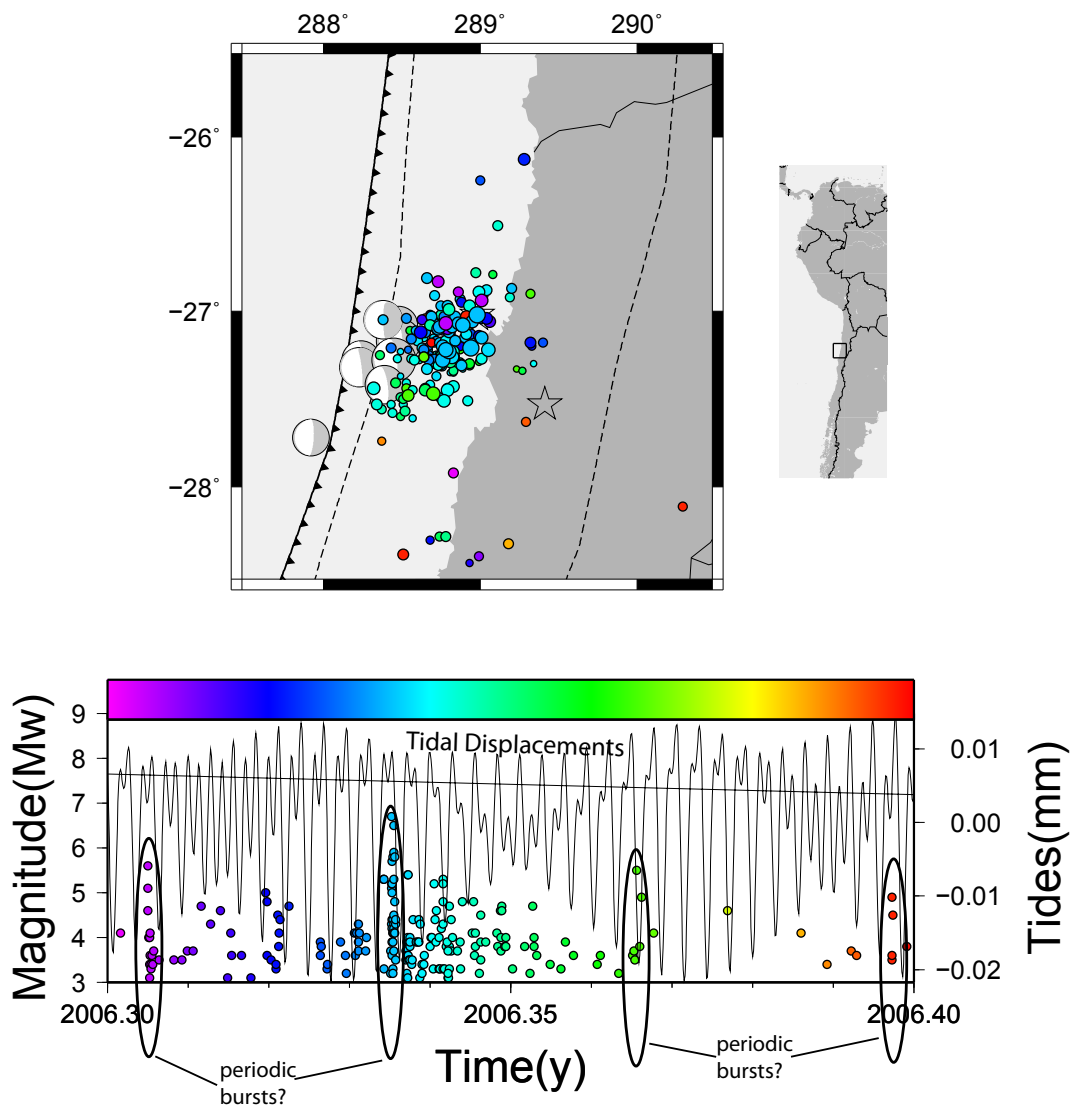


Figure 1.55: 2006 Copiapo Earthquake Swarm and comparison to tidal loading models.

[2007] attempt to remove the aftershock sequences from the catalog when computing earthquake statistics since they aren't believed to be caused by the same triggering event that caused the swarm. Figure 1.56 shows a conceptual model for how this may apply to the Ticsani Swarm.

We examined two of the three swarms caused by the 2001 Mw=8.5 Southern Peru earthquake for the possibility of static triggering via Coulomb stress changes. Several studies have shown that small Coulomb stresses, defined as a combination of shear and confining stresses, can have enough impact to trigger seismicity [King et al., 1994]. Coulomb stress changes as small as tenths of a bar has been shown to trigger seismicity. Earthquakes have also been shown to be triggered dynamically, with 1992 Landers earthquake providing the seminal example when it was shown to trigger earthquakes at volcanoes and hot springs several hundreds of kilometers away [Hill et al., 1993]. More recently, seismicity has been shown to be dynamically triggered by long period surface waves several thousands of kilometers away [e.g. Velasco et al., 2008]. We look to ascertain whether static triggering could have caused the swarms after the Southern Peru earthquake or if some sort of dynamic triggering must be involved.

Pritchard et al. [2007] calculate displacements associated with the 2001 earthquake by combining InSAR and teleseismic data in a joint inversion. Static changes in the Coulomb stress field due to the 2001 Peru earthquake were calculated using the solutions presented in Meade [2007] for stress and strain due to triangular tensile and shear faults in an elastic half space. The solutions of Meade [2007] are identical to Okada [1985] but are solved for triangular faults instead of rectangular faults. While there is no difference in this case because Pritchard et al. [2007] solve for displacements on rectangular fault patches, tri-

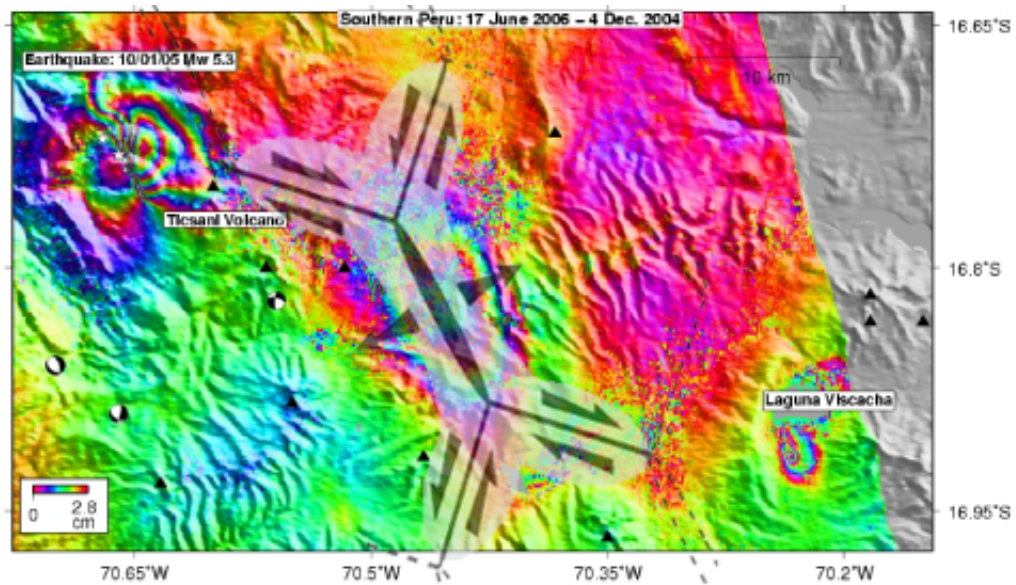


Figure 1.56: This conceptual model for the occurrence of the Ticsani swarm shows that stress changes due to deformation to the southeast of Ticsani Volcano could have caused the Ticsani earthquake swarm.

angles have the advantage of being able to tile curved interfaces without gaps between the edges. In the elastic half space, Poisson's ratio is taken to be 0.25 and the shear modulus of the fault is taken to be  $3.2 \times 10^{10} \text{ N}\cdot\text{m}$ .

The swarms in question did not occur coseismically but rather weeks to months after the event. The direct effects of dynamic triggering will only last on the order of minutes to hours, so it seems necessary that some static triggering is involved. Alternatively, a dynamic triggering mechanism that takes some time to manifest could be responsible. For the seismicity near Coropuna Volcano, strikes retrieved from the CMT catalog are consistent with the trend in the aftershocks, so the CMT solution strike ( $329^\circ$ ) and dip ( $88^\circ$ ) was used to construct the target fault. Only one CMT solution for seismicity southwest of lake Titicaca exists and it is not consistent with the trend of shocks associated with the swarm and so was not used. To be consistent with the trend in seismicity, a strike of  $50^\circ$  was used. Figure 1.57 shows Coulomb stresses resolved onto a fault plane consistent with seismicity near Coropuna Volcano and Figure 1.58 shows Coulomb stresses near lake Titicaca. However, both the Coulomb and confining stresses resolved onto fault planes consistent with swarm seismicity show very little static effect, on the order of  $10^{-5}$  bars. It therefore does not appear likely that these swarms were triggered by static stress changes due to the the  $M_w=8.5$  earthquake.

Since few volcanic swarms were discovered, their significance isn't as well determined. With the exception of the Ticsani swarm, all were associated with large megathrust earthquakes (the 2001  $M_w=8.5$  earthquake) or volcanic eruptions. Volcanic swarms in the north of the South American margin don't seem to be associated with eruptions, at least with magnitudes detectable by global

seismic networks, and many of these volcanoes are hot and frequently erupting. Southern Chilean volcanoes do produce sizable earthquake swarms, such as the Hudson and Chaiten Eruptions. The Cerro Hudson and Chaiten volcanoes both have infrequent eruptions, as their last eruptions were ~3600 and ~8000 years ago. The infrequency of the southern Chilean volcanoes and the magnitude of the swarms associated with those eruptions may both be related to the nature of the volcanoes, which are cooler than their northern counterparts. Swarms in the northern South American margin may require large triggering mechanisms, but there are too few swarms to make any clear inferences. Volcanic activity and volcanic earthquake swarms in the southern volcanoes can be triggered by large earthquakes as well, as the Mw=9.5 Chilean earthquake triggered the eruption of Cordon Caulle via movement of the LOFZ [Lara et al., 2004]. Key factors for the generation of earthquake swarms near volcanoes may be temperature and the presence of large faults near the volcano.

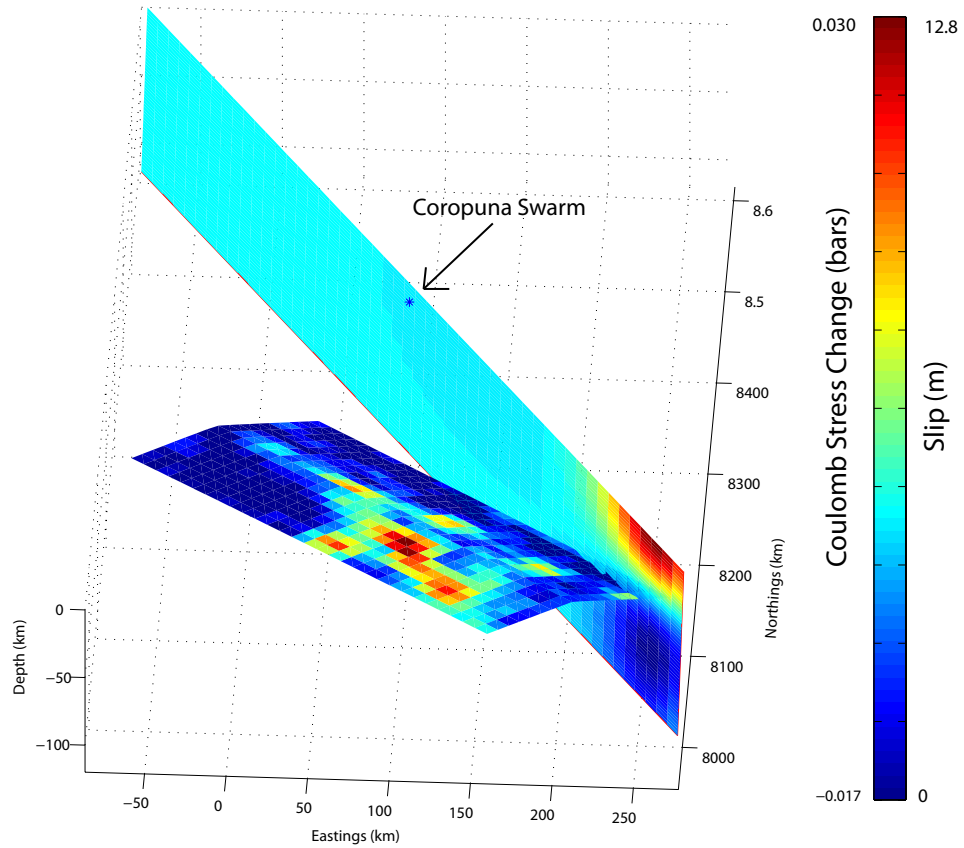


Figure 1.57: Coulomb stress changes at Coropuna Volcano due to the 2001 Peru earthquake. The blue star along the target fault plane shows the location of Coropuna Volcano.

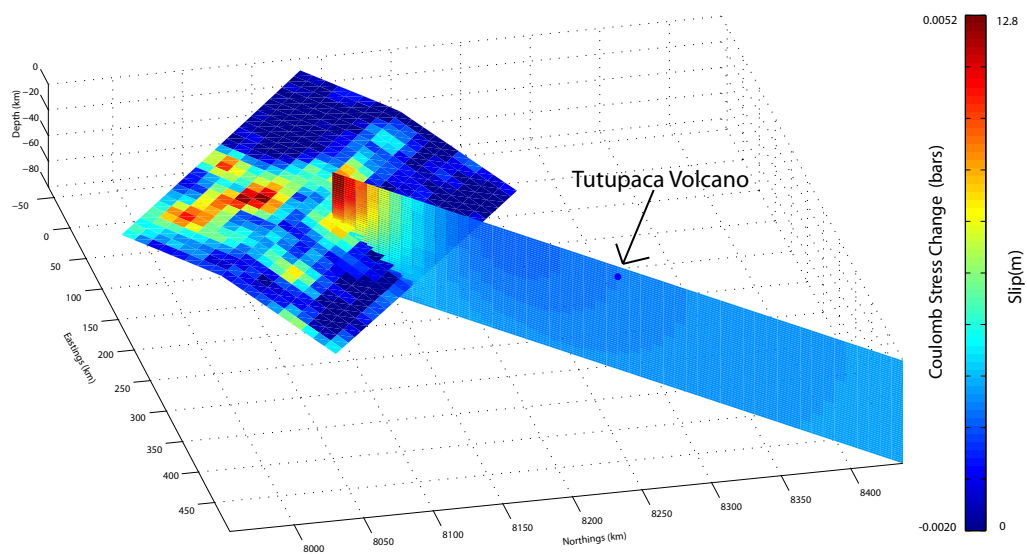


Figure 1.58: Coulomb stress changes at Tutupaca Volcano due to the 2001 Peru earthquake. The blue star along the target fault plane shows the location of Tutupaca Volcano.

## CONCLUSION

We performed a manual search for earthquake swarms in South America in order to identify earthquake swarms and determine their basic characteristics. We used the PDE catalog and identified 35 possible earthquake swarms of varying spatial scales and tectonic locations. We uncover indication that earthquake swarms may have some interaction with large megathrust events in South America, based on the observation that the termination of large megathrust ruptures sometimes end where swarms have recently occurred. We examine two of the swarms with InSAR geodetic data and conclude that no aseismic deformation is necessary to explain the observed surface deformation, however both of these swarms contain sudden bursts that make up most of the seismic moment release which is generally not indicative of aseismic slip. Seismicity that appears to have been triggered by the  $M_w=8.5$  2001 Peru earthquake is examined and shows that static changes in the Coulomb stress field did not trigger the events, indicating that some dynamic triggering process may have been responsible. We extended this idea to Kamchatka and showed that a similar process may have occurred there as well. We examined the frequency-magnitude content of our swarm catalog and found it to be in agreement with the regional swarm catalog from Japan despite large differences in catalog duration suggesting that we are observing the same process on a different scale. Although few volcanic swarms were found, we explore a possible relationship between swarm magnitudes, the frequency of eruption, and temperature of the volcano. With this South American earthquake swarm catalog we hope to provide the scientific community with a database that can help researchers better understand the earthquake process or their individual areas of interest in South America.

## BIBLIOGRAPHY

- Allmann, B. P. and Shearer, P. M. (2009). Global variations of stress drop for moderate to large earthquakes. *J. Geophys. Res.-Solid Earth*, 114:B01310.
- Barazangi, M. and Isacks, B. L. (1976). Spatial-distribution of earthquakes and subduction of nazca plate beneath south-america. *Geology*, 4(11):686–692.
- Barrientos, S., Bataille, K., Aranda, C., Legrand, D., Baez, J. C., Aguito, H., Pavez, A., Genrich, J., Vigny, C., and Bondoux, F. (2007). Complex sequence of earthquakes in fjordland, southern chile. *Proceedings Geosur*.
- Beck, S., Barrientos, S., Kausel, E., and Reyes, M. (1998). Source characteristics of historic earthquakes along the central Chile subduction zone. *J. South Am. Earth Sciences*, 11(2):115–129.
- Benoit, J. P. and McNutt, S. R. (1996). Global volcanic earthquake swarm database and preliminary analysis of volcanic earthquake swarm duration. *Annali de Geofisica*, 39:221–229.
- Biggs, J., Robinson, D. P., and Dixon, T. H. (2009). The 2007 Pisco, Peru, earthquake (M8.0): seismology and geodesy. *Geophys. J. Int.*, 176(3):657–669.
- Bird, P. (2003). An updated digital model of plate boundaries. *Geochem. Geophys. Geosyst.*, 4:1027.
- Boatwright, J. (1984). Seismic estimates of stress release. *J. Geophys. Res.*, 89(NB8):6961–6968.
- Brown, K. M., Tryon, M. D., DeShon, H. R., Dorman, L. M., and Schwartz, S. Y. (2005). Correlated transient fluid pulsing and seismic tremor in the Costa Rica subduction zone. *Earth Planet. Sci. Lett.*, 238(1-2):189–203.

- Comte, D., Eisenberg, A., Lorca, E., Pardo, M., Ponce, L., Saragoni, R., Singh, S. K., and Suarez, G. (1986). The 1985 central Chile earthquake - a repeat of previous great earthquakes in the region. *Science*, 233(4762):449–453.
- Comte, D., Haessler, H., Dorbath, L., Pardo, M., Monfret, T., Lavenu, A., Pontoise, B., and Hello, Y. (2002). Seismicity and stress distribution in the Copiapo, northern Chile subduction zone using combined on- and off-shore seismic observations. *Phys. Earth Planetary Interiors*, 132(1-3):197–217.
- Comte, D., Tassara, A., Farias, M., and Boroschek, R. (2006). 2006 Copiapo Chile seismic swarm analysis: Mapping the interplate contact. *Eos Trans. AGU*.
- Davis, D., Suppe, J., and Dahlen, F. A. (1983). Mechanics of fold-and-thrust belts and accretionary wedges. *J. Geophysical Research*, 88(NB2):1153–1172.
- Devlin, S. (2008). *Earthquakes in the Continental Crust*. PhD thesis, Cornell University.
- Dieterich, J. (1994). A constitutive law for rate of earthquake production and its application to earthquake clustering. *J. Geophysical Research-solid Earth*, 99(B2):2601–2618.
- Engdahl, E. R., Jackson, J. A., Myers, S. C., Bergman, E. A., and Priestley, K. (2006). Relocation and assessment of seismicity in the Iran region. *Geophys. J. Int.*, 167(2):761–778.
- Engdahl, E. R., van der Hilst, R., and Buland, R. (1998). Global teleseismic earthquake relocation with improved travel times and procedures for depth determination. *Bull. Seismol. Soc. Amer.*, 88(3):722–743.
- Evison, F. F. and Rhoades, D. A. (1993). The precursory earthquake swarm in New Zealand - hypothesis tests. *New Zealand J. Geology Geophysics*, 36(1):51–60.

- Fournier, T. J., Pritchard, M. E., and Riddick, S. N. (2009). The duration, magnitude, and frequency of subaerial volcano deformation events: New InSAR results from latin america and a global synthesis. *Geochem. Geophys. Geosyst.*, In press.
- Fujinawa, Y., Eguchi, T., Ukawa, M., Matsumoto, H., Yokota, T., and Kishio, M. (1983). The 1981 earthquake swarm off the Kii peninsula observed by the ocean bottom seismometer array. *J. Phys. Earth*, 31(6):407–428.
- Fukushima, Y. (2007). Ground deformation associated with a seismic swarm near Aysen, southern Chile, measured by ALOS/PALSAR interferometry (abstract). *European Space Agency FRINGE workshop*, page 124.
- Gardi, A., Lemoine, A., Madariaga, R., and Campos, J. (2006). Modeling of stress transfer in the Coquimbo region of central Chile. *J. Geophysical Research-solid Earth*, 111(B4):B04307.
- González, K., Froger, J. L., Rivera, M., and Audin, L. (2006). Deformación co-sísmica producida por el sismo mb = 5.4 del 01 de octubre de 2005 (carumas - moquegua), detectada por interferometría radar – insar. *XIII Congreso Peruano de Geología*.
- Heki, K., Miyazaki, S., and Tsuji, H. (1997). Silent fault slip following an inter-plate thrust earthquake at the Japan trench. *Nature*, 386(6625):595–598.
- Hill, D. P. (1977). Model for earthquake swarms. *J. Geophysical Research*, 82(8):1347–1352.
- Hill, D. P., Reasenber, P. A., Michael, A., Arabaz, W. J., Beroza, G., Brumbaugh, D., Brune, J. N., Castro, R., Davis, S., Depolo, D., Ellsworth, W. L., Gomberg, J., Harmsen, S., House, L., Jackson, S. M., Johnston, M. J. S., Jones, L., Keller,

- R., Malone, S., Munguia, L., Nava, S., Pechmann, J. C., Sanford, A., Simpson, R. W., Smith, R. B., Stark, M., Stickney, M., Vidal, A., Walter, S., Wong, V., and Zollweg, J. (1993). Seismicity remotely triggered by the magnitude 7.3 Landers, California, earthquake. *Science*, 260(5114):1617–1623.
- Hirose, H. and Obara, K. (2006). Short-term slow slip and correlated tremor episodes in the Tokai region, central Japan. *Geophys. Res. Lett.*, 33(17):L17311.
- Hsu, Y. J., Simons, M., Avouac, J. P., Galetzka, J., Sieh, K., Chlieh, M., Natawidjaja, D., Prawirodirdjo, L., and Bock, Y. (2006). Frictional afterslip following the 2005 Nias-Simeulue earthquake, Sumatra. *Science*, 312(5782):1921–1926.
- Husen, S., Taylor, R., Smith, R. B., and Healy, H. (2004). Changes in geyser eruption behavior and remotely triggered seismicity in Yellowstone National Park produced by the 2002 M 7.9 Denali fault earthquake, Alaska. *Geology*, 32(6):537–540.
- Ide, S., Beroza, G. C., Shelly, D. R., and Uchide, T. (2007). A scaling law for slow earthquakes. *Nature*, 447(7140):76–79.
- Jones, L. M. (1994). Foreshocks, aftershocks, and earthquake probabilities - accounting for the Landers earthquake. *Bull. Seismol. Soc. Amer.*, 84(3):892–899.
- Kelleher, J. A. (1972). Rupture zones of large south-american earthquakes and some predictions. *J. Geophysical Research*, 77(11):2087.
- King, G. C. P., Stein, R. S., and Lin, J. (1994). Static stress changes and the triggering of earthquakes. *Bulletin Seismological Soc. Am.*, 84(3):935–953.
- Kirby, S. H. (2000). Earth science - Taking the temperature of slabs. *Nature*, 403(6765):31.

- Lange, D., Cembrano, J., Rietbrock, A., Haberland, C., Dahm, T., and Bataille, K. (2008). First seismic record for intra-arc strike-slip tectonics along the Liquine-Ofqui fault zone at the obliquely convergent plate margin of the southern Andes. *Tectonophysics*, 455(1-4):14–24.
- Lara, L. E., Moreno, H., and Naranjo, J. (2004). Ryodacitic fissure eruption in southern Andes, Chile (40.5°S) after the 1960 ( $M_w$  9.5) Chilean earthquake: a structural interpretation. *J. Volcan. Geotherm. Res.*, 138:127–138.
- Lara, L. E., Pallister, J. S., and Ewert, J. W. (2008). The 2008 eruption of Chaitén volcano, Southern Chile: a tectonically controlled eruption? *Eos Trans. AGU* 89.
- Laursen, J. and Normark, W. R. (2002). Late Quaternary evolution of the San Antonio Submarine Canyon in the central Chile forearc (similar to 33 degrees s). *Marine Geology*, 188(3-4):365–390.
- Lay, T. and Wallace, T. C. (1995). *Modern Global Seismology*.
- Lemoine, A., Madariaga, R., and Campos, J. (2001). Evidence for earthquake interaction in Central Chile: the July 1997-September 1998 sequence. *Geophysical Research Lett.*, 28(14):2743–2746.
- Llenos, A. L., McGuire, J. J., and Ogata, Y. (2009). Modeling seismic swarms triggered by aseismic transients. *Earth Planetary Science Lett.*, 281(1-2):59–69.
- Lohman, R. B. (2004). *The inversion of geodetic data for earthquake parameters*. PhD thesis, California Institute of Technology.
- Lohman, R. B. and McGuire, J. J. (2007). Earthquake swarms driven by aseismic creep in the Salton Trough, California. *J. Geophysical Research-solid Earth*, 112(B4):B04405.

- Maggi, A., Jackson, J. A., Priestley, K., and Baker, C. (2000). A re-assessment of focal depth distributions in southern Iran, the Tien Shan and northern India: Do earthquakes really occur in the continental mantle? *Geophys. J. Int.*, 143:629–661.
- Matsuzawa, T., Uchida, N., Igarashi, T., Okada, T., and Hasegawa, A. (2004). Repeating earthquakes and quasi-static slip on the plate boundary east off northern Honshu, Japan. *Earth Planets Space*, 56(8):803–811.
- McNutt, S. R. and Marzocchi, W. (2004). Simultaneous earthquake swarms and eruption in Alaska, fall 1996: Statistical significance and inference of a large aseismic slip event. *Bull. Seismol. Soc. Amer.*, 94(5):1831–1841.
- Meade, B. J. (2007). Algorithms for the calculation of exact displacements, strains, and stresses for triangular dislocation elements in a uniform elastic half space. *Computers & Geosciences*, 33(8):1064–1075.
- Mogi, K. (1963). Some discussions on aftershocks, foreshocks, and earthquake swarms - the fracture of a semi finite body caused by an inner stress origin and its relation to the earthquake phenomena. *Bull. Earthquake Res. Inst.*, 41:615–658.
- Mora, C., Comte, D., Russo, R., Gallego, A., and Mocanu, V. (2008). The Liquiñe-Ofqui fault system and its relationship to the Aysen (Southern Chile) 2007 seismic swarm. *Eos Trans. AGU* 89.
- Motagh, M., Wang, R. J., Walter, T. R., Burgmann, R., Fielding, E., Anderssohn, J., and Zschau, J. (2008). Coseismic slip model of the 2007 August Pisco earthquake (Peru) as constrained by Wide Swath radar observations. *Geophysical J. Int.*, 174(3):842–848.

- Naranjo, J. A. and Stern, C. R. (1998). Holocene explosive activity of Hudson volcano. *Bull. Volc.*, 59:291–306.
- Ogata, Y. (2007). Seismicity and geodetic anomalies in a wide area preceding the Niigata-Ken-Chuetsu earthquake of 23 October 2004, central Japan. *J. Geophysical Research-solid Earth*, 112.
- Okada, Y. (1985). Surface deformation due to shear and tensile faults in a half-space. *Bulletin Seismological Soc. Am.*, 75(4):1135–1154.
- Ozawa, S., Murakami, M., Kaidzu, M., Tada, T., Sagiya, T., Hatanaka, Y., Yarai, H., and Nishimura, T. (2002). Detection and monitoring of ongoing aseismic slip in the Tokai region, Central Japan. *Science*, 298(5595):1009–1012.
- Ozawa, S., Suito, H., and Tobita, M. (2007). Occurrence of quasi-periodic slow-slip off the east coast of the Boso peninsula, Central Japan. *Earth Planets Space*, 59(12):1241–1245.
- Payero, J. S., Kostoglodov, V., Shapiro, N., Mikumo, T., Iglesias, A., Perez-Campos, X., and Clayton, R. W. (2008). Nonvolcanic tremor observed in the Mexican subduction zone. *Geophys. Res. Lett.*, 35(7):L07305.
- Peterson, C., Christensen, D., and McNutt, S. (2005). Episodic tremor in the Alaska/Aleutian subduction zone. *Eos Trans. AGU* 86.
- Pritchard, M. E. and Fielding, E. J. (2008). A study of the 2006 and 2007 earthquake sequence of Pisco, Peru, with InSAR and teleseismic data. *Geophysical Research Lett.*, 35(9).
- Pritchard, M. E., Norabuena, E. O., Ji, C., Boroschek, R., Comte, D., Simons, M., Dixon, T. H., and Rosen, P. A. (2007). Geodetic, teleseismic, and strong motion

- constraints on slip from recent southern Peru subduction zone earthquakes. *J. Geophysical Research-solid Earth*, 112(B3).
- Roeder, D. (1988). Andean-age structure of Eastern Cordillera (province of La-Paz, Bolivia). *Tectonics*, 7(1):23–39.
- Rogers, G. and Dragert, H. (2003). Episodic tremor and slip on the Cascadia subduction zone: The chatter of silent slip. *Science*, 300(5627):1942–1943.
- Rosen, P. A., Hensley, S., Peltzer, G., and Simons, M. (2004). Updated repeat orbit interferometry package released. *EOS*, 85.
- Sambridge, M. (1998). Exploring multidimensional landscapes without a map. *Inverse Probl.*, 14(3):427–440.
- Segall, P. and Rice, J. R. (1995). Dilatancy, compaction, and slip instability of a fluid-infiltrated fault. *J. Geophys. Res.-Solid Earth*, 100(B11):22155–22171.
- Segall, P., Rubin, A., and Rice, J. (2008). Mechanical models for slow-slip with focus on dilatant strengthening plus speculation on tremor and triggered earthquakes. *Report on the Aseismic Slip, Tremor, and Earthquakes Workshop*.
- Shcherbakov, R., Turcotte, D. L., and Rundle, J. B. (2004). A generalized Omori's law for earthquake aftershock decay. *Geophys. Res. Lett.*, 31(11):L11613.
- Shelly, D. R., Beroza, G. C., and Ide, S. (2007). Non-volcanic tremor and low-frequency earthquake swarms. *Nature*, 446(7133):305–307.
- Shelly, D. R., Beroza, G. C., Ide, S., and Nakamura, S. (2006). Low-frequency earthquakes in Shikoku, Japan, and their relationship to episodic tremor and slip. *Nature*, 442(7099):188–191.

- Shelly, D. R., Ellsworth, W. L., Ryberg, T., Haberland, C., Fuis, G. S., Murphy, J., Nadeau, R. M., and Burgmann, R. (2009). Precise location of San Andreas Fault tremors near Cholame, California using seismometer clusters: Slip on the deep extension of the fault? *Geophys. Res. Lett.*, 36:L01303.
- Shibutani, T., Nakao, S., Nishida, R., Takeuchi, F., Watanabe, K., and Umeda, Y. (2002). Swarm-like seismic activity in 1989, 1990 and 1997 preceding the 2000 Western Tottori earthquake. *Earth Planets Space*, 54(8):831–845.
- Slavina, L. B., Pivovarova, N. B., and Levina, V. I. (2007). A Study in the Velocity Structure of December 5, 1997, M-w=7.8 Kronotskii Rupture Zone, Kamchatka. *J. Volcanology Seismology*, 1(4):254–262.
- Swenson, J. L. and Beck, S. L. (1996). Historical 1942 Ecuador and 1942 Peru subduction earthquakes, and earthquake cycles along Colombia Ecuador and Peru subduction segments. *Pure Appl. Geophysics*, 146(1):67–101.
- Swenson, J. L. and Beck, S. L. (1999). Source characteristics of the 12 November 1996 M-w 7.7 Peru subduction zone earthquake. *Pure Appl. Geophys.*, 154(3-4):731–751.
- Sykes, L. R. (1970). Earthquake swarms and sea-floor spreading. *J. Geophysical Research*, 75(32):6598.
- Sykes, L. R. (1971). Aftershock zones of great earthquakes, seismicity gaps, and earthquake prediction for Alaska and Aleutians. *J. Geophysical Research*, 76(32):8021.
- Syracuse, E. M. and Abers, G. A. (2006). Global compilation of variations in slab depth beneath arc volcanoes and implications. *Geochemistry Geophysics Geosystems*, 7.

- Syracuse, E. M. and Abers, G. A. (2009). Systematic biases in subduction zone hypocenters. *Geophys. Res. Lett.*, 36:L10303.
- Thierer, P. O., Flueh, E. R., Kopp, H., Tilmann, F., Comte, D., and Contreras, S. (2005). Local earthquake monitoring offshore Valparaiso, Chile. *Neues Jahrbuch Fur Geologie Und Palaontologie-abhandlungen*, 236(1-2):173–183.
- Toda, S., Stein, R. S., and Sagiya, T. (2002). Evidence from the AD 2000 Izu islands earthquake swarm that stressing rate governs seismicity. *Nature*, 419(6902):58–61.
- Velasco, A. A., Hernandez, S., Parsons, T., and Pankow, K. (2008). Global ubiquity of dynamic earthquake triggering. *Nature Geoscience*, 1(6):375–379.
- Venzke, E., Wunderman, R. W., McClelland, L., Simkin, T., Luhr, J. F., Seibert, L., Sennert, S., and Mayberry, G. (2002). Global volcanism, 1968 to the present. Smithsonian Institution, Global Volcanism Program Digital Information Series, GVP-4.
- Vidale, J. E., Boyle, K. L., and Shearer, P. M. (2006). Crustal earthquake bursts in California and Japan: Their patterns and relation to volcanoes. *Geophys. Res. Lett.*, 33(20):L20313.
- Vidale, J. E. and Shearer, P. M. (2006). A survey of 71 earthquake bursts across southern California: Exploring the role of pore fluid pressure fluctuations and aseismic slip as drivers. *J. Geophys. Res.-Solid Earth*, 111(B5):B05312.
- vonHuene, R., Corvalan, J., Flueh, E. R., Hinz, K., Korstgard, J., Ranero, C. R., Weinrebe, W., Klaeschen, D., Naveas, J. L. D., Harms, G., Spiegler, D., Biebow, N., Locker, S., Kruger, D., Morales, E., Vergara, H., Yanez, G., Valenzuela, E., Wall, R., Trinhammer, P., Laursen, J., Scholl, D., Kay, S., Dominguez, S., Segl,

- M., Beese, D., Lamy, F., Bialas, J., Biegling, A., Gerdom, M., Hojka, A. M., Hoppenworth, R., Husem, S., Krastel, S., Kulowski, N., Morawe, M. P., Munoz, A. E. D., Lefmann, A. K., Vidal, N. M., Zelt, C., Hinz, K., Block, M., Damm, V., Fritsch, J., Neben, S., Reichert, C., and Schreckenberger, B. (1997). Tectonic control of the subducting Juan Fernandez Ridge on the Andean margin near Valparaiso, Chile. *Tectonics*, 16(3):474–488.
- Wech, A. G. and Creager, K. C. (2008). Automated detection and location of Cascadia tremor. *Geophys. Res. Lett.*, 35(20):L20302.
- Wolfe, C. J., Brooks, B. A., Foster, J. H., and Okubo, P. G. (2007). Microearthquake streaks and seismicity triggered by slow earthquakes on the mobile south flank of Kilauea Volcano, Hawaii. *Geophys. Res. Lett.*, 34(23):L23306.
- Yanez, G. A., Ranero, C. R., von Huene, R., and Diaz, J. (2001). Magnetic anomaly interpretation across the southern central Andes (32 degrees–34 degrees S): The role of the Juan Fernandez Ridge in the late Tertiary evolution of the margin. *J. Geophysical Research-solid Earth*, 106(B4):6325–6345.
- Zobin, V. M. (1996). Earthquake clustering in shallow subduction zones: Kamchatka and Mexico. *Phys. Earth Planetary Interiors*, 97(1-4):205–218.
- Zobin, V. M. (1999). Changes in earthquake source properties across a shallow subduction zone: Kamchatka peninsula. *Pure Appl. Geophysics*, 154(3-4):457–466.
- Zobin, V. M. and Ivanova, E. I. (1994). Earthquake swarms in the Kamchatka-Commander region. *Geophysical J. Int.*, 117(1):33–47.